

**UNIVERSITY OF TURKISH AERONAUTICAL ASSOCIATION
INSTITUTE OF SCIENCE AND TECHNOLOGY**

**DESIGN AND DEVELOPMENT OF A TWO-STROKE ENGINE
WITH RHOMBIC DRIVE MECHANISM**



Ph.D. THESIS

Erol GÜLTEKİN

DEPARTMENT OF MECHANICAL AND AERONAUTICAL ENGINEERING

MARCH 2019

**UNIVERSITY OF TURKISH AERONAUTICAL ASSOCIATION
INSTITUTE OF SCIENCE AND TECHNOLOGY**

**DESIGN AND DEVELOPMENT OF A TWO-STROKE ENGINE
WITH RHOMBIC DRIVE MECHANISM**



Ph.D. THESIS

**Erol GÜLTEKİN
1303947001**

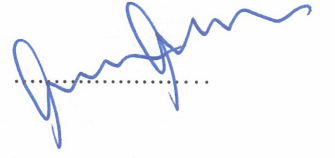
DEPARTMENT OF MECHANICAL AND AERONAUTICAL ENGINEERING

Supervisor: Prof. Dr. Can ÇINAR

Approval of the thesis:

Erol GÜLTEKİN, having student number 1303947001 and enrolled in the Ph.D. Program at the Institute of Science and Technology at the University of Turkish Aeronautical Association, after meeting all of the required conditions contained in the related regulations, has successfully accomplished, in front of the jury, the presentation of the thesis prepared with the title of “DESIGN AND DEVELOPMENT OF A TWO-STROKE ENGINE WITH RHOMBIC DRIVE MECHANISM”.

Supervisor: Prof. Dr. Can ÇINAR
Gazi University



Examining Committee Members:

Prof. Dr. Cihan KARATAŞ
University of Turkish Aeronautical Association



Prof. Dr. Can ÇINAR
Gazi University



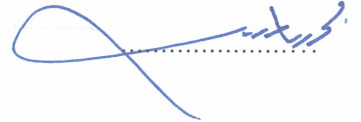
Assoc. Prof. Dr. Melih OKUR
Gazi University



Assoc. Prof. Dr. Tolga TOPGÜL
Gazi University



Assist. Prof. Dr. Mohamed Salem ELMNEFI
University of Turkish Aeronautical Association



Date of Thesis Defense: 7 March, 2019

UNIVERSITY OF TURKISH AERONAUTICAL ASSOCIATION
INSTITUTE OF SCIENCE AND TECHNOLOGY
STATEMENT OF NON-PLAGIARISM

I hereby declare that all information in this document I present as my Ph. D. Thesis, entitled: Design and development of a two-stroke engine with rhombic drive mechanism, has been presented in accordance with academic rules and ethical conduct. I also declare and certify with my honor that I have fully cited and referenced all the sources utilized in this study.

7 March, 2019

Erol GÜLTEKİN



ACKNOWLEDGEMENTS

I express my sincere appreciation to my thesis supervisor Prof. Dr. Can ÇINAR for his supervision, support and helpful critics throughout the progress of my thesis study.

I would like to thank members of thesis monitoring committee who are Assoc. Prof. Dr. Melih OKUR for his great contribution on preparing the experimental setup, and Assist. Prof. Dr. Mohamed Salem ELMNEFI for his comments.

I also would like to thank my former colleague Mehmet YAHŞI, classmate Assoc. Prof. Dr. Hamit SOLMAZ from Gazi University, and present colleague Assist. Prof. Dr. Ceyhun TOLA from UTAA for their support on software.

I have to acknowledge to Chairperson of Automotive Engineering Department in Gazi University due to utilization permit of the laboratories.

Many thanks to Orman Motor for supplying of the engine and spare parts, the next acknowledgement is to Çizgi Makine for manufacturing of the engine at his workshop.

Finally, I wish to give special thank my wife and all members of my family to whom this thesis is dedicated.

TABLE OF CONTENTS

	Page
ACKNOWLEDGEMENTS	iv
TABLE OF CONTENTS	v
LIST OF TABLES	vii
LIST OF FIGURES	viii
ABBREVIATIONS	xi
LIST OF SYMBOLS	xii
ABSTRACT	xiii
ÖZET	xiv
CHAPTER 1	
INTRODUCTION	1
1.1 Motivation	1
1.2 Objectives	1
1.3 Outline of the Thesis	2
CHAPTER 2	
LITERATURE OF TWO-STROKE ENGINES	4
2.1 Historical Development.....	4
2.2 Operating Principles	6
2.3 Comparison of Two-Stroke and Four-Stroke Engines.....	8
2.4 Literature Survey	9
2.5 Two-Stroke Engine Configurations	17
2.4.1 Three Port Two-Stroke Engine	17
2.4.2 Reverse Flow Scavenge (DKW) Engine	18
2.4.3 Lucas Engine	19
2.4.4 Trojan Engine	20
2.4.5 Opposed Piston Engine	20
2.4.6 Schnürle Engine	21
2.4.7 Orbital Engine	22
2.4.8 Omnivore Engine	23
2.4.9 Rhombic Drive Engine	24
CHAPTER 3	
KINEMATIC AND THERMODYNAMIC ANALYSIS OF THE ENGINE	25
3.1 Kinematics of the Engines.....	28
3.1.1 Slider-Crank Mechanism	28
3.1.2 Rhombic Drive Mechanism	31
3.2 Thermodynamic Analysis.....	32
3.2.1 Chemical and Physical Properties of Air	32
3.2.2 Properties of the Fuel and Excess Air Coefficient	33
3.2.3 Quantity and Temperature of Charging	34
3.2.4 Properties of Mixture Inside the Cylinder	35
3.2.5 Specific Heat Changing with Temperature	40

	Page
3.2.6 Quantity and Temperature of the Exhaust Residual Gases Inside the Cylinder with Temperature	42
3.2.7 Heat Addition to the Cylinder.....	44
3.2.8 Heat Transfer	45
3.3 Engine Performance Characteristics	47
3.3.1 Work	48
3.3.2 Mean Effective Pressure	49
3.3.3 Torque and Power.....	50
3.3.4 Air Fuel Ratio and Fuel Air Ratio	51
3.3.5 Specific Fuel Consumption	52
3.3.6 Engine Efficiencies	52
3.4 Exhaust Emissions.....	53
CHAPTER 4	
ENGINE DESIGN AND MANUFACTURING	55
4.1 Design of the Engine	55
4.1.1 Connecting Rod	57
4.1.2 Rhombic Links.....	60
4.1.3 Rhombic Pins.....	63
4.1.4 Gear Pins.....	64
4.1.5 Gears	66
4.1.6 Housing and Cover	67
4.1.7 Housing Connector	70
4.1.8 Flywheel	70
4.1.9 Pull Start Pulley	72
4.1.10 Assembly of the Designed Parts	72
4.2 Manufacturing of the Engine.....	75
4.2.1 Manufactured Components.....	76
4.2.2 Spare Components	80
4.2.3 Market Components.....	82
CHAPTER 5	
EXPERIMENTAL STUDIES	87
5.1 Dynamometer	91
5.2 Measurement of Fuel Consumption	94
5.3 Exhaust Emission Device	95
5.4 Measurement of Temperature	96
CHAPTER 6	
RESULTS AND DISCUSSION	98
6.1 Evaluation of the Thermodynamic Analysis	98
6.2 Evaluation of the Experimental Results	107
CHAPTER 7	
CONCLUDING REMARKS	111
REFERENCES	113
CURRICULUM VITAE.....	119

LIST OF TABLES

	Page
Table 3.1 Technical properties of the engine	25
Table 3.2 Chemical properties of isooctane fuel.....	33
Table 3.3 Mixture components and indexes that used at the mathematical model .	36
Table 3.4a C ₈ H ₁₈ , air and burned gas components coefficients (T<1000 K).....	38
Table 3.4b C ₈ H ₁₈ , air and burned gas components coefficients (T>1000 K).	39
Table 4.1 Properties of the designed rhombic drive engine	56
Table 4.2 2379 alloy tool steel physical and mechanical properties	59
Table 4.3 4340 normalized steel physical and mechanical properties.	65
Table 4.4 Design properties of gears	66
Table 4.5 Al 6061 alloy properties	68
Table 5.1 Technical properties of Bosch BEA350 exhaust analyser device	96
Table 5.2 Accuracy of the measurement and the uncertainty in the calculated result	97

LIST OF FIGURES

	Page
Figure 2.1 Two-stroke engine invented by Sir Dugald Clerk	5
Figure 2.2 Operation of the two-stroke cycle engine	6
Figure 2.3 Two-stroke engine PV diagram	8
Figure 2.4 View of single cylinder-pump assembly	10
Figure 2.5 Comparison of the relative best BSFC for the different architectures at engine target output conditions for the different altitudes	11
Figure 2.6 Neander Motor Vehicles AG, 4 stroke 2 cylinder turbo diesel engine ..	13
Figure 2.7 Parallel combustion two-stroke engine	14
Figure 2.8 Displacement Comparison of Parallel Combustion Two-Stroke Engine	14
Figure 2.9 Day three ports engine	17
Figure 2.10 DKW engine	18
Figure 2.11 Lucas engine	19
Figure 2.12 Trojan engine (front view)	20
Figure 2.13 Sultzer engine	21
Figure 2.14 Adolf Schnürle engine	22
Figure 2.15 Technical features of orbital combustion process engine	23
Figure 2.16 Omnivore Engine	24
Figure 3.1 Selected engine with slider-crank mechanism port timing diagram	26
Figure 3.2 Designed engine with rhombic drive mechanism port timing diagram ..	26
Figure 3.3 Slider-crank mechanism kinematics	28
Figure 3.4 Rhombic drive mechanism kinematics	31
Figure 3.5 Changing of Cp and k with temperature	40
Figure 3.6 Constant pressure specific heat of combustion products changing with temperature	42
Figure 3.7 Cumulative heat release function for a spark ignition engine	47
Figure 3.8 Heat transfer in air cooled engine	45
Figure 3.9 Determination of imep from the cylinder P-V diagram	50
Figure 4.1 Isometric view of critical components assembly model in CAD software	56
Figure 4.2 Isometric view of critical components finite element assembly model in CAE software	57
Figure 4.3 Isometric view of connecting rod	58
Figure 4.4 CAE inertia relief result of connecting rod	59
Figure 4.5 Isometric view of rhombic link	60
Figure 4.6 Compression analysis of rhombic link	61
Figure 4.7 Tensile analysis of rhombic link	61
Figure 4.8 Displacement analysis of rhombic link (compression).....	62
Figure 4.9 Displacement analysis of rhombic link (tensile)	62
Figure 4.10 Isometric view of rhombic pin	63

	Page
Figure 4.11 Compression analysis of rhombic pin	64
Figure 4.12 Isometric view of gear pin	65
Figure 4.13 Compression analysis of gear pin	65
Figure 4.14 Right view of LH helical gear	67
Figure 4.15 Isometric view of RH helical gear	67
Figure 4.16 Isometric view of assembled housing and cover	68
Figure 4.17 Isometric view of housing internal surface	69
Figure 4.18 Isometric view of cover internal surface	69
Figure 4.19 Transparent isometric view of housing connector	70
Figure 4.20 Isometric view of flywheel	71
Figure 4.21 Isometric view of flywheel assembly	71
Figure 4.22 Isometric view of pull start pulley	72
Figure 4.23 Isometric view of rhombic drive engine	73
Figure 4.24 Front view of rhombic drive engine	73
Figure 4.25 Transparent front view of rhombic drive engine	74
Figure 4.26 Right view of rhombic drive engine	74
Figure 4.27 Six standard views of the rhombic drive engine at 3rd angle projection	75
Figure 4.28 Exploded view of the rhombic drive engine	76
Figure 4.29 Connecting rod	77
Figure 4.30 Rhombic links	77
Figure 4.31 LH and RH helical gears	78
Figure 4.32 Housing internal surface	78
Figure 4.33 Cover external and internal surfaces	79
Figure 4.34 Housing connector	79
Figure 4.35 Flywheel	80
Figure 4.36 Pull start pulley	80
Figure 4.37 Cylinder	81
Figure 4.38 Piston, piston pin, and piston rings	81
Figure 4.39 Intake Manifold	82
Figure 4.40 Carburettor	82
Figure 4.41 Ball bearings for gear shafts	83
Figure 4.42 Assembled housing and cover with other parts	83
Figure 4.43 Front view of the rhombic mechanism	84
Figure 4.44 Rear view of the housing	84
Figure 4.45 Top view of the rhombic mechanism	85
Figure 4.46 Left side of the rhombic mechanism	85
Figure 4.47 Isometric view of the engine	86

	Page
Figure 4.48 Rear view of the engine	86
Figure 5.1 Experimental setup	87
Figure 5.2 Pull start pulley and thrust ball bearing on the output shaft	88
Figure 5.3 Circuit components of the ignition system	89
Figure 5.4 Initiator for magnetic pickup sensor and engine speed measurement sensor	89
Figure 5.5 Settlement of the external ignition system on the setup	90
Figure 5.6 Throttle adjustment system.....	90
Figure 5.7 Schematic view of prony brake	91
Figure 5.8 Prony type dynamometer	92
Figure 5.9 Load cell and force arm	92
Figure 5.10 Layout of the load cell, force arm and engine speed sensor	93
Figure 5.11 Engine mounting to the machine vice	93
Figure 5.12 Engine tachometer	94
Figure 5.13 CAS ED-H model electronic scale	94
Figure 5.14 Exhaust duct and sensor inputs	95
Figure 5.15 Bosch exhaust gas analyser	95
Figure 5.16 External cooling fan	96
Figure 5.17 Temperature measurement device	97
Figure 6.1 Piston displacement, velocity, acceleration-crank angle diagrams	100
Figure 6.2 Volume-crank angle diagrams	100
Figure 6.3 Cylinder pressure-crank angle diagram	101
Figure 6.4 Cylinder pressure-volume diagram	102
Figure 6.5 Cylinder temperature-crank angle diagram	103
Figure 6.6 Cylinder net work-crank angle diagram	103
Figure 6.7 Cylinder heat release-crank angle diagram	104
Figure 6.8 Cylinder cumulative heat release-crank angle diagram	105
Figure 6.9 Cylinder heat transfer coefficient-crank angle diagram	105
Figure 6.10 Cylinder heat transfer quantity-crank angle diagram	106
Figure 6.11 Piston gas force-crank angle diagram	107
Figure 6.12 Effective torque-effective power w.r.t. engine speed diagram	108
Figure 6.13 Brake specific fuel consumption w.r.t. engine speed diagram	109
Figure 6.14 Thermal efficiency w.r.t. engine speed diagram	109
Figure 6.15 CO, HC, NO, CO ₂ pollutant change w.r.t. engine speed	110

ABBREVIATIONS

aBDC	: After Bottom Dead Center
aTDC	: After Top Dead Center
bTDC	: Before Top Dead Center
BDC	: Bottom Dead Center
BSFC	: Brake Specific Fuel Consumption
CA	: Crank Angle
CAE	: Computer Aided Engineering
CE	: Combustion End
CS	: Combustion Start
EC	: Exhaust Port Closing
EO	: Exhaust Port Opening
Eq	: Equation
GDI	: Gasoline Direct Injection
IC	: Inlet Port Closing
ICE	: Internal Combustion Engine
IMEP	: Indicated Mean Effective Pressure
IO	: Inlet Port Opening
PV	: Pressure-Volume
SI	: Spark Ignition
TC	: Transfer Port Closing
TO	: Transfer Port Opening
UAV	: Unmanned Aerial Vehicle

LIST OF SYMBOLS

A	: Cylinder surface area (m^2)
H	: Stroke (m)
H_p	: Piston Pin Placement
H_u	: Lower Heating Value (kJ/kg)
L_r	: Rhombic Link Length (m)
N	: Engine speed (rpm)
P_g	: Internal cylinder gas pressure (kPa)
Q	: Transferred heat quantity (W)
R_r	: Gear Pin Placement Radius
T	: Temperature (K)
T_g	: Internal cylinder gas temperature (K)
T_w	: Cylinder surface temperature (K)
\bar{U}_p	: Mean Piston Speed (m/s)
U_p	: Instantaneous Piston Speed
X_b	: Percentage of Burned Fuel Mass
V_c	: Combustion Chamber Volume (m^3)
V_d	: Displacement volume (m^3)
V_s	: Stroke Volume (m^3)
V_t	: Total Cylinder Volume (m^3)
a	: Wiebe efficiency factor
h_c	: Convection heat transfer on the air coolant side (W/m^2K)
h_g	: Convection heat transfer on the gas side (W/m^2K)
k	: Adiabatic Coefficient
ks	: thermal conductivity of the cylinder wall (W/m^2K)
m	: Wiebe Form Factor
m_a	: Mass of air into the engine for one cycle (kg)
\dot{m}_a	: Steady state flow of air into the engine (kg/s)
n	: Number of revolutions per cycle (1 for two-stroke engines, 2 for four-stroke engines)
s	: Piston Displacement (m)
Δx	: Thickness of the combustion chamber wall
$\Delta\theta$: Total Combustion Duration ($^\circ$)
ε	: Compression Ratio
η_v	: Volumetric Efficiency
θ	: Crank Angle ($^\circ$)
θ_0	: Crank Angle at Start of Combustion ($^\circ$)
ω	: Angular Speed (rad/s)
ρ	: Density (kg/m^3)
ρ_a	: Air density outside of the engine at atmospheric condition (kg/m^3)

ABSTRACT

DESIGN AND DEVELOPMENT OF A TWO-STROKE ENGINE WITH RHOMBIC DRIVE MECHANISM

GÜLTEKİN, Erol

Doctorate, Department of Mechanical and Aeronautical Engineering

Thesis Supervisor: Prof. Dr. Can ÇINAR

March 2019, 119 pages

In this study, reciprocating motion of piston in a single cylinder, two-stroke spark ignition (SI) engine was achieved with a rhombic drive mechanism, which is estimated to reduce lateral forces of the piston on the cylinder. Kinematic and thermodynamic analyses were conducted for the engines with rhombic drive and slider-crank mechanisms. Mathematical model was conducted according to real cycle approach and some of the operating parameters such as compression ratio, swept volume, heat release time, and lambda were kept identical for both engines. Pressure, volume, temperature, heat release, heat transfer coefficient, work, piston speed and acceleration changes were examined. 3D model was created and 3D assembly strength analysis was carried out with inertia relief method in CAE. Then, a prototype of the engine was manufactured to test the engine performance and emissions. According to the theoretical results, maximum cylinder pressure obtained at 222° CA with 4188 kPa for rhombic drive while 190° CA with 4003 kPa for crank mechanism engine. According to finite element model, most critical component was gear pins and endurance limit for the mechanism was satisfied. Rhombic drive prototype engine could provide 0.98 Nm shaft torque at 2400 rpm and 0.3 kW at 3000 rpm. Maximum thermal efficiency was obtained as 23.55%. In total, 11% weight reduction was achieved and this lightness is seen as an advantage for aerial vehicles.

Key Words: Two-stroke Engine, Rhombic drive Mechanism, Performance, Thermodynamic Analysis.

ÖZET

İKİ ZAMANLI ROMBİK HAREKET MEKANİZMALI BİR MOTORUN TASARIMI VE GELİŞTİRİLMESİ

GÜLTEKİN, Erol

Doktora, Makine ve Uçak Mühendisliği Bilim Dalı

Tez Danışmanı: Prof. Dr. Can ÇINAR

Mart 2019, 119 sayfa

Bu çalışmada, pistonun silindire uyguladığı yanal kuvvetleri azaltmak amacıyla, tek silindirli iki zamanlı buji ile ateşlemeli bir motorda pistonun ileri geri hareketi, rombik mekanizması ile gerçekleştirilmiştir. Tasarlanan rombik mekanizmalı motor ile krank hareket mekanizmalı bir motorun kinematik ve termodinamik analizleri yapılmıştır. Gerçek çevrim yaklaşımı ile matematik modeli yapılmış ve sıkıştırma oranı, süpürme hacmi, ısı verilme süresi ve lamda eşit alınmıştır. Basınç, hacim, sıcaklık, toplam açığa çıkan ısı, ısı iletkenlik katsayısı, iş, piston hızı ve ivmelenme değişimleri incelenmiştir. Motorun 3 boyutlu modeli hazırlanarak CAE yazılımında 3 boyutlu montajın dayanım analizi, atalet kuvvetlerini dikkate alan metod ile yapılmıştır. Sonrasında motor performansını ve emisyonları incelemek üzere rombik mekanizmalı motorun prototipi üretilmiştir. Teorik sonuçlar, maksimum silindir basıncının rhombik mekanizmalı motorda 222° krank açısında 4188 kPa, krank mekanizmalı motorda ise 190° de 4003 kPa olduğunu göstermiştir. Sonlu elemanlar modeline göre en kritik parçanın dişli pimi olduğu görülmüş, mekanizma için sonsuz ömür limiti sağlanmıştır. Prototip rombik hareket mekanizmalı motor, 2400 dev/dak'da 0.98 Nm çıkış torku, 3000 dev/dak'da 0.3 kW çıkış gücü sağlamıştır. Maksimum ısıl verim %23.55 olarak elde edilmiştir. Toplamda %11 ağırlık düşürülmüş olup, bu hafiflik hava araçlarında bir avantaj olarak görülmektedir.

Anahtar Kelimeler: İki Zamanlı Motor, Rombik Hareket Mekanizması, Performans, Termodinamik Analiz

CHAPTER 1

INTRODUCTION

1.1 Motivation

Internal combustion engines (ICE) have been used since the latter half of the 1800s with a wide variety of land, navy and aviation vehicles. ICE's applied to the vehicles with different configurations to keep target from the point of power-torque, fuel type and consumption, environmental concerns, durability, simplicity and operating conditions. These targets have been performed by reciprocating motion of piston inside the cylinder via converting chemical energy of fossil fuels and as an output providing us a rotary motion from the slider-crank mechanism. Alternatives of this mechanism have been studied at least to reduce or totally eliminate drawbacks of the reciprocating motion such as lateral friction, vibration, high speed restrictions, et cetera.

With the increasing demand on unmanned aerial vehicles (UAV), alternative and optimized engines are searched to match and keep light, high power to weight ratio. In the USA, UAV market is expected to enlarge on nearly 10000 jobs and \$8.2 billion per year between the years of 2015 and 2025, performing a wide variety configuration for surveillance, monitoring and reconnaissance for military and civilian applications [1]. While electric motor and battery technologies are being developed, still internal combustion engines with fossil fuels are the main responsive power source for the requirements of long ranges and heavy duties. In the last two decades, researchers are focussed on changing the compression ratio, variable valve timing mechanisms, alternative engine cycles such as Atkinson and Miller cycles, different charging methods and combustion chamber designs to increase the thermal efficiency of internal combustion engines.

1.2 Objectives

The focus of this work is to develop a novel driving mechanism for a single cylinder, two-stroke, SI engine. For this purpose, a two-stroke engine with rhombic

drive mechanism was designed, manufactured and tested. Performance and emission characteristics of the engine were compared with a two-stroke engine with slider-crank mechanism. Experimental studies were performed at Department of Automotive Engineering in Gazi University. This engine is expected to stand for alternative national range extender engine for light/unmanned aviation vehicles or small size agricultural applications. This structure and configuration are used due to the following benefits and there is a wide variety and opportunities to develop:

- ✓ Two-stroke engines have simple design and less parts. It maintains light weight construction.
- ✓ Greater mechanical simplicity and light weight have made the two-stroke engines popular in light aerial vehicles.
- ✓ Rhombic drive mechanism was preferred because of the lower side thrust on piston and lower vibration.
- ✓ Rhombic drive mechanism allows easy compression ratio change.
- ✓ Usage of spark ignition systems in order to allow engine structure to maintain its light weight construction.
- ✓ Usage of gasoline direct injection (GDI) system allows a separate lubrication system for two-stroke engines.
- ✓ Supercharging or turbocharging is possible with GDI system. It is important for aviation vehicles.
- ✓ Usage of GDI system for better fuel economy and lower exhaust emissions.

1.3 Outline of the Thesis

Scope of this study consists of seven chapters which are introduction, literature of two-stroke engines, kinematic and thermodynamic analysis of the engine, engine design and manufacturing, experimental studies, result and discussion and concluding remarks, respectively.

At the first chapter, today's expectations from the internal combustion engines and the objective of the study are given. At the second chapter, historical development and operation principles of two-stroke engines, comparisons of two and four-stroke engines, literature survey and different types of two-stroke engines from the point of structure and mechanism at literature are given. At the third chapter, foremost kinematics of slider-crank and rhombic drive mechanisms are given, then, thermodynamic analysis is introduced. At the fourth chapter, engine design concept

with structural analysis is given, then, manufacturing of the engine is introduced. At the fifth chapter, technical properties of used testing apparatus and devices are introduced and experimental procedure is given. At the sixth chapter, thermodynamic analysis results of both engines are compared and then experimental result of the rhombic drive engine is given. At last seventh chapter, concluding remarks are given.



CHAPTER 2

LITERATURE OF TWO-STROKE ENGINES

2.1 Historical Development

The first fairly practical internal combustion engine was invented by Etienne Lenoir and appeared on the scene about 1860. During the following years, several hundreds of these engines were designed and output power was raised to 4.5 kW while mechanical efficiency was up to 5%. In 1867, the Otto-Langen engine was put on public display, with efficiency improvement about 11%, and many of Langen engines were produced during the next decade. This was a type of normally aspirated engine with the expansion stroke propelled by atmospheric pressure acting against a vacuum. At this time interval, many engines were invented by Nicolaus A. Otto and Eugen Langen.

During this period, engines operating on the same basic four-stroke cycle as the modern automobile engine began to evolve as the best design.

In the 1880s, the internal combustion engines first appeared in automobiles [2]. Four-stroke cycle power output limitations with increasing expectations from the vehicles, urged the designers to seek alternative cycle which should eliminate the idle exhaust and charging strokes which occupy one complete revolution of the crankshaft [3]. That decade, the two-stroke cycle engine was invented by Sir Dugald Clerk in England which is shown in Figure 2.1.

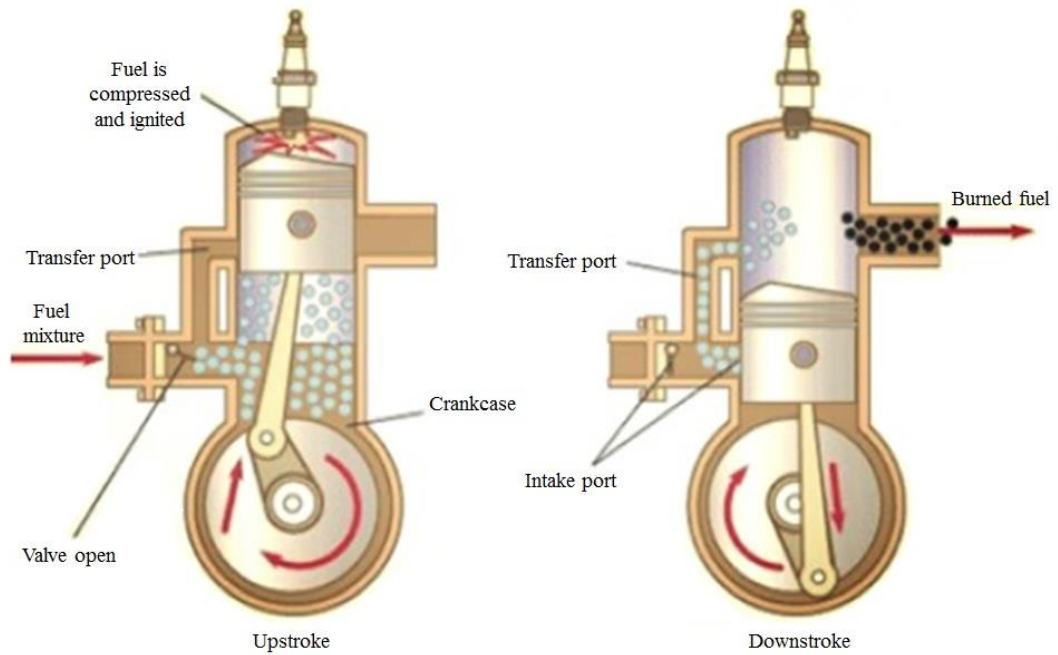


Figure 2.1: Two-stroke engine invented by Sir Dugald Clerk [4]

In 1879, first stationary two-stroke engine was developed by Karl Benz [5]. The form of the engine using crankcase compression for the intake process, including the control of the timing and area of the exhaust, transfer and intake ports by the piston, was patented by Joseph Day in England in 1891. His engine was the original “three port engine” and is the forerunner of the simple two-stroke engine which has been in common usage since that time. Two-stroke engines have been used by many different applications such as motorcycles, agricultural off-road vehicles, locomotives, medium size vessels and ships, stationaries, lawn mowers, snow blowers, light aircrafts, automobiles, etc. Outboard motors have been dominated by two-stroke engines since 1909 [6] and many attempt could be seen after that time. In 1925, German engineer Adolf Schnürle achieved a gas flow in a loop and took the patent of a two-stroke engine [7]. In 1932, Caunter studied on a 60 HP two-stroke, light aero engine [8]. In the 1930s, supercharged DKW engines used in motorcycle races but after World War II, supercharging was not allowed to use in the races so two-stroke engines faded until MZ machines adopted tuned exhaust expansion chambers and disc valve induction systems in 1959. In the 1960s, two-stroke engines were used on road vehicles by today automotive manufacturers but after 1990s, two-stroke engines have not been preferred due to environmental constraints and fuel

consumption rates [6]. Trabant model with a 0.6 L two-cylinder air cooled engine and Wartburg model with 1 L three-cylinder water cooled engines were the last used two-stroke engines in automobiles [2].

Manufacturers and researchers have been focusing on gasoline direct injection (GDI) systems, alternative fuels, alternative charging methodologies to overcome emissions and to develop fuel consumption since last two decades.

In two-stroke engines, required structural strength could be reduced due to lower engine loads and that makes these engines a remarkable alternative as a power source on light weight vehicles and preferred on range extender for hybrid electric vehicles nowadays [9]. Also two-stroke diesel engines are still pioneer the large power output applications such as ships and stationary electric generation plants for mining, aircraft ground support equipment, high-end marine pleasure craft, armies and navies requirements [10].

2.2 Operating Principles

A two-stroke engine has two piston motion from top dead center (TDC) to bottom dead center (BDC) over one revolution for each cycle [2]. These strokes are called compression stroke and expansion or power stroke, shown in Figure 2.2.

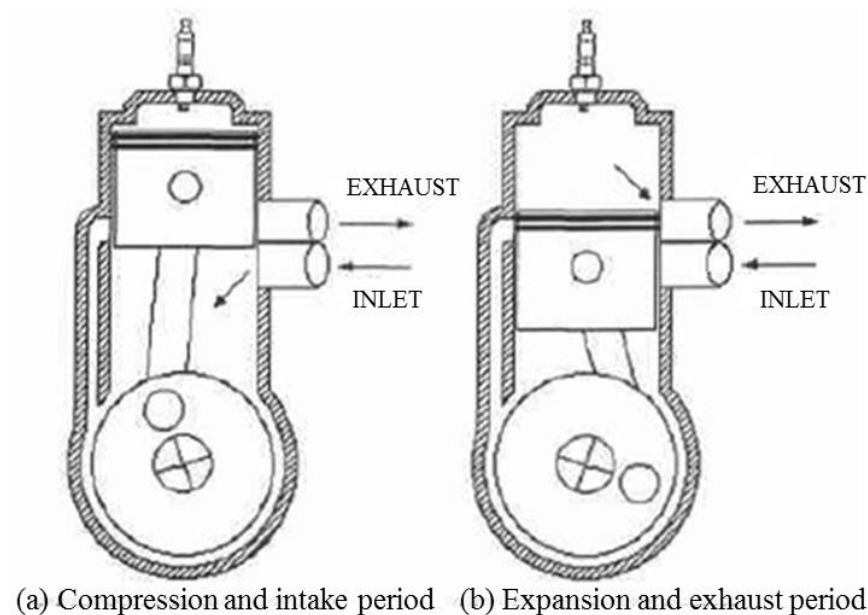


Figure 2.2: Operation of the two-stroke cycle engine [6].

Piston moves towards TDC from BDC and starts to compress air-fuel mixture and residual exhaust gases. Exhaust port is located a bit above from the transfer ports so that compression is not applied efficiently without passing exhaust port closing. During that time some of the fresh charging is scavenged to the exhaust port with exhaust gases. After closing of exhaust port, mixture is compressed efficiently at the polytropic condition and mixture pressure and temperature is increased. Simultaneously, while piston moves upward to the TDC inlet port is opened and fresh charge is taken by the crankcase. That is shown in Figure 2.2a.

Piston arrives to nearly TDC and with respect to ignition advance spark plug ignites and mixture of compressed gases and fuel vapour starts to burn. Almost at constant volume, pressure and temperature are at peak. Obtained pressure, forces the piston downward to the BDC. Connected crank mechanism starts to rotate which is called useful work at the engine. Combustion chamber is expanding during that time and pressure and temperature is dropping. When the piston approaching to the BDC, firstly exhaust port is starting to open and blowdown occurs. When nearly completion of blowdown, transfer port ones more opens and fresh air-fuel mixture enters to the cylinder under pressure. This low pressure also pushes remaining burned gases to the exhaust manifold. During this period transfer port and exhaust port are open and this condition is called scavenging [6]. It is shown in Figure 2.2b.

Two-stroke gasoline engines are formed by theoretical Otto cycle which consists of isentropic compression, constant volume heat addition, isentropic expansion, exhaust blowdown, intake and exhaust scavenging. Thermodynamics of compression and expansion strokes produce work which is represented with sum of the enclosed area cyclic integral of the pressure-volume diagram in Figure 2.3 [6]. In the figure both theoretical and experimental pressure change depending on volume could be seen.

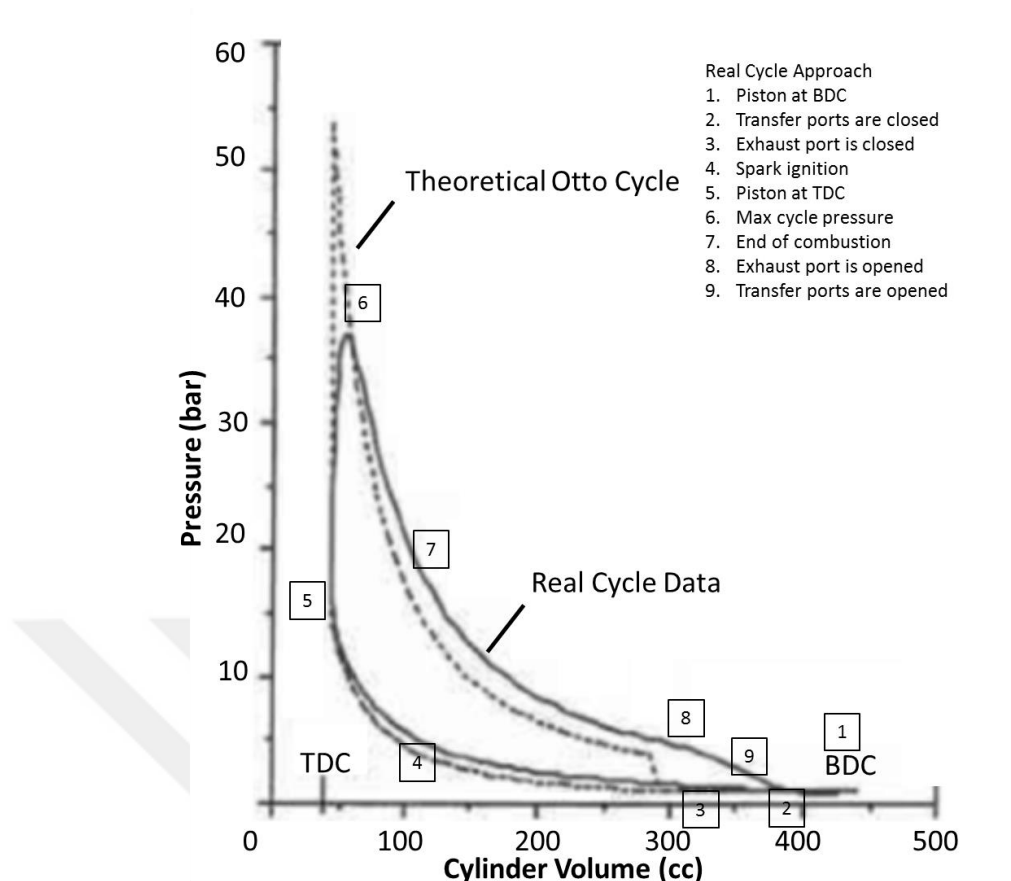


Figure 2.3: Two-stroke engine PV diagram [6].

2.3 Comparison of Two-Stroke and Four- Stroke Engines

General advantage and disadvantages of the two-stroke engines over the four stroke ones could be denoted as:

1. With identical size of cylinder diameter and stroke, cylinder number and engine speed, two-stroke engines produce two times more power theoretically than the four-stroke engines.
2. Two-stroke engines have simpler structure due to having any valve mechanism, so production cost is less and lighter weight is the reason to be applicable to many vehicles easily. Fresh air and fuel charging to the cylinder and discharging of exhaust gases from the cylinder is performed by means of ports on the cylinder wall according to design configuration. Ports are governed by piston top and bottom ends.

3. Two-stroke engines have simpler maintenance operations.
4. Two-stroke engines have a wide variety engine speed to operate, such as for large size low speed diesel engines and small and medium size high speed spark ignition engines.
5. Mechanical efficiency is higher at two-stroke engines.
6. A lighter flywheel meets engine requirements and prevents speed variations caused by the torque fluctuations.
7. On the other hand, two-stroke engines have relatively lower thermodynamic efficiency, higher HC and CO emissions, lower life time, and higher fuel consumption rates due to the scavenging period. Lubrication oil must be mixed with fuel for its lubrication. Also remarkable attention should be employed on the crankcase design which creates negative pressure to draw air and fuel mixture from inlet port and creates positive pressure to transfer the mixture to the cylinder.

2.4 Literature Survey

Cantore et al. (2014) developed a new concept for aircraft diesel engines which focus on to reach a power target, at sea level, of 150 kW at 4000 rpm and minimum power of 100 kW at the altitude 20000 feet. They used 1500 cc three-cylinder, turbocharged and intercooled engine. The engine was configured with a patented rotary valve mechanism which controls inlet flow through a set of inlet ports. This configuration enables supercharging and achieves extremely high power densities compared to typical solutions. The scavenging is operated by using an external pump inside the crankcase, which uses additional cylinder for housing, and piston is connected to the same crankshaft. Construction of one of the cylinders is shown in Figure 2.4. The piston pump allows the crankcase to be used as a conventional oil sump and supports to improve crankshaft balance. Mixture flows with piston controlled ports by two sets of reed valves so neither poppet valve nor camshafts need to be installed. Study shows that 2 stroke diesel engine overall dimensions are reduced nearly half sizes when compared with 4 stroke automotive diesel engine. Specific fuel consumption was reported as 235 g/kWh which is close to 230 g/kWh at the 4 stroke motorcycle engines. The peak pressure inside the cylinders greatly

reduced to 110 bars while 4 stroke engine at the same brake power facing with 150-180 bar cylinder pressure. Heat rejection is 15% less at the 2 stroke three-cylinder engine when compared with the calculated reference V6 diesel automotive engine [11].

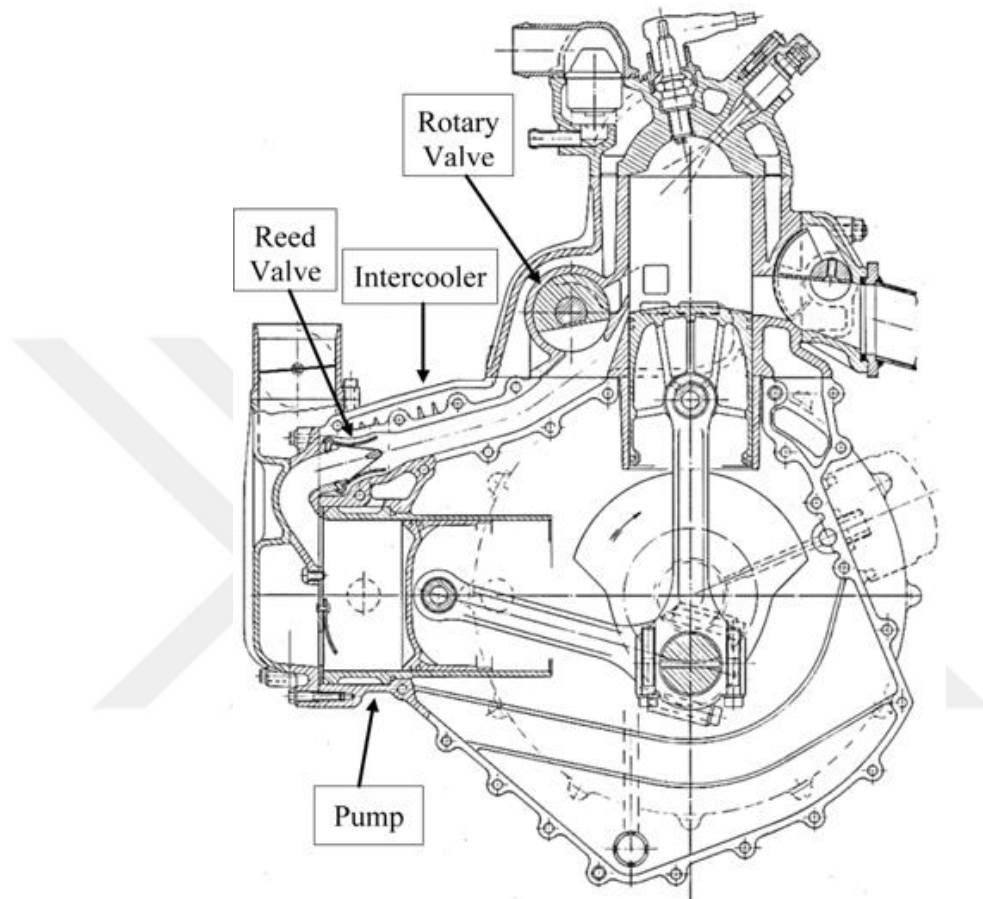


Figure 2.4: View of single cylinder-pump assembly [11].

Herold et al. (2011) studied on an opposed piston two-stroke engine (OP2S) to present thermodynamic benefits over a standard four stroke engine (4S). They performed the studies for three different engine configurations which are a baseline six-cylinder four-stroke engine, a hypothetical three cylinder opposed-piston four-stroke engine and a three cylinder opposed-piston two-stroke engine. Constant bore and stroke parameters were used for all three types. Close cycle performance was compared with a custom zero dimensional analysis tool which detects the source of the thermal efficiency differences with prediction of cylinder pressure during the cycle. They found that opposed piston with two-stroke combination increased the indicated thermal efficiency due to reducing heat transfer with better area/volume

ratio, increasing specific heat ratio with leaner operating conditions and decreasing combustion duration with lower energy release density. Peak pressure at OP2S engine is 126 bars while 175 bars at 4S engine. Pumping work which is required to produce operating conditions, consumes 3.3% of fuel at OP2S engine while 3.9% of fuel at 4S engine. Weighted average indicated brake specific fuel consumption benefit is 10.4% at OP2S engine [12].

Carlucci et al. (2015) studied on supercharging system behaviour of high altitude operation of a two-stroke diesel aircraft engine. To compare supercharging systems, they selected different architectures such as single turbocharger (TC), double turbocharger (TTC), single turbocharger combined with a mechanical compressor (CTC), single turbocharger with an electrically assisted turbocharger (TTC Hybrid) with intercooler or aftercooler which were designed for general aviation two-stroke diesel engine and unmanned aerial vehicles to use at very high altitude operation and long fuel distance. The comparison from the point of power and specific fuel consumption at four different altitudes which are sea level, 3050 m, 5180 m and 10670 m revealed that, TTC aftercooler architecture has advantages from the point of lower weight, bulk, intake and exhaust system simplicities to improve energy utilization at heavy conditions. Brake specific fuel consumption hybrid supercharging system which comprised a classic high pressure TC and a low pressure compressor and a turbine electrically connection provides nearly low BSFC as much as single TC and keep the power targets at all altitudes [13]. That is shown in Figure 2.5.

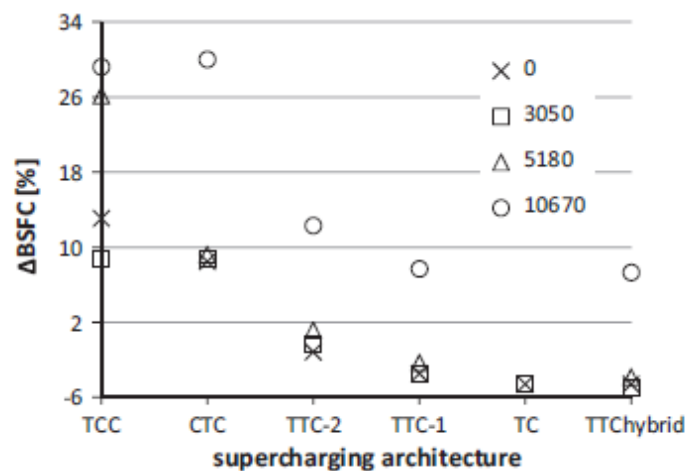


Figure 2.5: Comparison of the relative best BSFC for the different architectures at engine target output conditions for the different altitudes [13]

Carlucci et al. (2016) studied on performance optimization of a two-stroke supercharged diesel engine for aircraft propulsion from the point of brake power at sea level and brake specific fuel consumption at cruise condition. They used a validated AVL Boost 0D/1D numerical engine model which is compared with Ansys Fluent 3D simulations, has capability to reflect the effect of exhaust valves opening and closing angles and maximum valve lift, scavenging ports opening angle, distance between bottom edge of the scavenging ports and bottom dead center, area of the single scavenging port and number of ports, engine volumetric compression ratio, low and high pressure compressor pressure ratios, air/fuel ratio on a reasonable operation ranges. These parameters effects are examined with a pareto front statistical estimation methods such as effect size and significance. The study revealed that Air/Fuel ratio, low and high compressor pressure ratios are most crucial parameters to affect the brake power and brake specific fuel consumption [14].

A German company, Neander Motor Vehicles AG developed a 4-stroke turbo diesel engine which consists of an engaged gear mechanism with double parallel crankshaft and connecting rod connection for each cylinder. This mechanism compensates all rotating inertial forces and 1st order oscillating forces so reducing vibration, eliminates reactive effects arise from torque impulses on the exterior of the engine, eliminates torque which occurs due to the inertial effect and its phase differences from compensation measures, reduces lateral friction losses between piston and cylinder with the guidance of connecting rod. Obtaining better thermodynamic efficiency, this mechanism uses large single swept volumes. Power range is from 12 HP to 110 HP, cylinder volume range is from 400 cc to 1400 cc and torque range is from 25 Nm to 120 Nm obtained at 2000-3000 rpm [15]. Engine construction is seen in Figure 2.6.

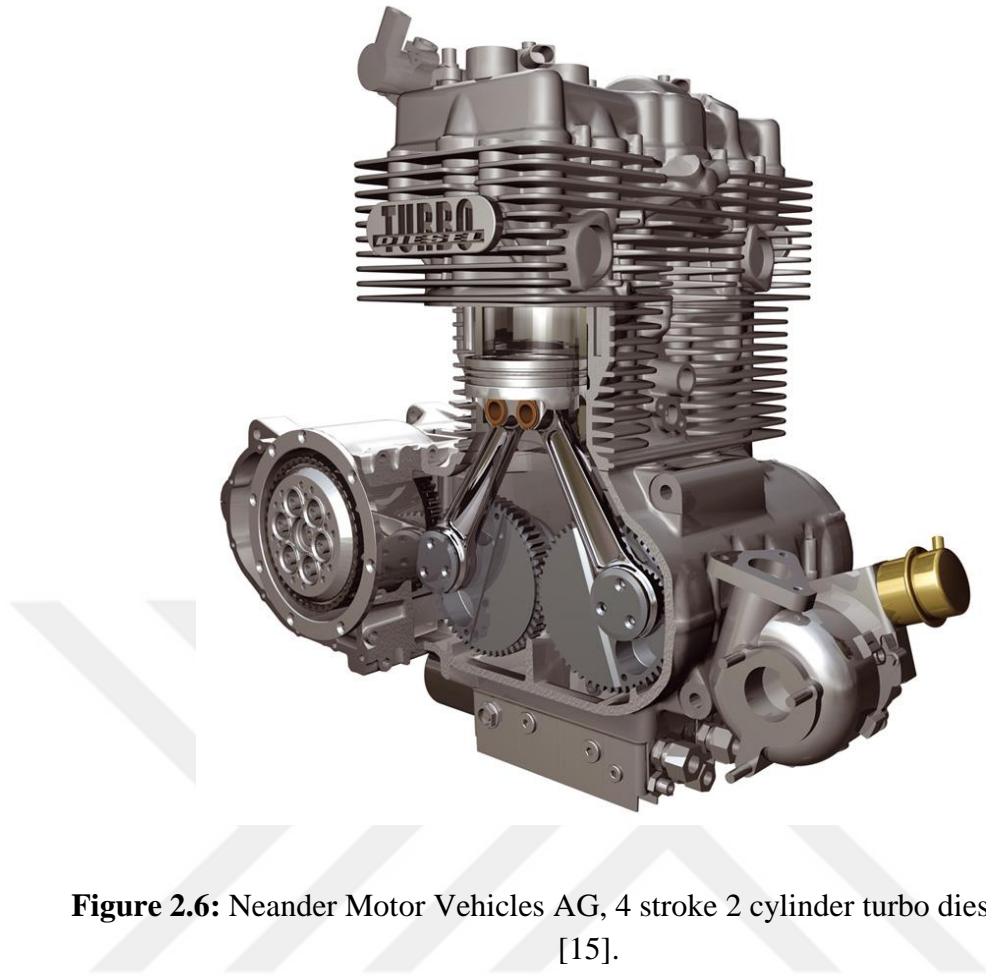


Figure 2.6: Neander Motor Vehicles AG, 4 stroke 2 cylinder turbo diesel engine [15].

Rucker studied on the analysis of a parallel combustion two-stroke engine. This engine consists of a hypocycloid gear mechanism and parallel two combustion chambers. The hypocycloid linear drive mechanism ensures mechanical balance, sinusoidal motion, increased mechanical efficiency and linear rod motion. As a result, piston lateral forces are eliminated and structure creates two chambers in the working cylinder. These two chambers are mounted to combustion chambers externally to the working cylinder. The engine is shown in Figure 2.7 [16].

The resulting engine combines the many advantages of four-stroke engine and rotary engines and external combustion engines. The piston travels slower than the conventional two-stroke engine which provides a higher pressure at the expansion process. Piston displacements are shown in Figure 2.8. The linear gear drive mechanism provides greater overall mechanical advantages than the crankshaft mechanism which have 1.5 at 90 degrees shaft rotation and 1.42 at 70 degrees shaft rotation respectively.

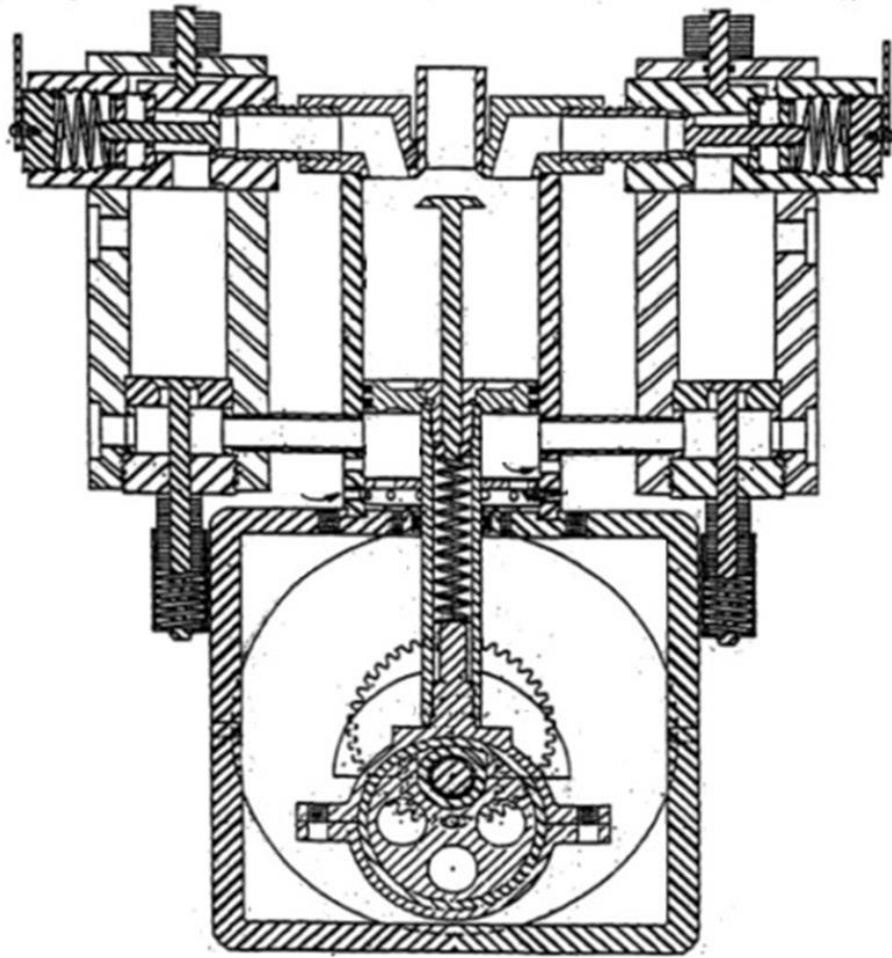


Figure 2.7: Parallel combustion two-stroke engine [16]

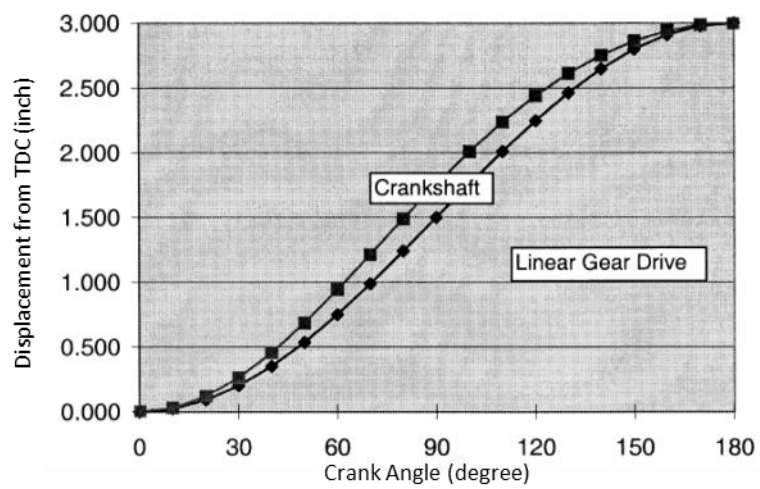


Figure 2.8: Displacement comparison of parallel combustion two-stroke engine [16]

Ausserer et al. (2017) measured the loss pathways in two-stroke, spark ignition, naturally aspirated engines having 28 cc and 55 cc displacements. The objective of the work was the experimental quantification of energy balances for two engines that are representative of remotely piloted aircraft (RPA) engines and the identification of the dominant loss pathways. The pathways are brake power, cooling load, sensible exhaust enthalpy, incomplete combustion and short circuiting. According to complete energy balance test results losses caused by mostly short circuiting with 44% at 28 cc engine and 36% at 55 cc engine. Then with respect to incomplete combustion comes with 16% at 28 cc engine and 23% at 55 cc engine. at exhaust enthalpy with a 17% at 28 cc engine and 16% at 55 cc engine. Thermal efficiencies are comparable with conventional size engine which are considered bigger than 100 cc. For two-stroke ICE, increasing efficiencies mostly related with improving short circuiting and incomplete combustion [1].

Boretti et al. (2015) analysed a two-stroke spark ignition engine featuring crankcase scavenging, precise oiling, direct injection and jet ignition by using CAD, CFD and CAE tools for unmanned aerial vehicles. With this configuration, running the engine at stoichiometric homogeneous, lean stratified, diesel diffusion like, and mixed, availability on changing the timings of jet ignition and main chamber injections is possible but increases the complexity of the engine dramatically [17].

Nuccio et al. (2003) studied on performance improvement of two-stroke SI engines for motor-glidors and ultra-light aircrafts by means of a GDI fuel system. Experimental tests have been carried out on a 345 cc positive displacement single cylinder, crankcase-scavenged two-stroke engine, with both indirect (GII) and direct gasoline injection (GDI), in order to compare the power, brake specific fuel consumption (BSFC) and emission results obtained with these two different fuel-feeding systems. Also carburettor feeding is compared from the point of BSFC. Experiments show that only HC reduction with 80% on average obtained from the GDI when compared with GII. Other pollutants are nearly same. On the other hand, BSFC is 17% on average lower at GDI. When compared with carburettor feeding at maximum tested engine speed is about 40% while at minimum tested engine speed is 60% reduction [18].

Shankar et al. (2015) studied on performance analysis of gasoline direct injection system in two-stroke spark-ignition engines. They modified a two-stroke conventional engine for GDI to compare conventional engine of a comparable size.

The GDI engine provides approximately 10% greater outputs at all speed. At heavy loads and higher engine speeds homogeneous charging seems better to catch diesel like fuel economy on gasoline engines. CO₂ production is reduced by nearly 20%. Smooth transition between operating modes is achieved. GDI engine provides improved torque and achieves future emission restrictions. GDI is simple to implement and can be retrofitted in two-stroke engines. Fuel consumption reduction is obtained by 15-20%. Higher torque 5-10% is produced. Also good and spontaneous throttle response behaviour is obtained [19].

Savioli et al. (2017) reviewed development of a 2-stroke GDI prototype engine which could be used as a range extender with a target power of 30 kW. An electric supercharged is used to deliver air to the cylinder to eliminate throttle valve. An experimentally calibrated CFD-1D model simulation carried out to predict full load engine performance. They obtained a specific power of 60 kW/L and brake specific fuel consumption of 222 g/kWh while indicated mean effective power is just 9 bars [20].

Antonelli et al. (2004) developed a new GDI 2-stroke engine prototype to meet future emission limits from a modified 4 stroke 4-cylinder engine. The work was intended to substantially reduce pollutant emissions and fuel consumption of 2-stroke engines for motorcycle applications. At the prototype engine GDI, forced-fed lubrication, roots compressor as an external scavenging pump and unidirectional scavenging process architecture is used. Valve timing system is also modified according to unidirectional process. At low speeds around 1000 rpm the preliminary experiment shows 80% HC emission reduction when compared with usual carburettor feeding systems [21].

Dube et al. (2016) searched influence of injection parameters on the performance and emissions of a direct injection two-stroke spark ignition engine. They compared 2S-GDI, 2S-manifold injection and four stroke port fuel injection engine (4S-MI) at various throttle positions. Experiments show that end of injection timing has an important effect on reduction of HC and CO emissions but it does not affect so much power output and brake thermal efficiency. Spark plug position at near of exhaust port provides higher heat release rates and lower HC emissions at 2S GDI engines. Also trapping efficiency with 11.3% improvement is obtained from the 2S-GDI when compared with 2S-MI engine at 70% throttle position. 2S-GDI engines have 40.6% more fuel efficient, 90% lower HC and 80% lower CO rates over 2S-MI

engine. NO emissions nearly same for both engines. Higher brake thermal efficiency, lower CO and HC emissions are obtained from 4S-MI engine but 2S-GDI has comparable results [22].

2.5 Two-Stroke Engine Configurations

2.5.1 Three Port Two-Stroke Engine

In Figure 2.9, Joseph Day three ports engine architecture is given which represents still the basic two-stroke engine principles. In the figure, E stands for exhaust port, which will be governed by the piston after arriving about 80% of its stroke. T represents transfer port, which the charge is pumped from the crankcase pressure. Transfer port is opened slightly later than the exhaust port to prevent the hot exhaust gases flow through the crankcase and ignition of the new charge. The transfer port is closed by the piston motion towards the upward just before the exhaust port closing. As a result, the final pressure in the cylinder, and therefore the total quantity of air fuel mixture is not only affected by the pump delivery pressure but also by extent to which the throttling and impulse of the exhaust pipe, silencer, etc., increase the indicated pressure of cylinder above the atmosphere pressure. A specific attention should be given to design of the piston head shape which deflects the entering gases to the top of the cylinder during the scavenging. That is called as cross flow scavenge [3].

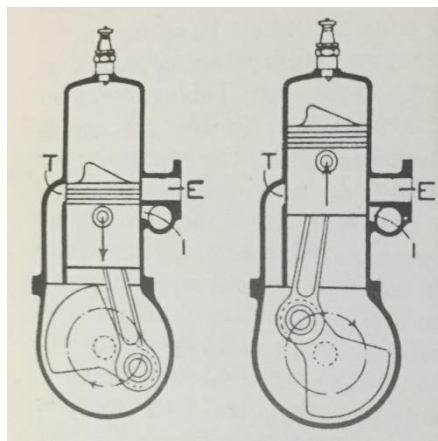


Figure 2.9: Day three ports engine [3]

2.5.2 Reverse Flow Scavenge (DKW) Engine

A different application of three port engine is German DKW small car engine which operates as reverse flow scavenge. Crankcase pressurizing is used but charging is achieved by means of two transfer ports which take place each side of the exhaust port, delivers the charging flow tangentially to upward.

The piston deflector on the head is removed. So disposing of pressure and inertia tilt due to lack of symmetry, which cause rattle in the two-stroke, is also eliminated and tangential scavenge flow becomes as indicated at the Figure 2.10 below [3].

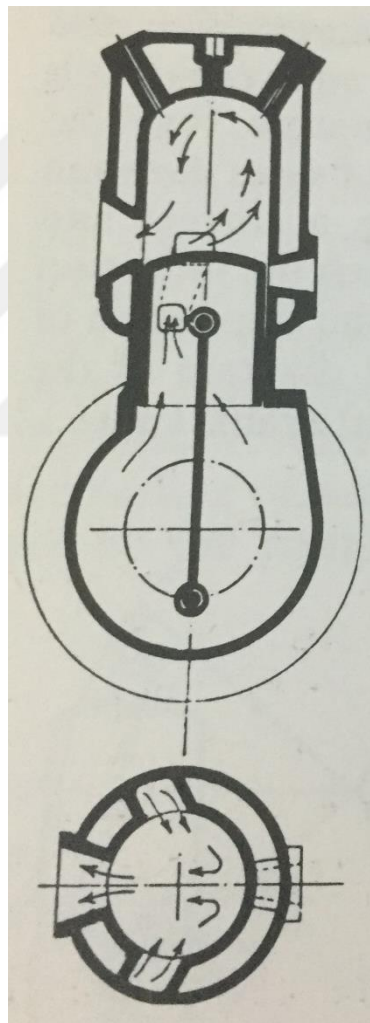


Figure 2.10: DKW engine [3]

Transfer port passages could be shorter through lateral surface of the piston at this design but due to the direction changes in the flow, which could cause transfer resistances. At the cylinder design that should be considerably taken account [3].

2.5.3 Lucas Engine

At this design construction, two cylinders are used with a common combustion chamber and spark plug to eliminate the fresh charge flow through the exhaust port for increasing the two-stroke efficiency. Each cycle per revolution is exposed to just one impulse due to the combustion. That makes flexible arrangement of connecting rod and crank as gear connections [3]. Layout of the Lucas engine is shown in Figure 2.11 below which is not produced nowadays.

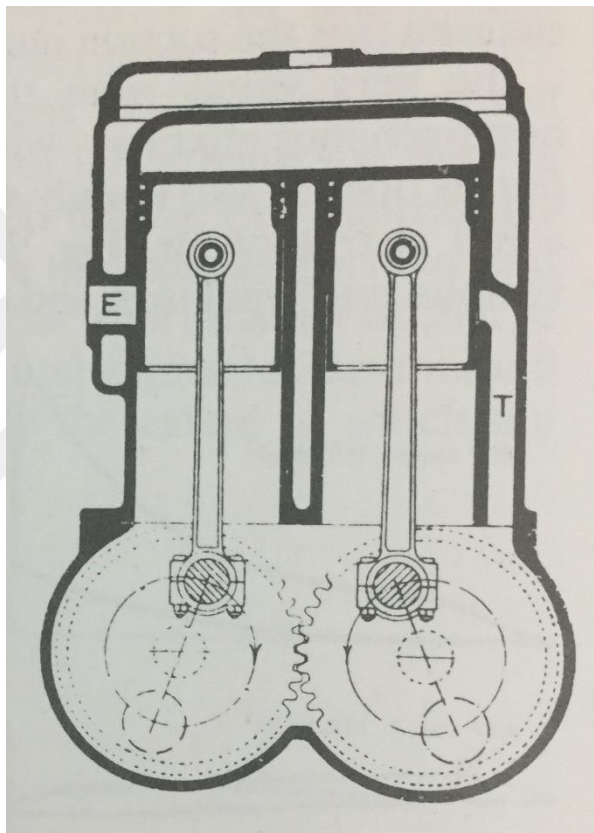


Figure 2.11: Lucas engine [3]

The two pistons are connected to two independent connecting rods operating on parallel two cranks, which are located to operate in a harmony by two gears in the concentricity of the circular crank webs. Only one of the cranks is used to locate the flywheel on and clutch connection, so that half of the power is transmitted through the gear teeth. Due to the gear engagement, the cranks are rotated reversely, and connection is made of this fact to accomplish complete primary balance. Each crank assembly is carrying counter balance weights [3].

2.5.4 Trojan Engine

Trojan engine does not use crankcase to scavenge the mixture into the cylinder instead, pump and piston are used for transfer and exhaust port respectively. All the pistons are controlled with a well arranged cylinder. So pressure sealing of the crankcase is not required. Lubricant is not mixed with the fuel due to having separate system [3]. Front view of the engine is given in Figure 12.

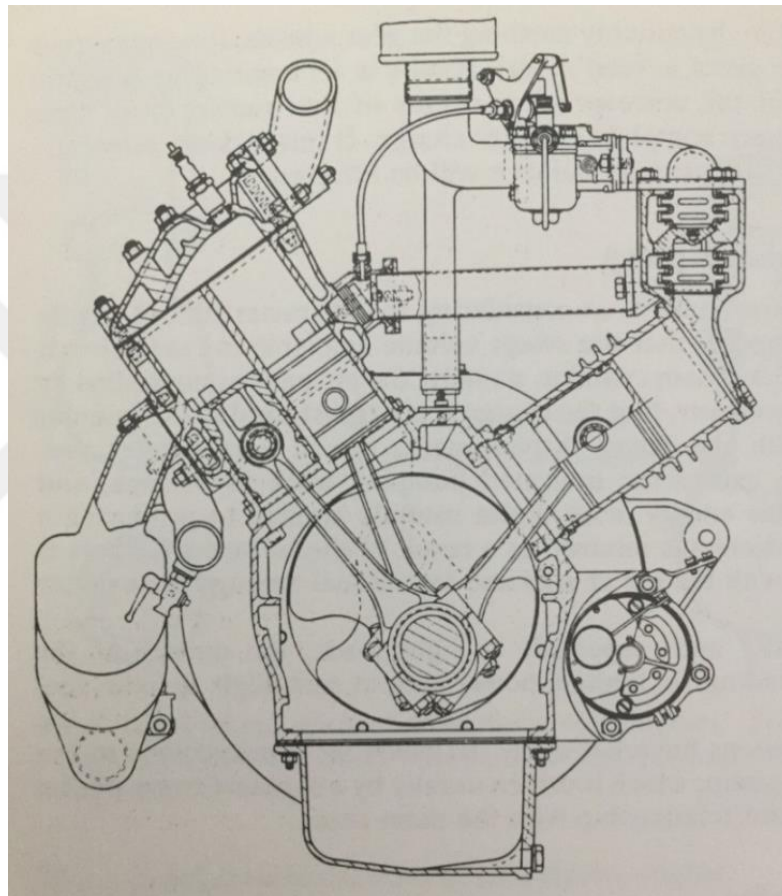


Figure 2.12: Trojan engine (front view) [3]

2.5.5 Opposed Piston Engine

At uniflow opposed piston engine compression is performed by two pistons moving to each other while moving away for expansion stroke. Inlet port continuous air flow is taken into the cylinder by a piston while one more piston is used for exhaust port.

The structure consists of two crankshafts phased by gear mate or such a mechanism, or a single crankshaft to which the power of one piston is transmitted directly, and that of the other by means of a pair side connecting rods, or alternatively by means of a symmetrical reversing rocker system for each piston. At Figure 2.13 Sultzer engine structure is shown which is produced in about 1936. Sultzer engine used an opposed piston rocker configuration which is integrated with a phased reciprocating scavenge pump [3].

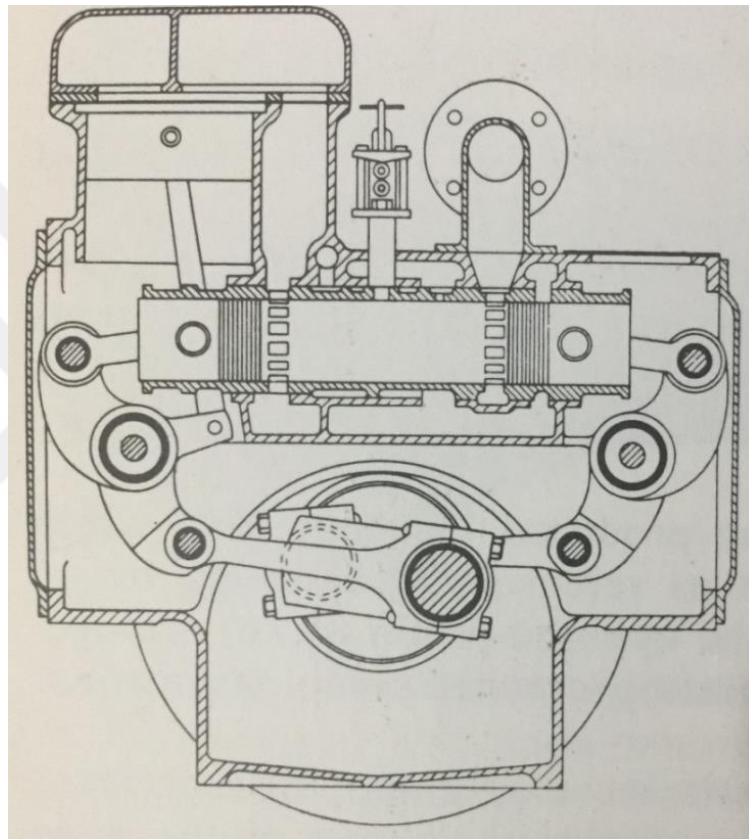


Figure 2.13: Sultzer engine [3]

2.5.6 Schnürle Engine

In 1925, a German engineer Adolf Schnürle designed and manufactured 2-stroke engine which use a piston to scavenge air into the cylinder and took the patent from the USA Patent Office. Additional piston was connected to the same crankshaft of the power cylinder and tried to increase scavenge pressure of the fresh charging. That is why the piston is called scavenge pump inside the crankcase. It was designed

to use at high speed two-stroke engines. A rotary valve controlled the pressurized air inlet [23, 24]. Construction of the engine is shown in Figure 2.14.

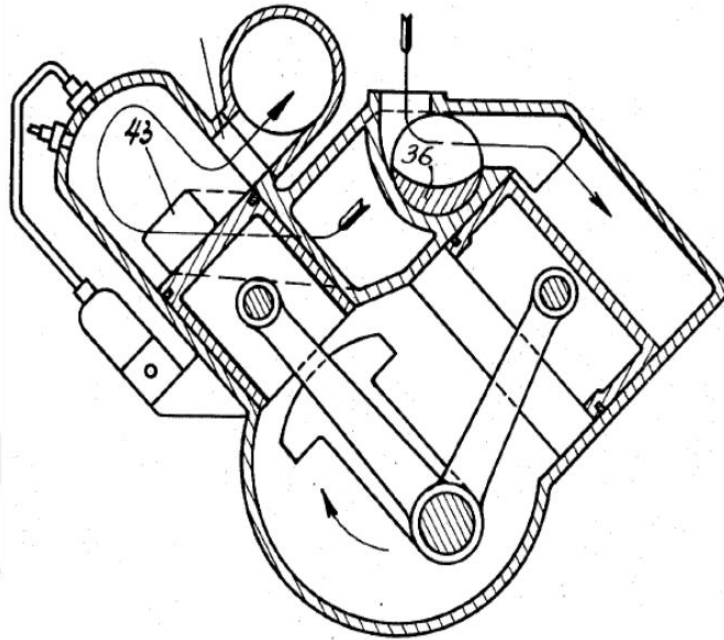


Figure 2.14: Adolf Schnürle engine [24].

2.5.7 Orbital Engine

Orbital Engine Corp detected that a sophisticated fuel injection and combustion system could be used on two-stroke engines which are developed for orbital engine. As a result, much more power is obtained and fuel used efficiently and it is clean from the point of pollutants. The Orbital Combustion Process engine has been adapted to a two-stroke engine that ensures 50% lighter, 30% more fuel efficient, 20% cheaper production, 70% smaller size, and exposes 30% less pollutant than conventional engines [25]. Configuration of the engine is shown in Figure 2.15.

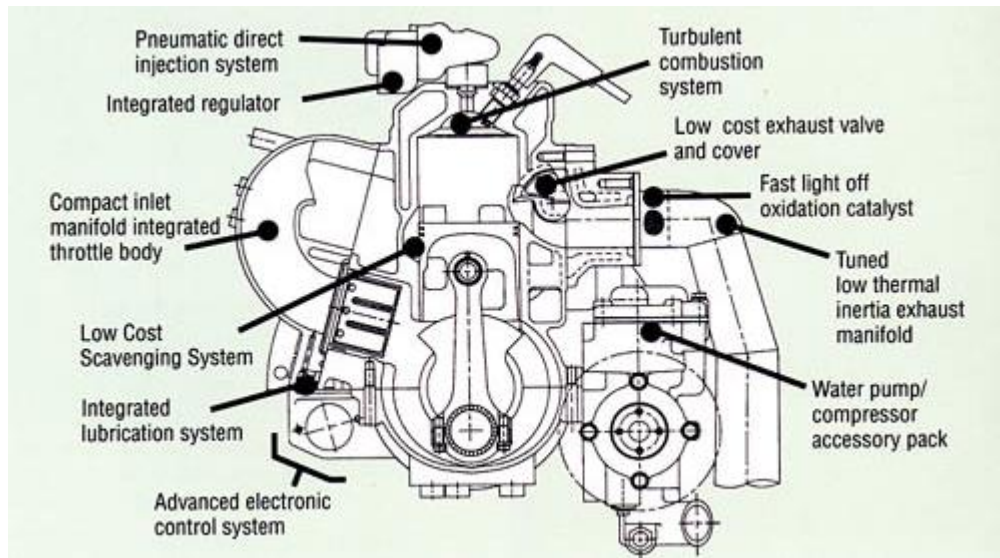


Figure 2.15: Technical features of orbital combustion process engine [25].

2.5.8 Omnivore Engine

Lotus presented a novel exhaust valve mechanism for 2-stroke engines as a part of their OMNIVORE engine as shown in Figure 2.16. This system has an oscillating valve controlling the opening and closure of the exhaust port. For each crankshaft rotation the valve performs a full oscillation cycle. The opening of the exhaust is controlled by the upward movement of the valve while the closure is controlled during its downward movement. The oscillatory movement of the valve is produced by an eccentric shaft system and the angle of the oscillation is controlled by an actuator allowing for a different timing to be set at both the opening and the closure of the port. This induces a continuous variation of the exhaust timings [26].

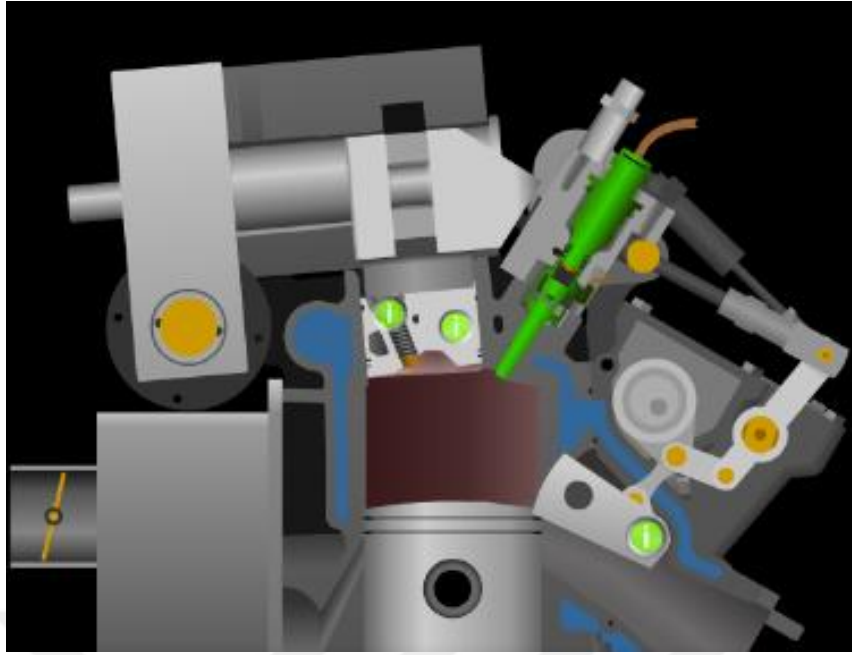


Figure 2.16: Omnivore engine [26]

2.5.9 Rhombic Drive Engine

Rhombic drive mechanism was identified with the usage on Stirling engine by Meijer in 1959. With the reduction in lateral force acting to the cylinder wall by the piston makes the rhombic drive mechanism superior on decreasing the friction loss [27]. Different from the Stirling engine displacer is removed and at two-stroke spark ignition engine the rhombic drive mechanism consists of two gears, a modified connecting rod and two links which connect gears and connecting rod to each other.

CHAPTER 3

KINEMATIC AND THERMODYNAMIC ANALYSIS OF THE ENGINE

Design parameters of single-cylinder, two-stroke, spark ignition engine with rhombic drive mechanism are given at this section. Design sizes were determined according to developed mathematical model in MATLAB. For this purposes, kinematic relations and thermodynamic model were obtained. To compare differences from the point of engine performance and emissions, a single cylinder, two-stroke, spark ignition engine with slider-crank mechanism which could be used at different applications such as scythe, lawn mower or UAV was selected from the market and analysed. Some technical properties of the engine are given in Table 3.1.

Table 3.1: Technical properties of the engine

Engine Type	2-stroke, SI engine
Cylinder number	1
Total cylinder volume (cc)	57.96
Stroke (mm)	35.18
Cylinder diameter (mm)	43.213
Connecting rod length (mm)	61.5
Geometric compression ratio	9.1:1
Cooling system	Air
Lubrication oil	2-stroke engine oil
Max power	3.1 HP-2.14 kW
Mass (kg) (without accessories)	3.6

Selected model slider-crank mechanism and designed rhombic drive mechanism engines port timing diagrams are given in Figure 3.1 and Figure 3.2, respectively.

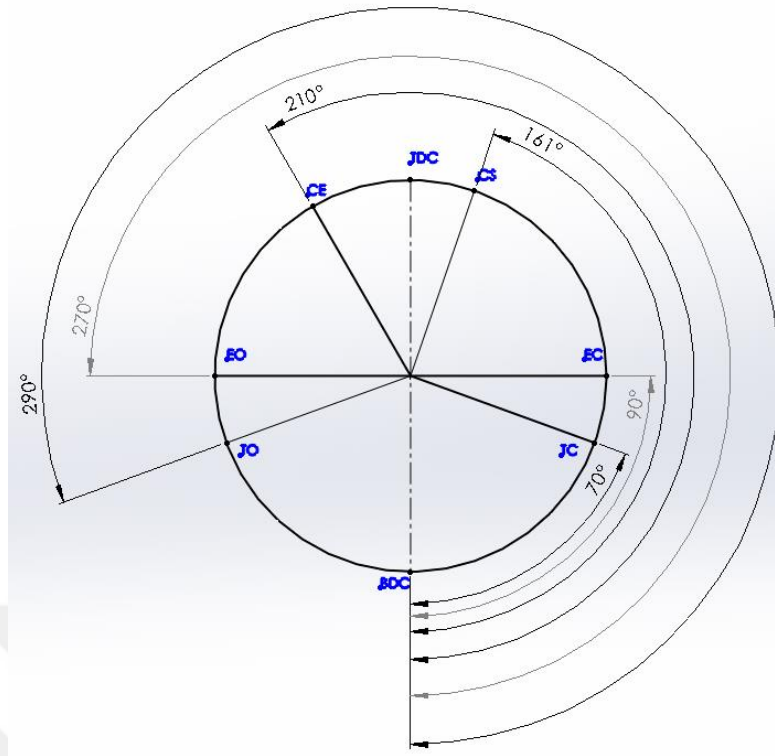


Figure 3.1: Selected engine with slider-crank mechanism port timing diagram

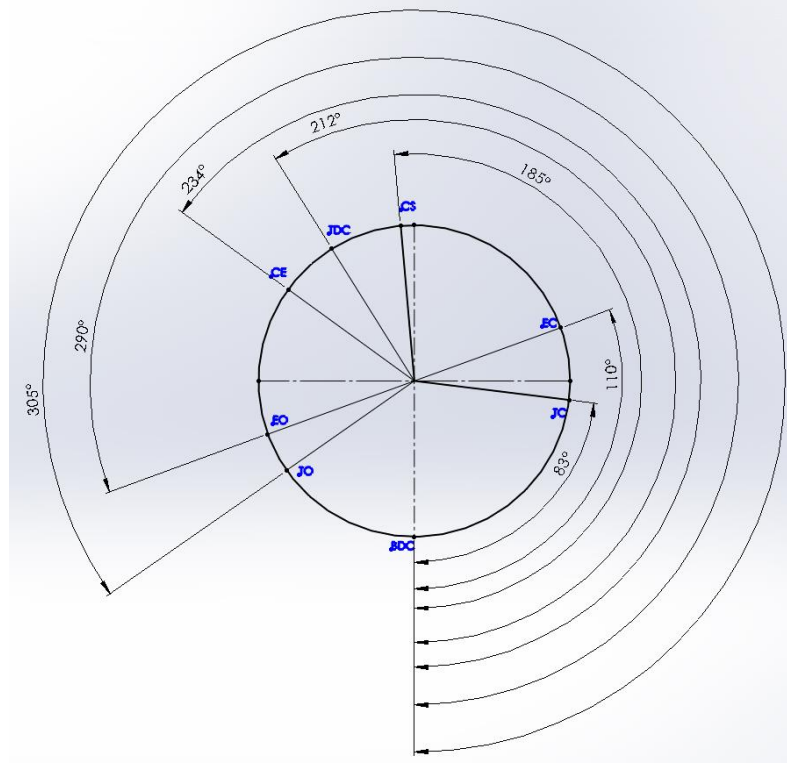


Figure 3.2: Designed engine with rhombic drive mechanism port timing diagram

To obtain closer results from the thermodynamic analysis, real-cycle approach was taken into account and JANAF tables were used to determine specific heat constants changes with respect to temperature at each cycle phases.

Both engines were air cooled. For the thermodynamic models, the heat transfer quantity with conduction and convection was calculated and Nusselt equation was used to find convective heat transfer coefficient. Frictional losses were taken into account.

Volumetric efficiency was considered as 70% for both engines due to intake phase mixture and exhaust phase residual gases.

We assume cycle starts at BDC and piston moves towards TDC to compress the fresh charging to the cylinder but still exhaust port is open due to previous cycle exhaust gases discharging so there will be no compression efficiently. Isooctane (C_8H_{18}) was used as a fuel and lambda (λ) was assumed as 1.

Transfer ports are closed at 70° CA for slider-crank mechanism and 83° CA for rhombic drive mechanism aBDC. Exhaust port is closed at 90° CA for crankshaft mechanism while 110° CA for rhombic drive mechanism aBDC and compression process continues efficiently with the upward movement of the piston at the polytrophic conditions. Pressure and temperature increase and isooctane inside the charging mixture starts to vaporize and is suitable for ignition. Heat addition starts at 161° CA and 185° CA aBDC for slider-crank and rhombic drive engines, respectively. Heat addition was considered as close as real conditions and Wiebe function was used. Duration of heat addition was assumed 50° CA for both engines. Thermal energy of the isooctane increases the pressure and temperature rapidly and piston moves downward from the TDC. Expansion lasts till exhaust port opens at 270° CA and 290° CA aBDC slider-crank and rhombic drive engines, respectively. Expansion stroke provides rotation of the connected crankshaft at slider-crank mechanism or rotation of the links over the gears at rhombic drive mechanism which transmit the power to the output shaft of the gear so the torque is obtained. Transfer ports are opened to take fresh charging into the cylinder for upcoming cycle at 290° CA and 305° CA aBDC for slider and rhombic drive, respectively. During that time scavenging provides residual gases output faster.

According to the thermodynamic analysis for both mechanisms, pressure (P), volume (V), temperature, heat transfer quantity, heat release, cumulative heat release, net work, heat transfer coefficient graphs were obtained with respect to crank angle

and evaluated. P-V diagrams were prepared to compare engine performance. According to kinematic analysis volume, stroke, piston velocity and acceleration, imposed piston forces with respect to crank angle were compared with both mechanisms.

3.1 Kinematics of the Engines

Both slider-crank mechanism and rhombic drive mechanism engine kinematic relations are given below.

3.1.1 Slider-Crank Mechanism

Slider-crank mechanism kinematic relations are given in Figure 3.3. According to these kinematic relation and parameters, stroke volume, combustion chamber volume, total cylinder volume, piston position and stroke with respect to (w.r.t.) crank angle is calculated below.

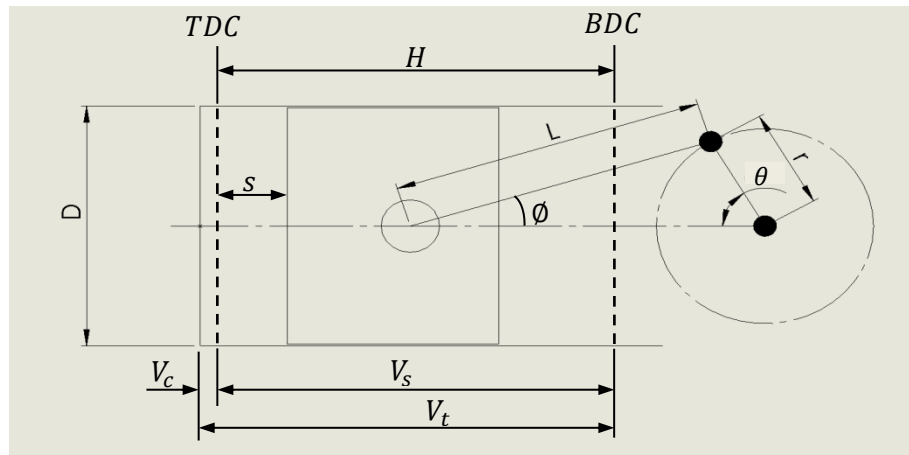


Figure 3.3: Slider-crank mechanism kinematics

Stroke volume is calculated via Equation (3.1) below

$$V_s = \frac{\pi D^2}{4} H \quad (3.1)$$

where, cylinder diameter is D, and length of stroke is H.

Combustion chamber volume is obtained using Eq (3.1). ε is here compression ratio which is given in Table 3.1.

$$V_c = \frac{V_s}{\varepsilon - 1} \quad (3.2)$$

Total cylinder volume is obtained as:

$$V_t = V_c + V_s \quad (3.3)$$

Piston position is derived from the trigonometric relations as below

$$s = L + r(1 - \cos\theta) - L\cos\emptyset \quad (3.4)$$

where, L is length of the connecting rod, r is crank radius, (θ) is crank angle and (\emptyset) is connecting rod angle w.r.t. horizontal axis. To obtain the piston position w.r.t. crank angle (θ) following trigonometric relations could be written:

$$L\sin\emptyset = r\sin\theta \quad (3.5)$$

$$\sin\emptyset = \frac{r}{L}\sin\theta \quad (3.6)$$

$$\sin^2\emptyset + \cos^2\emptyset = 1 \quad (3.7)$$

$$\cos\emptyset = \sqrt{1 - \sin^2\emptyset} \quad (3.8)$$

$$\cos\emptyset = \sqrt{1 - \left(\frac{r}{L}\sin\theta\right)^2} \quad (3.9)$$

So piston displacement could be written as derived equation from the Eq (3.4), (3.5), (3.6), (3.7), (3.8) and (3.9).

$$s(\theta) = L + r(1 - \cos\theta) - \sqrt{L^2 - (r\sin\theta)^2} \quad (3.10)$$

Total cylinder volume w.r.t. crank angle, (θ), could be written as

$$V_t = V_c + \frac{\pi D^2}{4} s(\theta) \quad (3.11)$$

Mean piston speed is defined as:

$$\bar{U}_p = 2sN \quad (3.12)$$

N is here engine speed in revolutions per minute (rpm). The maximum mean piston speed for all engines will normally be in the range of 5 to 20 m/s, with large diesel engines on the low end and high performance vehicle engines on the right end [2]. Instantaneous piston speed U_p is obtained with the differentiating the s w.r.t. time (t):

$$U_p = ds / dt \quad (3.13)$$

The ratio of instantaneous piston speed divided by the mean piston speed can be defined as

$$U_p / (\bar{U}_p) = \frac{\pi}{2} \sin\theta \left(1 + \frac{\cos\theta}{\sqrt{\left(\frac{L}{r}\right)^2 - \sin^2\theta}} \right) \quad (3.14)$$

or

$$U_p = r\omega(\sin\theta - \frac{r}{2L} \sin 2\theta) \quad (3.15)$$

where ω is angular speed (rad/s) of the crankshaft.

Piston acceleration could be written as

$$a = r\omega^2(\cos\theta - \frac{r}{L} \cos 2\theta) \quad (3.16)$$

3.1.2 Rhombic Drive Mechanism

Kinematic diagram of the rhombic drive mechanism is given in Figure 3.4. Counter clockwise is taken positive w.r.t. vertical axis for the angle changes.

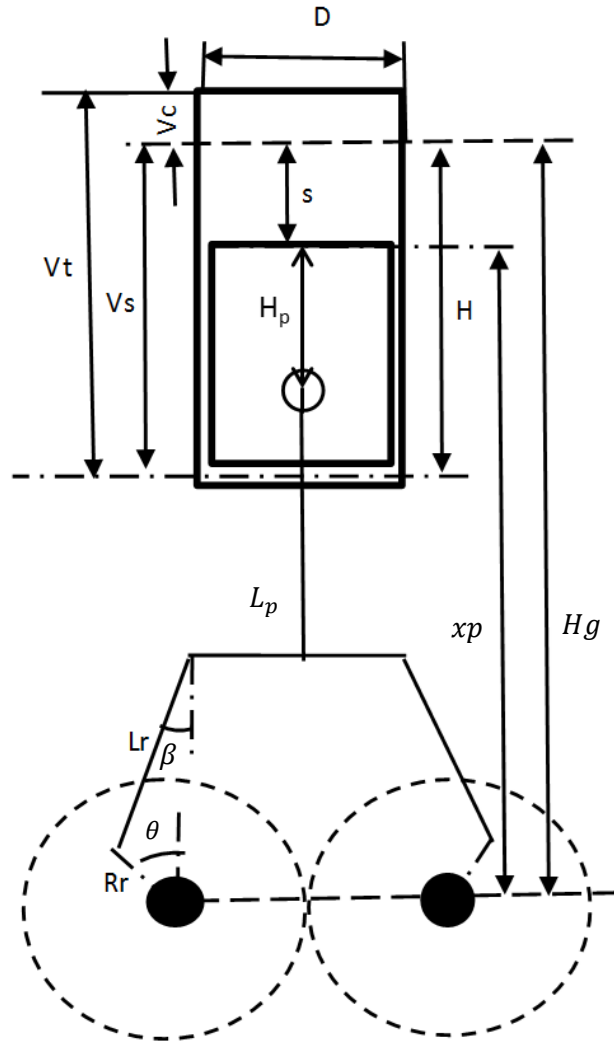


Figure 3.4: Rhombic drive mechanism kinematics

Rhombic drive mechanism kinematic relations are given below to obtain piston displacement w.r.t. gear rotation angle. As being on slider-crank mechanism gear rotation angle is defined with crank angle, θ , to compare the model graphics simultaneously in Matlab and also to reduce unknown parameters. Left side gear center is taken as the coordinate center.

$$\sin\beta = \frac{1}{2} - \frac{R_r}{L_r} \sin\theta \quad (3.17)$$

where R_r is rotational radius of the link rod (at literature this rods could be called rhombus) that connected to the gear, L_r is the length of the link rod, and β is the angle of link rod w.r.t. connecting rod connection center vertical axis.

$$\beta = \arcsin\left(\frac{1}{2} - \frac{R_r}{L_r} \sin\theta\right) \quad (3.18)$$

$$R_r = \frac{L_r}{2.666} \quad (3.19)$$

$$x_p = L_r \cos\beta + R_r \cos\theta + L_p + H_p \quad (3.20)$$

Rhombic drive piston displacement is obtained as [28-33]:

$$s_r(\theta) = H_g - x_p \quad (3.21)$$

3.2 Thermodynamic Analysis

3.2.1 Chemical and Physical Properties of Air

Components of the ideal air is taken as 78.08% nitrogen, 20.95% oxygen, 0.93% argon and 0.03% carbon dioxide, 0.015% neon, 0.0005% helium and so on by mole [34]. But generally to simplify the calculations, components are taken as 79% nitrogen and 21% oxygen by mole.

Molecular mass of the dry air is [35, 36]

$$M = 0.7808 \times 28.0134 + 20.95 \times 31.998 + 0.093 \times 39.948 + 0.003 \times 44.009 = 28.962 \text{ kg/kmole} \quad (3.22)$$

During the combustion process, volumetric ratio of nitrogen and oxygen is

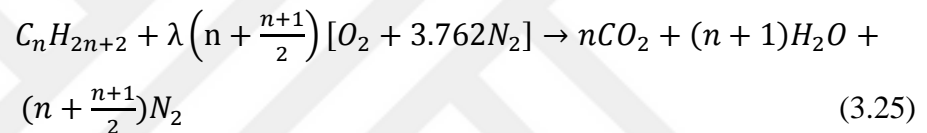
$$\frac{N_2}{O_2} = \frac{79}{21} = 3.762 \quad (3.23)$$

Total molecular mass of the air is

$$1 \text{ kmole } O_2 + 3.762 \text{ kmole } N_2 = 4.762 \text{ kmole air} \quad (3.24)$$

3.2.2 Properties of the Fuel and Excess Air Coefficient

Spark ignition engine thermodynamic analysis was conducted with isooctane to catch closer results for the real conditions with its known thermal properties according to temperature in BURCAT Tables. Hydrocarbon fuels obey C_nH_{2n+2} chemical structures and reaction with O_2 is



where n is number of carbon and hydrogen atoms per one mole fuel, λ is excess air coefficient [37]. To make simplified combustion λ is taken 1 and constant at the models.

Table 3.2: Chemical properties of isooctane [37].

Molecular formula	Isooctane $CH_3C(CH_3)_2CH_2CH(CH_3)CH_3$
Structure of molecule	C_8H_{18}
Weight of molecule	114.23 g/mole
Density	0.69 g/cc (20° C)
Melting point	-107 °C
Boiling point	99 °C (1013 hPa)
Self ignition temperature	410 °C
Flash point	-12 °C
Solubility	0.56 mg/L

3.2.3 Quantity and Temperature of Charging

Two-stroke engines charged with crankcase compression and w.r.t. design, there could be double transfer port as our selected engine construction. Intake port takes a place which is slightly lower than the exhaust port. In these types of engines, the crankcase performs as a pre-combustion compression chamber. Charging could be by naturally aspirated or by forced flow, supercharging or turbocharging. Our engine is charged with normally aspirated and this pre compression process is irreversible process which reduces the thermodynamic efficiency. The two-stroke engines fresh mixture is scavenged with crankcase pressure may have at most 1.5 times the power of four-stroke engines having the same cylinder volume. Fresh air flow from the crankcase to the cylinder is transient flow in the form of a pulse. When engine speed is increased, the pulsing period of the fresh air is reduced as the exhaust gases. To solve this problem, high speed engines are designed with a larger crankcase compression ratio, which is statistically about 1.4-1.5 at moderate engine speeds, as well as designing ports that opens relatively earlier [38]. At our mathematical models volumetric efficiency is assumed 70% and for simplification, air components are 79% N₂ and 21% O₂.

Mole quantities of the fresh charging components are:

$$N_{N_2} = \frac{PV_s}{RT} \eta_v N_2 \quad (3.26)$$

$$N_{O_2} = \frac{PV_s}{RT} \eta_v O_2 \quad (3.27)$$

where in Eq (3.26) and Eq (3.27) N_{N_2} and N_{O_2} mole quantities of the charging air components to the cylinder (kmole), N₂ and O₂ are percentage of volumetric quantities (79% and 21%), P is atmospheric pressure (kPa), T is temperature (K), V_s is stroke volume (m³), R is universal gas constant, and η_v is volumetric efficiency (%).

So mole quantity of the air is;

$$N_{air} = N_{N_2} + N_{O_2} \quad (3.28)$$

Mole quantity of the exhaust gases is;

$$N_{ex} = N_{CO_{2ex}} + N_{HO_{2ex}} + N_{O_2} + N_{N_2} \quad (3.28)$$

Total mole quantity is;

$$N_{tot} = N_{air} + N_{ex} \quad (3.29)$$

Temperature (K) of total mixture inside the cylinder is [39];

$$T_{totmix} = T + \left(\frac{N_{ex} (T_{ex} - T)}{N_{ex} + N_{air}} \right) \quad (3.30)$$

3.2.4 Properties of Mixture Inside the Cylinder

After pulsing of the exhaust gases, the transfer port is uncovered by the piston top. For a certain time interval both ports remain open which is in terms of crank angle called scavenging angle. Due to nature of the two-stroke engines, residual gases will mix with fresh charging during the scavenging period. Exhaust port is placed somewhere before the bottom dead center of the cylinder. Exhaust gases start discharging when the upper piston ring intersects with upper end of the exhaust port. Discharge of exhaust gases is transient flow in the form of a pulse Determination of discharging period of exhaust gases is a comprehensive fluid mechanic problem. So this condition reduces the volumetric efficiency [38]. Temperature increases due to the compression process and changing the mixture chemical and physical properties dramatically. That's why we need to take care components properties in terms of temperature which is given at JANAF or BURCAT tables. These tables show enthalpy, internal energy, constant volume and pressure specific heats, and viscosity of the mixture components w.r.t. temperature.

Changing of the internal energy, enthalpy and specific heat due to the reaction inside the cylinder is made suitable to use in Matlab software model after conversion and obtained from the BURCAT tables [37]. These equations are defined below.

Table 3.3: Mixture components and indexes that used at the mathematical model.

Component	CO ₂	H ₂ O	O ₂	N ₂	C ₈ H ₁₈
Index(i)	1	2	3	4	5

Mixture properties w.r.t. temperature is obtained with following Eq(3.31) to calculate air components and fuel enthalpy individually.

$$h_i(T) = R_{mol}T \left(a_{i1} + a_{i2} \frac{T}{2} + a_{i3} \frac{T^2}{3} + a_{i4} \frac{T^3}{4} + a_{i5} \frac{T^4}{5} + \frac{b_i}{T} \right) \quad (3.31)$$

where a index defines lower temperature than 1000 K and b index is higher than 1000 K which are given at Table 3.4a and Table 3.4b respectively. Then internal energy of the components will be found one by one. Relation between enthalpy and internal energy is given below [37,40,41]

$$u = h + pV \quad (3.32)$$

From the ideal gas equation RT could be written instead of pV in Eq (3.32),

$$u = h - RT \quad (3.33)$$

So each component internal energy could be found with [37];

$$u_i(T) = h_i(T) - RT \quad (3.34)$$

Total enthalpy and internal energy is obtained with;

$$\sum h_{mix} = \frac{1}{N_{mix}} \left(h_1 N_{CO_2} + h_2 N_{H_2O} + h_3 N_{O_2} + h_4 N_{N_2} + h_5 N_{C_8H_{18}} \right) \quad (3.35)$$

$$\sum u_{mix} = \frac{1}{N_{mix}} \left(u_1 N_{CO_2} + u_2 N_{H_2O} + u_3 N_{O_2} + u_4 N_{N_2} + u_5 N_{C_8H_{18}} \right). \quad (3.36)$$

$$N_{mix} = N_{CO_2} + N_{H_2O} + N_{O_2} + N_{N_2} + N_{C_8H_{18}} \quad (3.37)$$

where h_{mix} is total enthalpy of the mixture (kJ/kmole), u_{mix} is total internal energy (kJ/kmole), N_{mix} is mole quantity of the mixture and N_{CO_2} , $N_{\text{H}_2\text{O}}$, N_{O_2} , N_{N_2} , $N_{\text{C}_8\text{H}_{18}}$ are mole quantities of the components of the mixture.



**Table 3.4a: C₈H₁₈, air and burned gas components coefficients (T<1000 K)
[37,40].**

Components	a_1	a_2	a_3	a_4	a_5	a_6
C ₈ H ₁₈	8.15741071e-01	7.32647307e-02	1.78301503e-05	-6.93592790e-08	3.21630852e-11	-3.04774255e+04
N ₂	3.53100528e+00	-1.23660988e-04	-5.02999433e-07	2.43530612e-09	-1.40881235e-12	-1.04697628e+03
O ₂	3.78245636e+00	-2.99673416e-03	9.84730201e-06	-9.68129509e-09	3.24372837e-12	-1.06394356e+03
H ₂ O	0.41986352e+01	-0.20364017e-02	0.65203416e-05	-0.54879269e-08	0.17719680e-11	-0.30293726e+05
CO ₂	0.23568130e+01	0.89841299e-02	-0.71220632e-05	0.24573008e-08	-0.14288548e-12	-0.48371971e+05

Table 3.4b: C₈H₁₈, air and burned gas components coefficients (T>1000 K) [37,40].

Components	b_1	b_2	b_3	b_4	b_5	b_6
C ₈ H ₁₈	1.76160941e+01	5.13323108e-02	-1.65307266e-05	2.43232275e-09	-1.35572757e-13	-3.63461118e+04
N ₂	2.95257637e+00	1.39690040e-03	-4.92631603e-07	7.86010195e-11	-4.60755204e-15	-9.23948688e+02
O ₂	3.66096065e+00	6.56365811e-04	-1.41149627e-07	2.05797935e-11	-1.29913436e-15	-1.21597718e+03
H ₂ O	0.26770389e+01	0.29731816e-02	-0.77376889e-06	0.94433514e-10	-0.42689991e-14	-0.29885894e+05
CO ₂	0.46365111e+01	0.27414569e-02	-0.99589759e-06	0.16038666e-09	-0.91619857e-14	-0.49024904e+05

3.2.5 Specific Heat Changing with Temperature

Required heat to increase temperature 1 K of the 1 kg substance is called specific heat [42]. The specific heat of the gases is influenced dramatically by the conditions of the heating process [43]. Specific heat could change up to 30% in the temperature range of an engine [2]. In Figure 3.5, changing of C_p and k w.r.t. temperature is shown. From the figure, it is clear that increasing C_p causes reduction of k with more increase of C_v and reducing k results with less net work and thermal efficiency due to reduction of combustion end temperature.

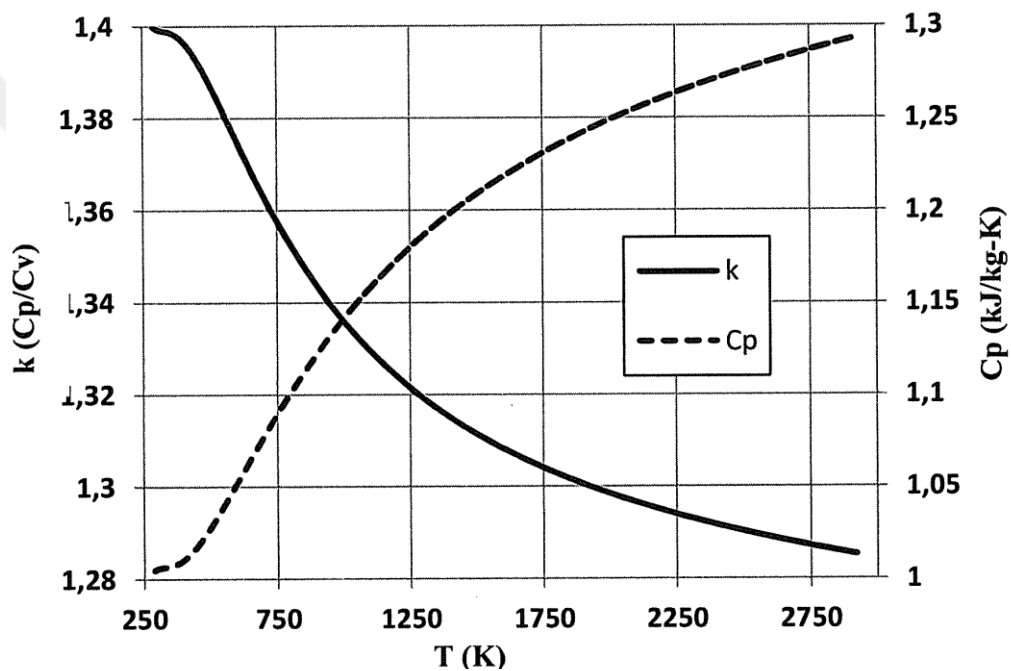


Figure 3.5: Changing of C_p and k with temperature [35].

Constant volume and pressure specific heat is calculated with Eq (3.38) and Eq (3.39) respectively below

$$c_v = \left(\frac{\partial u}{\partial T} \right)_v = \frac{du}{dT} \quad (3.38)$$

$$c_p = \left(\frac{\partial h}{\partial T} \right)_p = \frac{dh}{dT} \quad (3.39)$$

The ratio of specific heats, k , is a useful quantity [44]

$$k = \frac{c_p}{c_v} \quad (3.40)$$

Specific heat of the all components for the combustion is calculated one by one with Eq (3.41) and Eq (3.42);

$$c_{vi}(T) = \frac{u_{i2} - u_{i1}}{T_2 - T_1} \quad (3.41)$$

$$c_{pi}(T) = \frac{h_{i2} - h_{i1}}{T_2 - T_1} \quad (3.42)$$

Then all component total constant volume and pressure specific heats are obtained from Eq (3.43) and Eq (3.44) respectively.

$$\sum C_v = \frac{1}{N_{mix}} \left(C_{v1}N_{CO_2} + C_{v2}N_{H_2O} + C_{v3}N_{O_2} + C_{v4}N_{N_2} + C_{v5}N_{C_8H_{18}} \right) \quad (3.43)$$

$$\sum C_p = \frac{1}{N_{mix}} \left(C_{p1}N_{CO_2} + C_{p2}N_{H_2O} + C_{p3}N_{O_2} + C_{p4}N_{N_2} + C_{p5}N_{C_8H_{18}} \right) \quad (3.44)$$

In Figure 3.6, C_p changing of combustion products w.r.t. temperature is given. Temperature affects the components with different function.

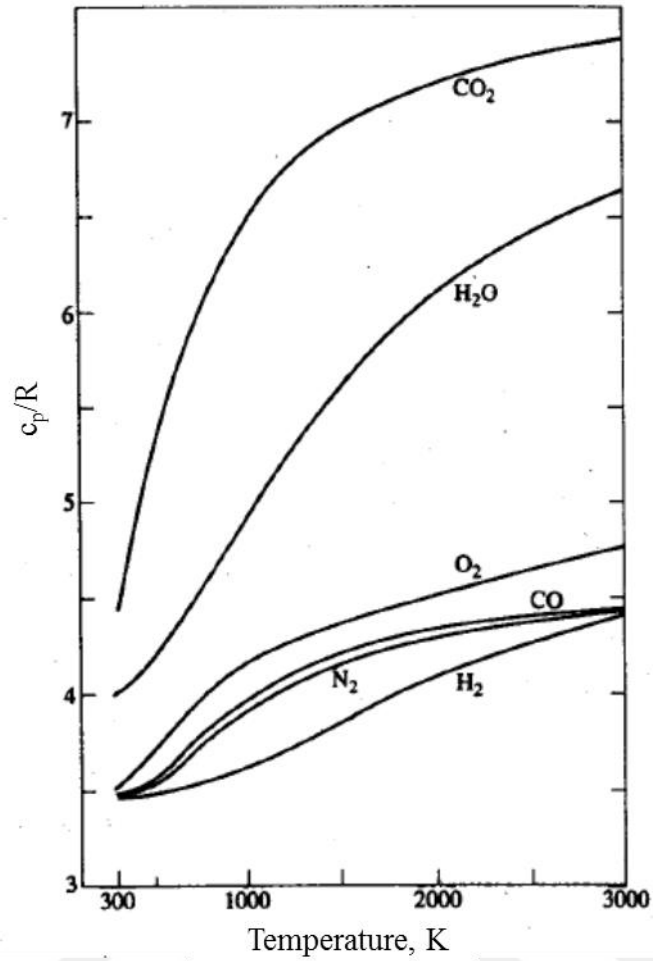


Figure 3.6: Constant pressure specific heat of combustion products changing with temperature [44].

3.2.6 Quantity and Temperature of the Exhaust Residual Gases Inside the Cylinder

At the end of the exhaust process, quantity of the residual gases equal to the combustion chamber volume. Residual gases increase temperature of the intake charging. That is why we need to find out pressure, temperature and mole quantity of the charging at the compression real cycle for thermodynamic analysis. Exhaust port opening and closing temperatures are obtained from Eq (3.45) and Eq (3.46) respectively [45].

$$T_{ex} = T_{exo} \left(\frac{P_{ex}}{P_{exo}} \right)^{\left(\frac{n-1}{n} \right)} \quad (3.45)$$

$$T_{exc} = T_{ex} \left(\frac{P_{atm}}{P_{ex}} \right)^{\left(\frac{n-1}{n} \right)} \quad (3.46)$$

where T_{ex} is exhaust gas temperature, T_{exo} is temperature at the exhaust port opening, T_{exc} is temperature at the exhaust port closing, P_{atm} is atmospheric pressure, P_{exo} is pressure at the exhaust port opening, P_{ex} is reverse pressure of exhaust, and n is polytropic coefficient.

Total mole quantity of the exhaust gases is derived from the ideal gas law and obtained Eq (3.47) below.

$$N_{ex} = \frac{P_{ex} V_{com}}{RT_{ex}} \quad (3.47)$$

where N_{ex} is mole quantity of the exhaust gases (kmole), R is universal gas constant which is 8.314 kJ/kmoleK, V_{com} is volume of the combustion chamber (m^3).

Each component of residual gases mole quantity is calculated from the point of volumetric contribution to the residual gases.

$$N_{CO_{2ex}} = \frac{P_{ex} V_{com}}{RT_{ex}} CO_{2ex} \quad (3.48)$$

$$N_{H_2O_{ex}} = \frac{P_{ex} V_{com}}{RT_{ex}} H_2O_{ex} \quad (3.49)$$

$$N_{O_{2ex}} = \frac{P_{ex} V_{com}}{RT_{ex}} O_{2ex} \quad (3.50)$$

$$N_{N_{2ex}} = \frac{P_{ex} V_{com}}{RT_{ex}} N_{2ex} \quad (3.51)$$

where $N_{CO_{2ex}}$, $N_{H_2O_{ex}}$, $N_{O_{2ex}}$, $N_{N_{2ex}}$ is mole quantity of the components at the residual gases(kmole) and CO_{2ex} , H_2O_{ex} , O_{2ex} , N_{2ex} is percentage of the components at the residual gases (%).

3.2.7 Heat Addition to the Cylinder

In the Otto cycle, fuel is assumed to burn at constant volume but actual process is not matched with this simple model. Reflecting more realistic conditions to the combustion, finite heat release model, which is a differential model of an engine power cycle depending on crank angle, is used. Engine work and efficiency could be answered with heat release models. In Figure 3.7, cumulative heat release (burn fraction) curve for a spark ignition engine is given. The curve could be separated three regions which are initial ignition delay, a rapid burning region and a burning completion region. The ignition delay is represented with initial small slope at the curve and beginning with the spark ignition. Then rapid growth and more gradual decay occur [40]. Burn fraction could be obtained analytically with Wiebe function as shown in Eq (3.52) below [44].

$$X_b = 1 - \exp \left[-a \left(\frac{\theta - \theta_0}{\Delta\theta} \right)^{m+1} \right] \quad (3.52)$$

The mass fraction burning gradient arises from zero, where zero mass fraction burn represents combustion start, and then nearly acts exponentially to one indicating the end of combustion. The variation of those two ends is known as the duration [46].

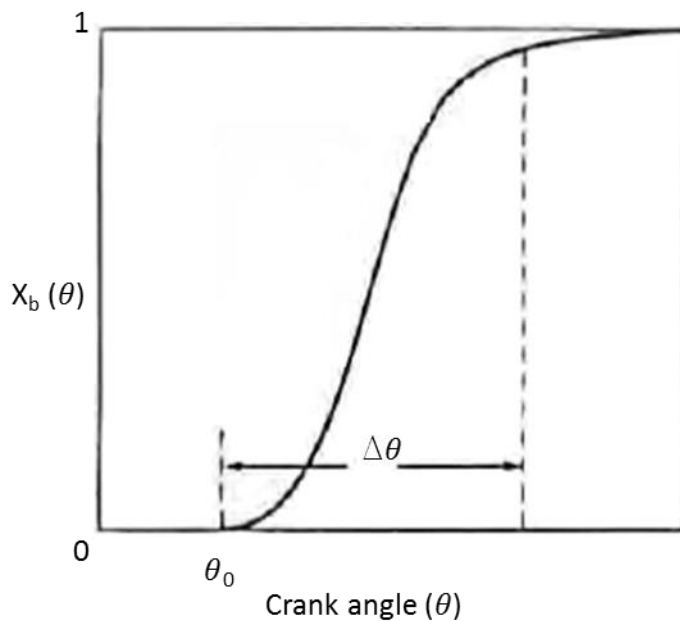


Figure 3.7: Cumulative heat release function for a spark ignition engine [40].

3.2.8 Heat Transfer

The air-cooled engines have the heavier operation than the liquid cooled engines due to irregular cooling of the cylinder surface [47]. Produced heat by the combustion is released toward the ambient air that surrounds the engine by a series of fins located onto the external cylinder surface and swept by the air stream flowing externally to the cylinder itself. Non-uniform flow of the air at the surrounding is compensated with non-symmetrical fin arrangement over the cylinder [48].

In a two-stroke engine the cooling heat flow contains only two factors: conduction and convection. The radiation occupies only trivial part of the total cooling heat by reason of absence of the soot in the exhaust gases. Heat transfer with convection occurred between gas inside the cylinder and the cylinder wall. The heat of the conduction which is arose from molecular motion and interaction is transferred through the wall of the cylinder liner, cylinder body, combustion chamber, the piston, piston rings and the exhaust duct [47]. Then again heat transfer with convection occurred from the outer surface of the cylinder to the air around the engine body. So at the analysis convection and conduction provide transfer of the heat while radiation effect is ignored. Heat transfer on a cylinder is shown in Figure 3.8.

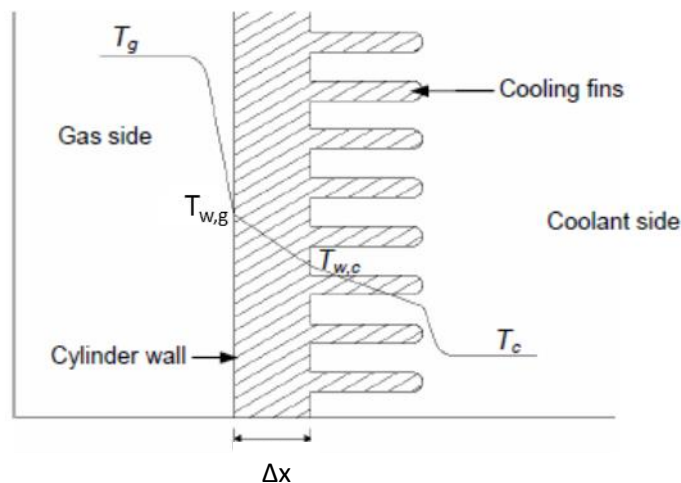


Figure 3.8: Heat transfer in air cooled engine [49].

Heat transfer per unit surface area is denoted in Eq (3.53)

$$Q = \frac{A(T_g - T_w)}{\left[\left(\frac{1}{h_g} \right) + \left(\frac{\Delta x}{k_s} \right) + \left(\frac{1}{h_c} \right) \right]} \quad (3.53)$$

Heat transfer relation with crank angle is defined by averaged heat flux and rises at fully open throttle and at maximum engine speed [40]. Heat flux allows predicting power output or efficiency with a quasi-steady process. Meaning of this, at any instant of the time heat transfer rate could be taken as proportional to the temperature variation between working fluid and the body surface. Uniform distribution of the gas temperature in the cylinder is assumed for simplification.

The convection heat transfer coefficient could be calculated with a few empirical approaches which are offered and developed by Nusselt (1923), N. Brillling, Eichelberg (1939), Annand (1963), G. Woschni (1967), Hohenberg (1979), Elser (1995) etc, [43].

Nusselt heat transfer coefficient is as given in Eq (3.54) below.

$$h_g = 5.388 \times 10^{-4} \left(1 + 1.24 \bar{V}_p \right) T_g^{\frac{1}{3}} P_g^{\frac{2}{3}} + 0.421 \left[\frac{\left(\frac{T_g}{100} \right)^4 - \left(\frac{T_w}{100} \right)^4}{T_g - T_w} \right] \quad (3.54)$$

N. Brillling expanded Nusselt equation for low speed diesel engine and detected intense swirl formation caused by pneumatic spraying of the fuel, increases heat transfer coefficient of 2.5 times [50]. Denoted in Eq (3.55) below

$$h_g = 5.388 \times 10^{-4} \left(1 + 1.45 + 0.185 \bar{V}_p \right) T_g^{\frac{1}{3}} P_g^{\frac{2}{3}} + 0.421 \left[\frac{\left(\frac{T_g}{100} \right)^4 - \left(\frac{T_w}{100} \right)^4}{T_g - T_w} \right] \quad (3.55)$$

Eichelberg offered Eq (3.56)

$$h_g = 77.9 \times 10^{-4} \left(T_g P_g \right)^{\frac{1}{2}} + V_p \quad (3.56)$$

G. Woschni expressed heat transfer coefficient as in Eq (3.57)

$$h_g = 0.12793 \times D^{-2} T_g^{-0.53} P^{0.8} \left[C_1 V_p + C_2 \frac{V_t + T_r}{P_r + V_r} (P - P_0) \right]^{0.8} \quad (3.57)$$

where the values P and T_g, which correspond to the instantaneous conditions inside the cylinder, working values P_r and T_r correspond to a volume V_r of a reference state, such as beginning of combustion, exhaust valve closure or inlet valve closure.

G.Woschni offers following coefficients:

$$C_1 = 6.18 \times +0.417 \frac{c_u}{V_p} \text{ for scavenging period}$$

$$C_1 = 2.28 \times +0.308 \frac{c_u}{V_p} \text{ for compression and expansion period}$$

$$C_2 = 0.00324 \text{ for diesel engines with direct injection}$$

$$C_2 = 0.0062 \text{ for diesel engines with separate combustion chambers}$$

Hohenberg developed Eq (3.58) below

$$h_g = C_1 V_\theta^{-0.06} T_g^{-0.4} P^{0.8} + (V_p + C_2)^{0.8} \quad (3.58)$$

where C₁=130 and C₂=1.4

3.3 Engine Performance Characteristics

Internal combustion engines could be operated at a wide range starting with idle which is the lowest engine speed that engine operates in stability by itself, and ending at maximum engine speed which is restricted by efficiency of intake and exhaust process, thermal stresses of the components, excess of inertia forces, reduction in mechanical efficiency, etc.

Optimum operation range for the engines is supplied when maximum power (P_{e_max}), maximum torque (M_{e_max}) or lowest fuel consumption (b_{e_min}) are provided. These parameters have correlation with operating target and condition of the engines [51].

Operating characteristics of the engines include mechanical output parameters of work, mean indicated pressure and indicated efficiency, indicated torque and

power, the input requirements of air, fuel, and combustion; efficiencies; and emission measurement of engine exhaust [2].

3.3.1 Work

Any heat engine output is called work and the gases generate the work during the combustion process of the ICE. Work is the result of a force acting through a distance which is due to gas pressure on the moving piston.

$$W = \int F dx = \int P A_p dx \quad (3.59)$$

where P is pressure in combustion chamber, A_p is area of piston top surface which the pressure acts, x is distance the piston moves.

$$A_p dx = dV \quad (3.60)$$

where dV is differential volume displaced by the piston as it reciprocates between top dead center and bottom dead center inside the cylinder.

$$W = \int P dV \quad (3.61)$$

If P represents the pressure inside the cylinder combustion chamber, then it is called indicated work (W_i). Due to mechanical friction and parasitic load of the engine, some of the indicated work is lost and called brake work (W_b) which is taken from the crankshaft. It is clear that at P-V diagram during compression and expansion strokes, output work is generated and called gross indicated work. During intake and exhaust lost work against piston and crankcase pressure is called pumping work [2].

$$W_b = W_i - W_f \quad (3.62)$$

where W_f is work lost due to the friction and parasitic loads.

$$W_{net} = W_{gross} + W_{pump} \quad (3.63)$$

Per unit of mass of gas m within the cylinder, volume V is replaced with specific volume, v , and work is replaced specific work, w .

Mechanical efficiency which is the ratio of brake work to indicated work could be shown as Eq (3.64) below.

$$\eta_m = w_b / w_i \quad (3.64)$$

3.3.2 Mean Effective Pressure

It is clear from Figure 3.9, pressure in the cylinder is changing cyclically that is why mean effective pressure (mep) denoted as

$$(mep) = w / \Delta v \quad (3.65)$$

If brake work is used, break mean effective pressure is shown as Eq (3.66)

$$(bmep) = w_b / \Delta v \quad (3.66)$$

In Figure 3.9, rectangular shaded area, equal in area to the enclosed cylinder P-V diagram which is the total work on the piston. Rectangle is of height indicated mean effective pressure (IMEP) and of length V_{sv} is stroke volume. IMEP is related any two similar or dissimilar stroke volume engines of equal development or performance status will have identical values of mean effective pressure to compare [6]. IMEP is obtained as;

$$(IMEP) = w_i / \Delta v \quad (3.67)$$

Indicated efficiency is;

$$\eta_i = \frac{P_i}{m_f Q_{HV}} \quad (3.68)$$

where P_i is indicated power (kW), \dot{m}_f is mass flow of fuel (kg/s) and Q_{HV} is lower heating value of the fuel (kJ/kg)

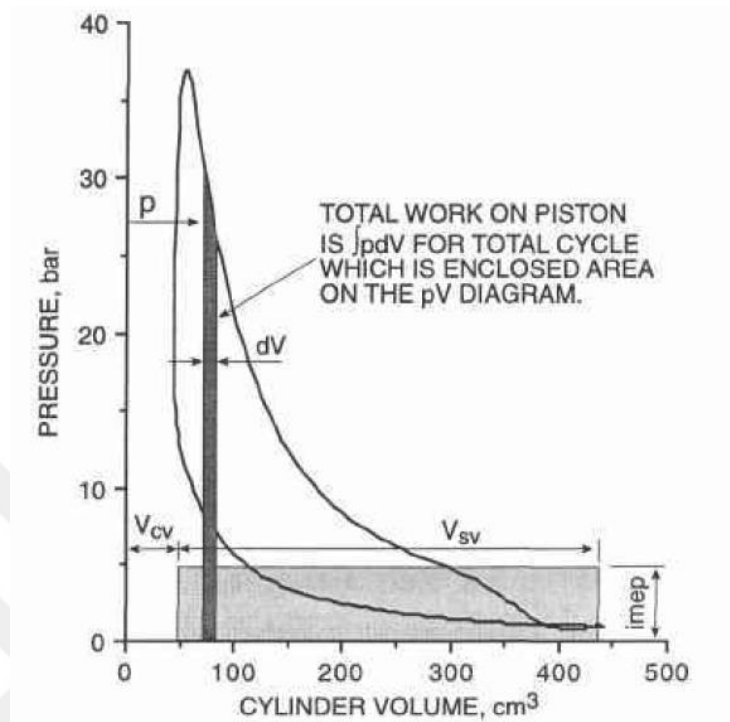


Figure 3.9 Determination of IMEP from the cylinder P-V diagram [6].

3.3.3 Torque and Power

Effective torque, M_e , is an indicator of an engine's ability to do work as derived in Eq (3.69).

$$M_e = m_l g l_m \quad (3.69)$$

where M_e is in (Nm), m_l dynamometer load cell measurement (kg), g is gravity (m/s^2) and l_m torque rod length (m) on the dynamometer which will be introduced in Chapter 5.

For two-stroke engines, brake mean effective pressure could be used to define effective torque on the output shaft.

$$M_e = (bmep)V_s / 2\pi \quad (3.70)$$

Engine power is obtained with work rate of the engine such as

$$\dot{W} = WN / n \quad (3.71)$$

where W is work per cycle, N is engine speed, and n is number of revolution per cycle.

Effective (brake) power which is taken from the engine output shaft is denoted;

$$P_e = \frac{M_e N}{9549} \quad (3.72)$$

where P_e is engine effective power (kW), M_e is effective torque (Nm), and N is engine speed (rpm)

3.3.4 Air Fuel Ratio and Fuel Air Ratio

Air fuel ratio (AF) and fuel air ration (FA) defines the mixture ratio that enters to the cylinder at intake process.

$$AF = m_a / m_f = \dot{m}_a / \dot{m}_f \quad (3.73)$$

$$FA = 1 / AF \quad (3.74)$$

where m_a and m_f are mass of air and fuel, \dot{m}_a and \dot{m}_f is mass flow rate of air and fuel, respectively.

Equivalence ratio, ϕ , is defined as the actual ratio of fuel-air to ideal or stoichiometric fuel-air:

$$\phi = (FA)_{act} / (FA)_{stoich} = (AF)_{stoich} / (AF)_{act} \quad (3.75)$$

Also fuel air ratio could be represented with lambda value;

$$\lambda = 1 / \phi \quad (3.76)$$

3.3.5 Specific Fuel Consumption

Specific fuel consumption is given by

$$sfc = m_f / \dot{W} \quad (3.77)$$

where m_f is rate of fuel flow (g/h) into engine and \dot{W} is engine power

Brake specific fuel consumption (g/kWh) could be obtained with effective power (kW);

$$sfc = m_f / \dot{W}$$
$$bsfc = \frac{m_f}{P_e} \quad (3.78)$$

3.3.6 Engine Efficiencies

Combustion process is a bit complicated and during the process all fuel molecules may not find an oxygen molecule to be combined or the local temperature may not favour a reaction. That is why a combustion efficiency η_c is defined to take care the fraction of fuel that burns. Generally, the range of η_c is 0.95 to 0.98 for well operating engines [2]. For our analysis it is taken 0.98. For one engine cycle in one cylinder, the heat addition is;

$$Q_{in} = m_f Q_{HV} \eta_c \quad (3.79)$$

For steady state,

$$Q_{in} = m_f Q_{HV} \eta_c \quad (3.80)$$

and thermal efficiency is

$$\eta_t = \frac{W}{Q_{in}} = \frac{\dot{W}}{\dot{Q}_{in}} = \dot{W} / m_f Q_{HV} \eta_c \quad (3.81)$$

Volumetric efficiency is related with air taken into the cylinder during one cycle which affects obtained power and performance from the engine. Volumetric efficiency, η_v , is

$$\eta_v = \frac{m_a}{\rho_a V_d} = \frac{n m_a}{\rho_a V_d N} \quad (3.82)$$

Volumetric efficiency range is 75% to 90% at wide open throttle condition of the engine. Lower efficiency is obtained when throttle is closed and this air flow restriction governs power control of spark ignition engine [2]. At our analysis η_v is assumed 70%.

3.4 Exhaust Emissions

One of the comparisons is made on exhaust emissions to control their environmental effects. Due to unburned fuel, some pollutants inside the exhaust gases exist such as nitrogen oxides (NO), carbon monoxide (CO), hydrocarbons (HC). Generally, two methods are used to define the amounts of the exhaust products which are specific emissions (SE) and emission index (EI). Units are g/kWh and emission flow per fuel flow respectively [2].

Specific emissions are denoted:

$$(SE)_{NO_x} = \dot{m}_{NO_x} / P_e \quad (3.83)$$

$$(SE)_{CO} = \dot{m}_{CO} / P_e \quad (3.84)$$

$$(SE)_{HC} = \dot{m}_{HC} / P_e \quad (3.85)$$

where \dot{m} is flow rate of emissions in g/h, and P_e is brake power in kW.

Emission indexes are denoted:

$$(EI)_{NO_x} = \dot{m}_{NO_x} / \dot{m}_f \quad (3.86)$$

$$(EI)_{CO} = \dot{m}_{CO} / \dot{m}_f \quad (3.87)$$

$$(EI)_{HC} = \dot{m}_{HC} / \dot{m}_f \quad (3.88)$$

where \dot{m} is flow rate of emissions in g/s, and \dot{m}_f is flow rate of fuel in kg/s.



CHAPTER 4

ENGINE DESIGN AND MANUFACTURING

In this chapter, two-stroke engine with rhombic drive mechanism 3D solid model which was created at SolidWorks CAD software was analysed with 3D finite element assembly model. Strength analysis of the engine was run at Hypermesh, Abaqus and SolidWorks Simulation CAE software. Components of the engine were simplified with removing some details at finite element models to analyse in a shorter time. Manufacturing of the engine is given at the second topic.

4.1 Design of the Engine

Rhombic drive is a novel mechanism for two-stroke engines. Different from the slider-crank mechanism engine rhombic links and gears were used to obtain reciprocating motion of the piston inside the cylinder. Cylinder, piston, piston rings and piston pin patterns were made w.r.t. coordinate measurement machine (CMM) data of a mass production engine components. Rhombic drive mechanism mainly consisted of a connecting rod, two rhombic links, two gears, two couple connection pins. One of the couple pin was rotation centers between connecting rod and rhombic links and other couple was between rhombic links and gears. All drive mechanism components were surrounded by housing and its cover. Gears were seated on bearings inside the housing. Engine output shaft was unique part with one of the gear which was on the right side and over this output shaft pull start pulley and flywheel was integrated.

Some of the design properties are given in Table 4.1.

Table 4.1: Properties of the designed rhombic drive engine

Engine	2-stroke, SI engine
Cylinder number	1
Total cylinder volume (cc)	57.98
Stroke (mm)	35.2
Cylinder diameter (mm)	43.213
Connecting rod length (mm)	47.84
Geometric compression ratio	9.1:1
Cooling system	Air
Lubrication	2-stroke engine oil
Mass (kg) (without accessories)	3.2

Critical components were assembled according to thermodynamic and kinematic analysis and simplified for finite element model as shown in Figure 4.1.

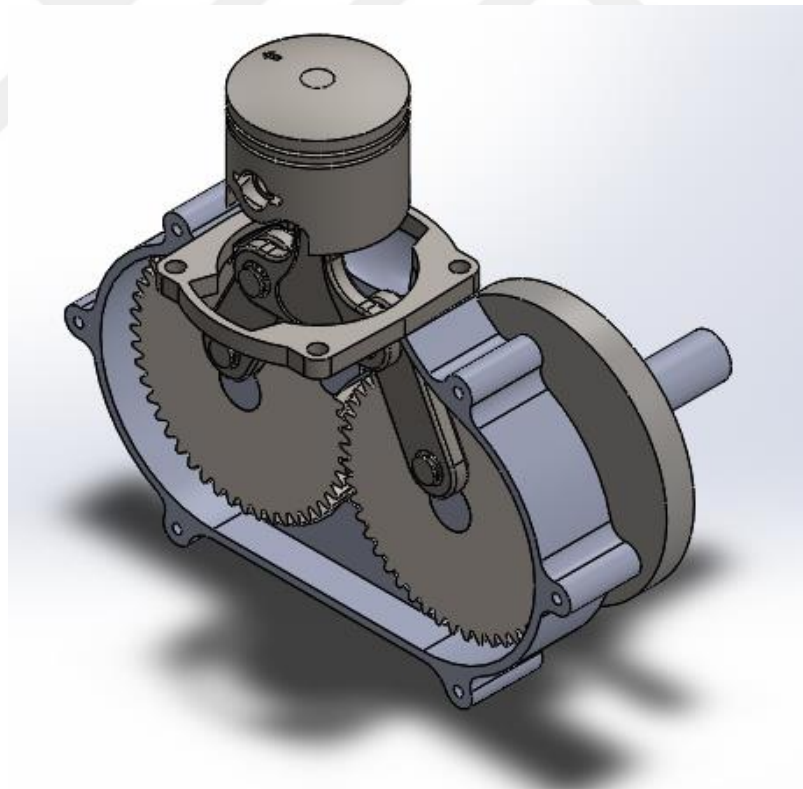


Figure 4.1: Isometric view of critical components assembly model in CAD software

Then critical components finite element assembly model was created to analyse its strength and displacement behaviour in both static condition and inertia relief condition which took into account inertia moment of the components individually. The model is shown in Figure 4.2. All critical component analysis was examined under compression and tension stresses with different material properties and only most critical results were shared here.

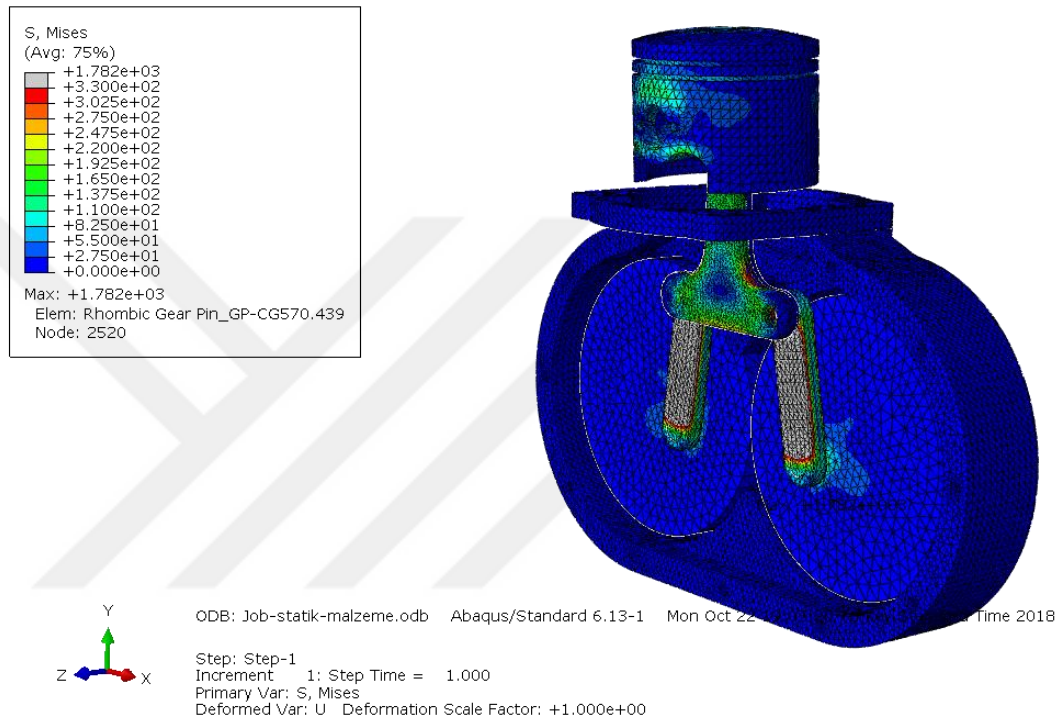


Figure 4.2: Isometric view of critical components finite element assembly model in CAE software

4.1.1 Connecting Rod

Connecting rod was designed to transmit all forces between the piston and rhombic links. It is exposed almost all types of stresses at vertical direction. Due to the operating condition of the rhombic links, connecting rod was fixed with two shrink fitted keys to the piston and piston pin mid points. Rotational and translational motion were prevented on the piston pin. Connecting rod is shown in Figure 4.3.



Figure 4.3: Isometric view of connecting rod

Result of analysis is given in Figure 4.4. Material and size of the connecting rod was determined w.r.t. CAE analysis result and selected 2379 alloy tool steel and pattern was obtained with machining. Due to its chemical content with high carbon and chromium, it can resist to high abrasive forces [52]. It is clear that selected material could satisfy easily maximum stress on the radius of connecting rod at any heavy conditions. 2379 alloy tool steel properties are given in Table 4.2.

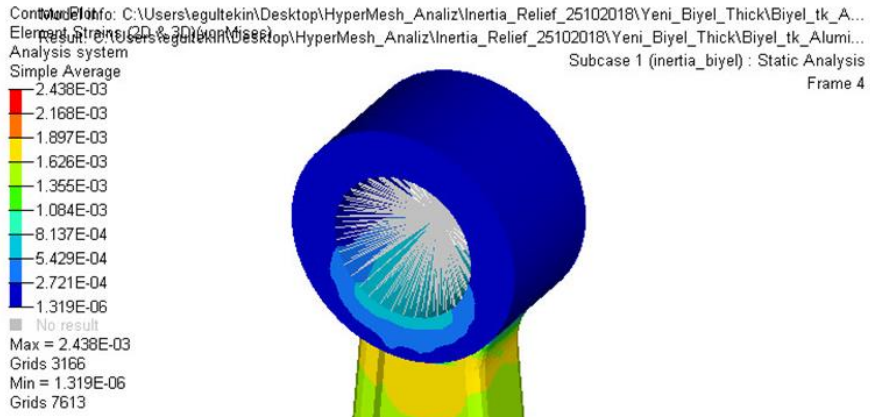


Figure 4.4: CAE inertia relief result of connecting rod

Tablo 4.2: 2379 alloy tool steel physical and mechanical properties [53,54].

2379 Tool Steel	
Density	$7.7 \times 10^3 \text{ kg/m}^3$
Melting Point	1421°C
Thermal Expansion	$10.4 \times 10^{-6} \text{ }^\circ\text{C}$
Poisson's Ratio	0.27-0.30
Elastic Modulus	190-210 GPa
Tensile Strength, Ultimate	965-1030 MPa
Tensile Strength, Yield	827-862 MPa
Compressive Strength	862 MPa

4.1.2 Rhombic Links

Rhombic links are the connections between connecting rod and gears. Reciprocating motion of the piston inside the cylinder was performed by these two rhombic links which were located onto the gears. Connections of rhombic links were achieved by two pins which kept a determined offset according to the gear centers. They were located symmetrically on both side of connecting rod. Geometry of the rhombic link is given in Figure 4.5.



Figure 4.5: Isometric view of rhombic link.

According to inertia relief analysis, compression pressure on the pin bearing of rhombic link was 94.7 MPa and tension stress was 328.7MPa. Compression and tension stress results are given in Figure 4.6 and in Figure 4.7. Displacement was higher in tension than compression which was 0.01018 mm and 0.00618 mm, respectively. They are given in Figure 4.8 and in Figure 4.9. Material is same as the connecting rod which is 2379 tool steel and so stresses could be easily accomplished by the selected material at experimental conditions.

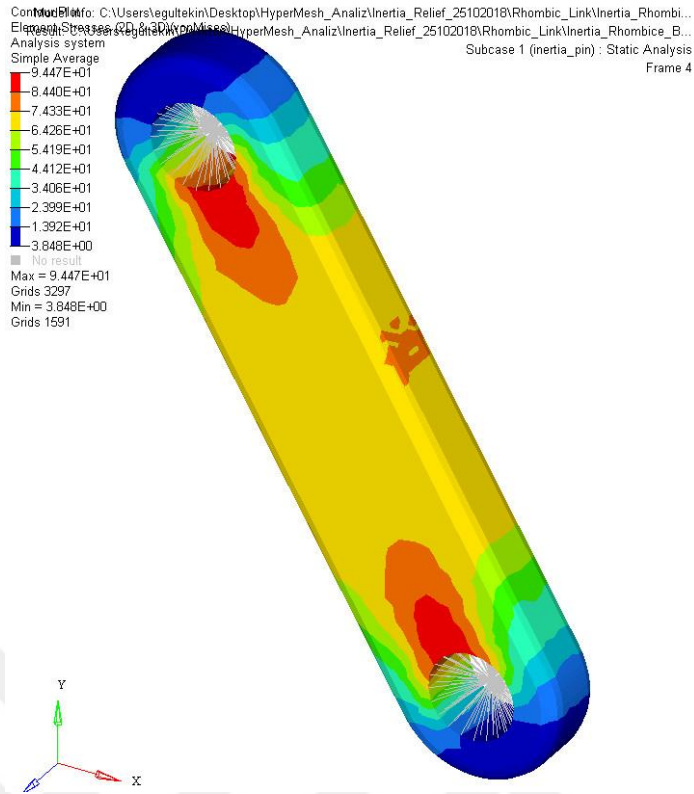


Figure 4.6: Compression analysis of rhombic link

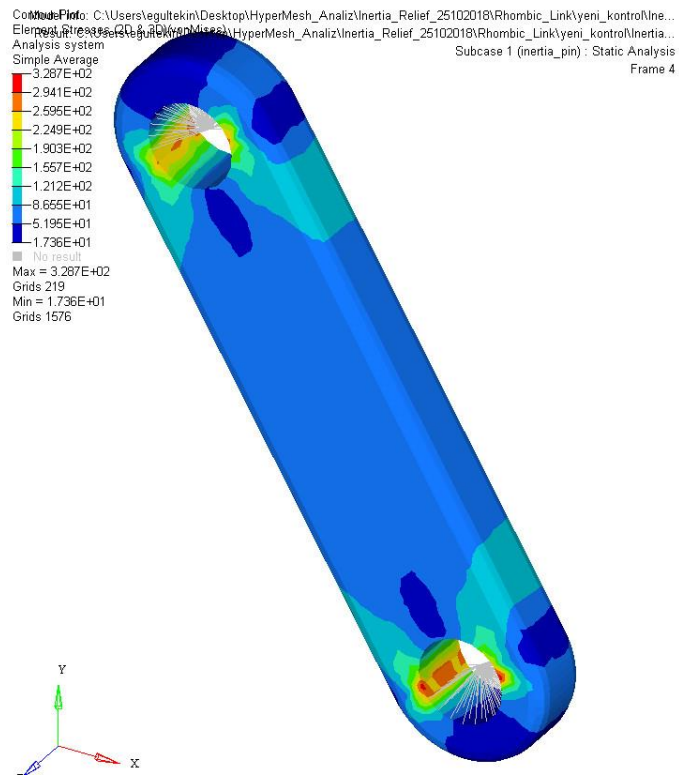


Figure 4.7: Tensile analysis of rhombic link

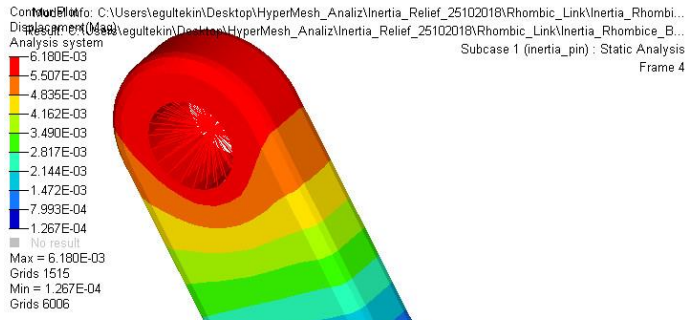


Figure 4.8: Displacement analysis of rhombic link (compression)

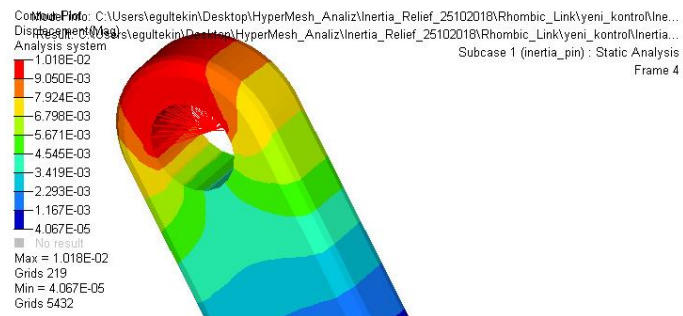


Figure 4.9: Displacement analysis of rhombic link (tensile)

4.1.3 Rhombic Pins

Rhombic pin makes connecting rod bottom end free on rotation while restricts on vertical and horizontal directions. Rhombic pin for each upper end of the rhombic link was shrink fitted. Pins were surrounded by impregnated oil bushing when inserted to the connecting rod bottom ends and rhombic links upper ends. In front of the pins there is a groove for a retaining ring which prevents longitudinal motion of the rhombic links. Rhombic pin is shown in Figure 4.10.

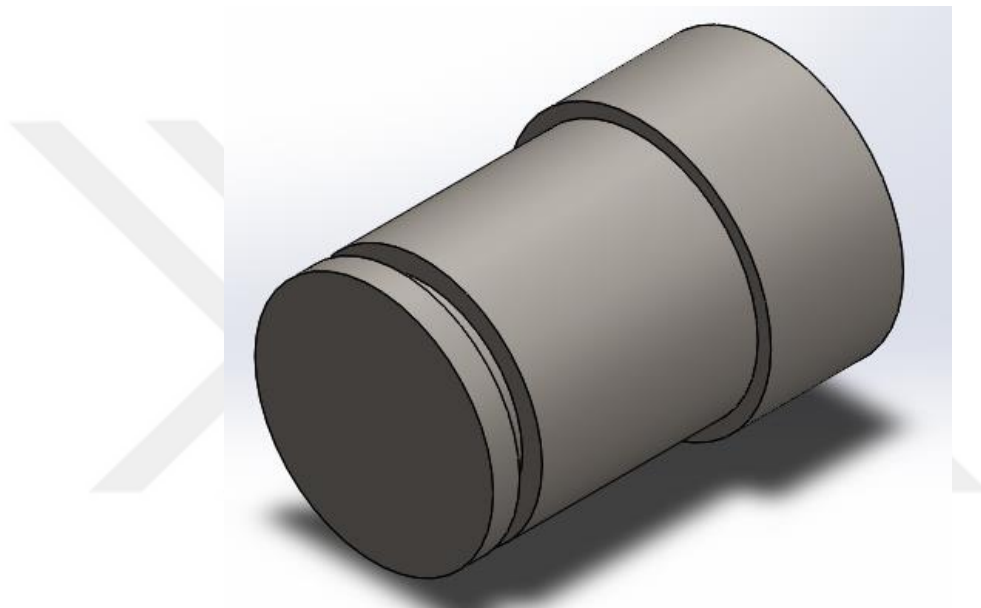


Figure 4.10: Isometric view of rhombic pin

Compression analysis result is given in Figure 4.11 and it seems not a critical element when any steel is selected at the assembly for heavy conditions. From the point of material supply, material was selected as same as gear pin which we had forecasted more critical conditions exist for.

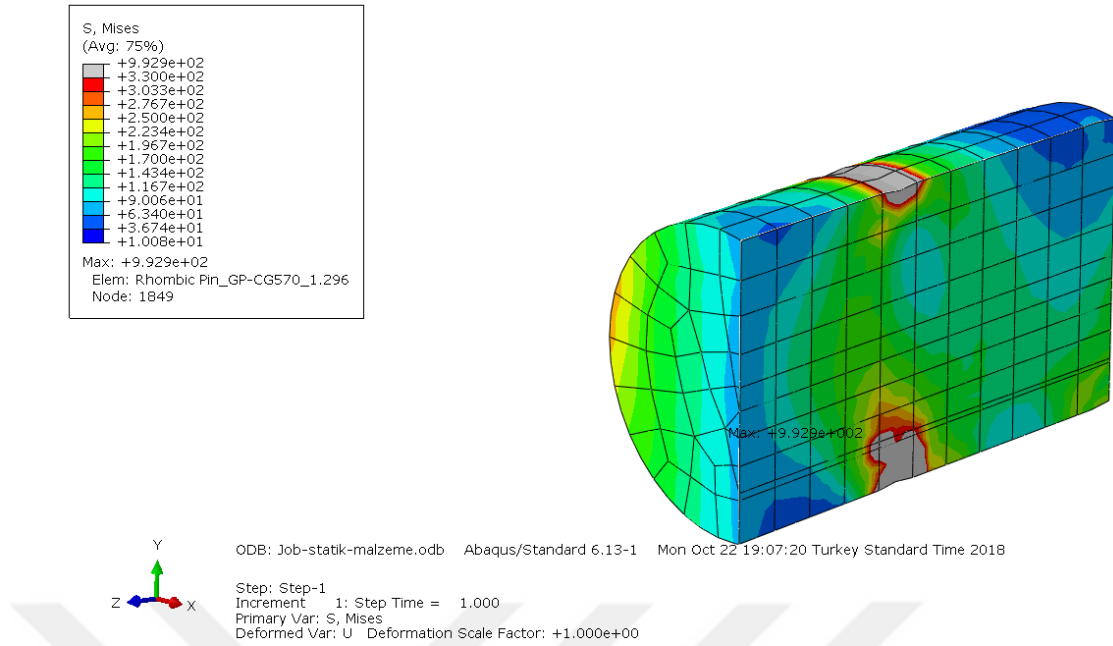


Figure 4.11: Compression analysis of rhombic pin

4.1.4 Gear Pins

Gear pins are different from the rhombic pins only at lengths. Due to gear thickness gear pin is a bit longer and shrink fitted on the gear with impregnated oil bushing. According to static and dynamic analysis at CAE, gear pins were the most critical components to carry the loads and different stresses. The pins provide freely rotation of the rhombic links while blocking translational motion of the rhombic links with its inserted retaining ring onto the groove. Gear pin is shown in Figure 4.12.

Compression pressure was obtained as shown in Figure 4.13. Material was selected which had physical and mechanical properties such as given in Table 4.3.

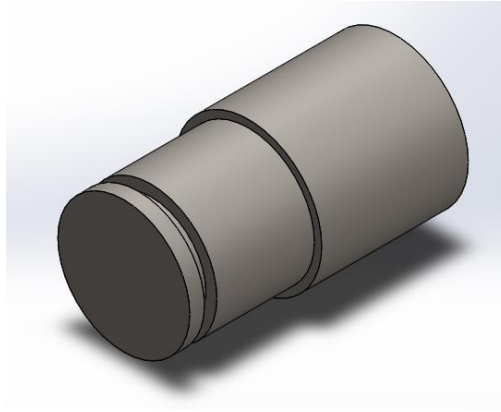


Figure 4.12: Isometric view of gear pin

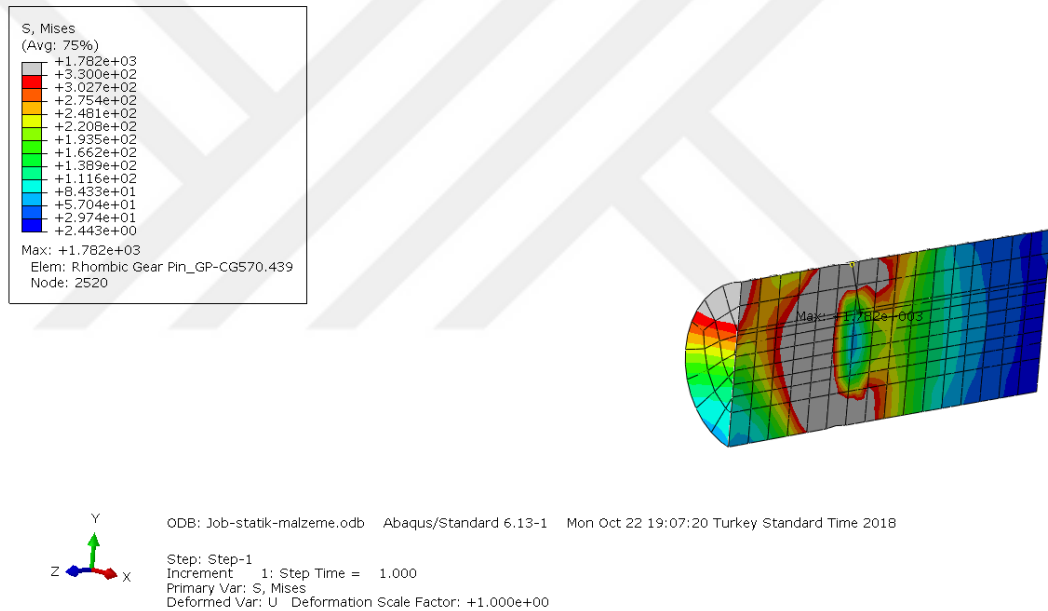


Figure 4.13: Compression analysis of gear pin.

Tablo 4.3: 4340 normalized steel physical and mechanical properties.

Density	$7.85 \times 10^3 \text{ kg/m}^3$
Thermal Expansion	$1.23 \times 10^{-5} \text{ K}$
Poisson's Ratio	0.32
Elastic Modulus	205 GPa
Shear Modulus	80 GPa
Tensile Strength	1110 MPa
Yield Strength	710 MPa

Material of the rhombic pin was also determined 4340 normalized steel same as gear pin.

4.1.5 Gears

Reciprocating motion of the piston were converted into rotational motion with two rhombic links and these rhombic links were seated on the gear pins which were shrink fitted on two engaged gears. The gears are helical to transmit more power smoothly at high speeds and reduce noise because of the gradual engagement. Thanks to this operation and connections, drive mechanism gains friction advantage between piston and cylinder wall which causes less lateral forces inside the cylinder.

Each helical gear was seated onto two ball bearings to increase their stiffness on the housing. Gear sizes were determined w.r.t. rhombic drive kinematics. Design properties of the gears are shown in Table 4.4. Left hand (LH) side and right hand (RH) side gears have identical pitch diameters, teeth and module but shaft lengths are different. LH side gear shaft is shorter and shown in Figure 4.14. RH side gear shaft was used as an output shaft of the engine and extended to out of the housing. RH side gear is shown in Figure 4.15. To keep less crankcase volume inside the housing, shaft integrated gear was designed as a unique component and so assembly constraints were reduced.

A keyway was machined onto the RH side gear shaft to set a shrink fitted square key for providing correlated rotational motion of engine output shaft and flywheel and pull start pulley. Also onto lateral axis of the RH side gear shaft, a thread was settled to insert a set screw to prevent longitudinal motion of flywheel over the shaft when loaded with dynamometer.

Cemented steel was used as a material and both gears were heat treated.

Table 4.4: Design properties of gears.

Number of teeth	48
Module	1.5
Pitch circle (mm)	77.67
Pressure angle	20°
Gear thickness (mm)	10
Shaft diameter (mm)	15

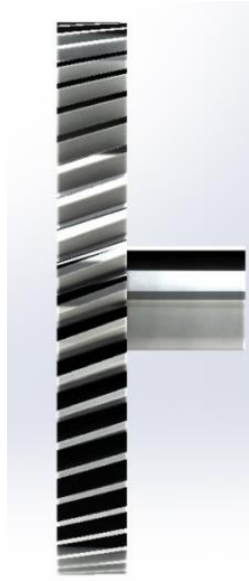


Figure 4.14: Right view of LH helical gear

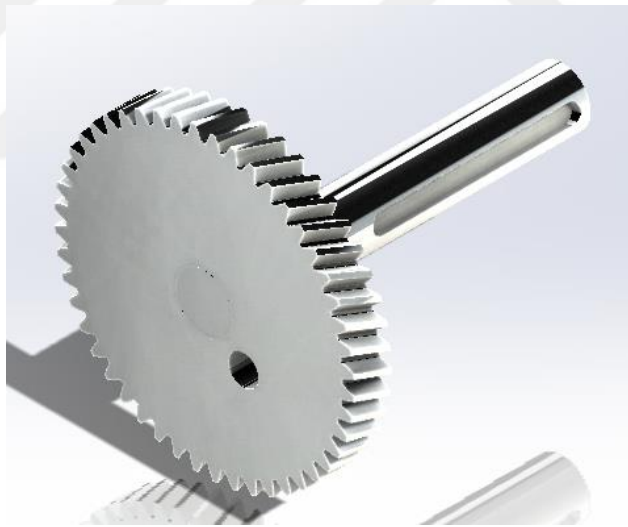


Figure 4.15: Isometric view of RH helical gear

4.1.6 Housing and Cover

Housing and cover were used for mainly fuel and air mixture to provide them crankcase volume at intake when engaged as being on slider-crank mechanism in conventional two-stroke engines and surroundings of the drive mechanism.

Assembled housing and cover is shown in Figure 4.16. Top surface of the housing and cover provide connection with cylinder by means of inserted helicoils which are preferred generally on aluminium to avoid thread damage.

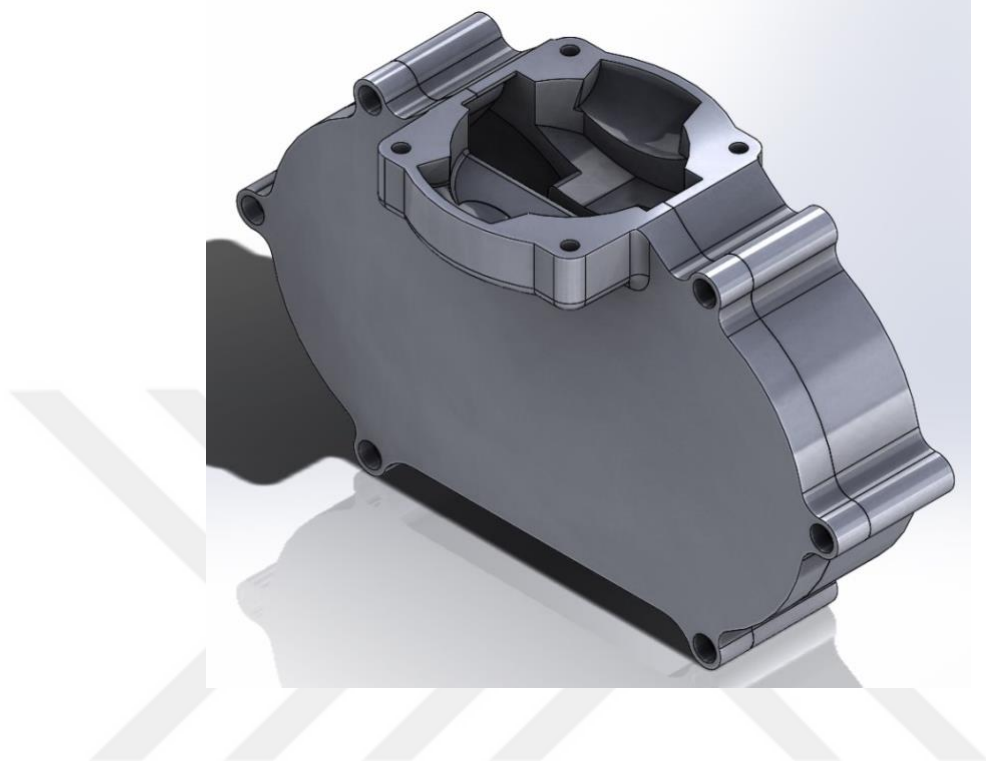


Figure 4.16: Isometric view of assembled housing and cover.

According to CAE analysis it was observed that housing and cover loads were not so critical and so they were optimized with material reduction method to reduced mass and lighter material was selected as soon as possible. As a result aluminium 6061 alloy was used for both component. Material properties are given in Table 4.5.

Table 4.5: Al 6061 alloy properties.

Density	$2.7 \times 10^3 \text{ kg/m}^3$
Thermal Expansion	$2.4 \times 10^{-5} \text{ K}$
Poisson's Ratio	0.33
Elastic Modulus	69 GPa
Shear Modules	26 GPa
Tensile Strength	124.084 MPa
Yield Strength	55.1485 MPa

Housing carries nearly all components' loads on its bearings. Housing is shown in Figure 4.17. Helicoils were also used on the housing to assemble and disassemble the cover easily for a long time.

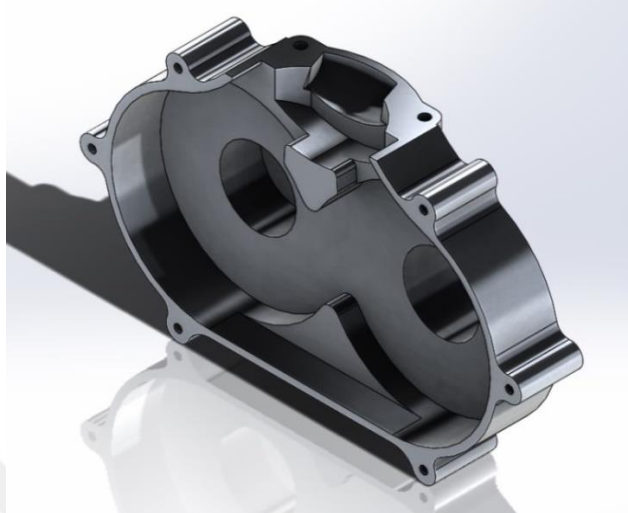


Figure 4.17: Isometric view of housing internal surface.

Cover was designed to construct a close form for crankcase volume while ensuring minimal sizes and preventing fuel or air leakages to outside of it (Figure 4.18).



Figure 4.18: Isometric view of cover internal surface

4.1.7 Housing Connector

Housing connector is a kind of spacer between housing - cover assembly and cylinder while performing as a gate for transfer ports and air fuel mixture. Also that simplifies the housing and cover construction. Besides that it makes disassembly of the connecting rod easier. Due to designing a prototype engine, that offers changing compression ratio easily for experiments. Material was selected Al 6061 alloy as being on housing and cover. Housing connector is shown in Figure 4.19 below.

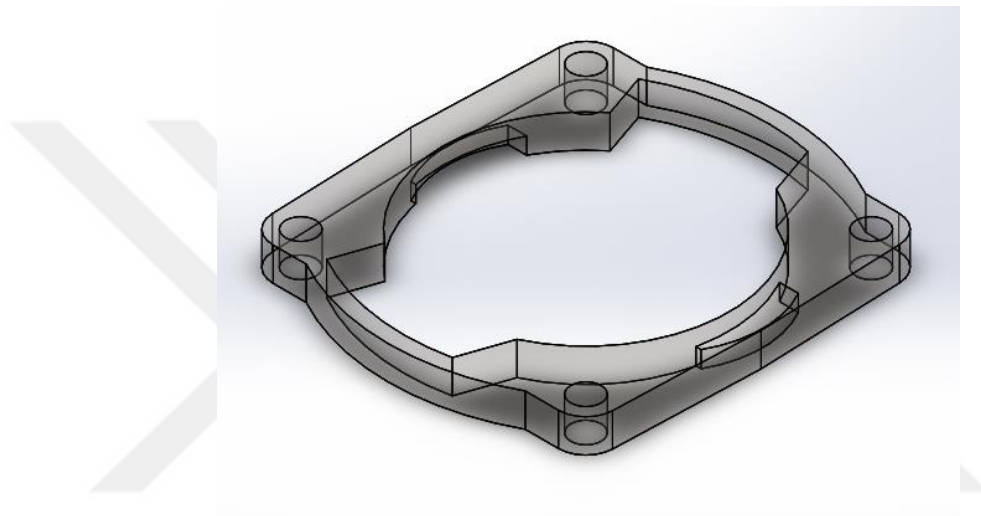


Figure 4.19: Transparent isometric view of housing connector.

4.1.8 Flywheel

Flywheel assists engine start, dynamic balancing of engines parts and it makes easier for the piston to pass dead points. At rhombic drive engine, flywheel was also used for frictional surface during the dynamometer loading at the experiments. Considering different dynamometer loading constraints, longitudinal and rotational axis braking was applied separately to observe buckling and compression strength of the flywheel in CAE software by means of finite element method. Rotational motion of the flywheel was integrated with output shaft rotation by means of a keyway set on the hub. It is shown in Figure 4.20. A set screw was inserted to the flywheel to carry longitudinal loadings over the output shaft as shown in Figure 4.21.

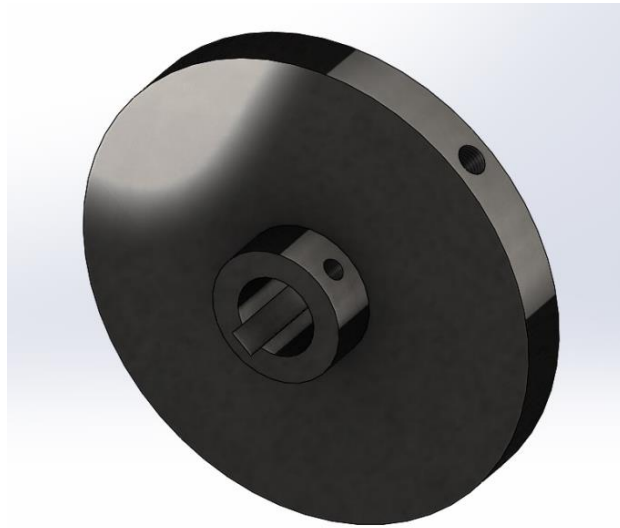


Figure 4.20: Isometric view of flywheel.

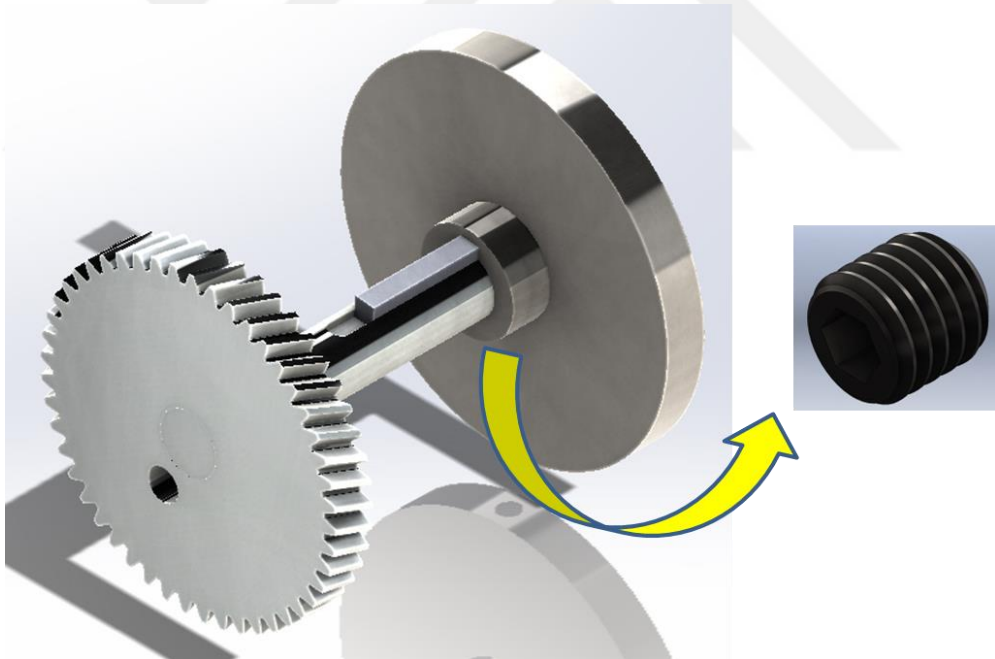


Figure 4.21: Isometric view of flywheel assembly

4.1.9 Pull Start Pulley

A simple pull start pulley and a rope were used for the first start of the engine due to designing a prototype engine. A notch was made on the circumference of the pulley to keep the rope on the pulley during the start and to be slipped after accessing wrapped rope end. The pull start pulley is given in Figure 4.22.

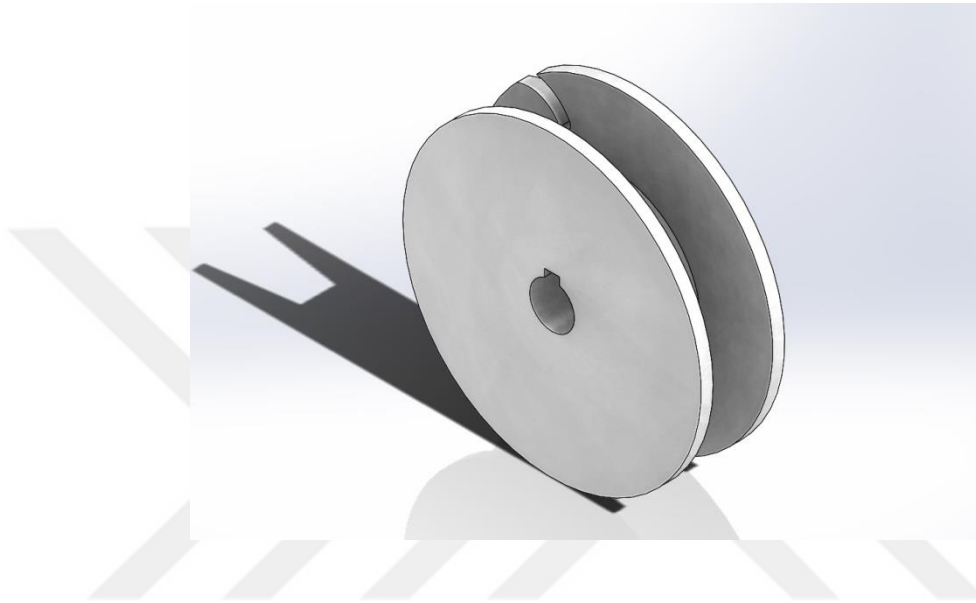


Figure 4.22: Isometric view of pull start pulley.

4.1.10 Assembly of the Designed Engine

All engine components denoted above were assembled in a sequence at CAD. A housing cap was designed to prevent leakage between output shaft and housing. A thrust ball bearing was adopted between housing cap and pull start pulley to absorb longitudinal forces arises from the loading phase at experiments. Assembly figures are shown in Figure 4.23-27.

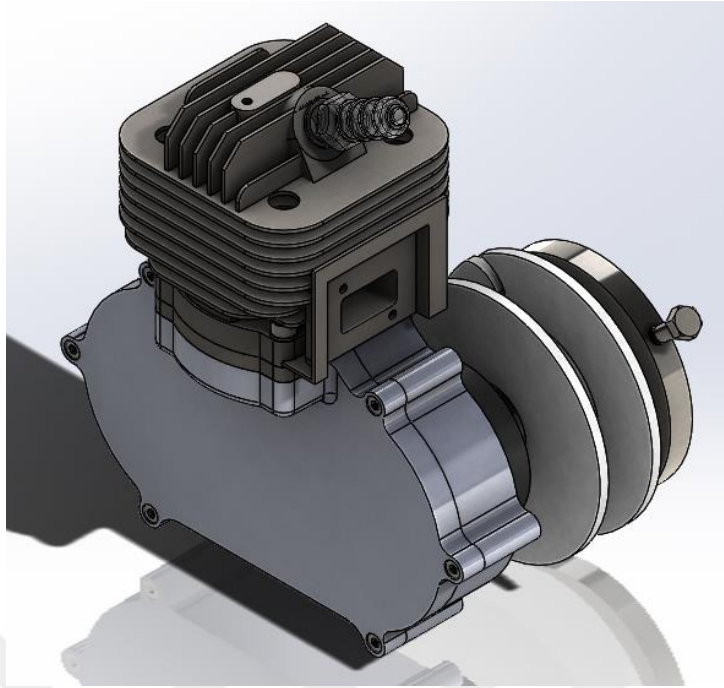


Figure 4.23: Isometric view of rhombic drive mechanism engine.

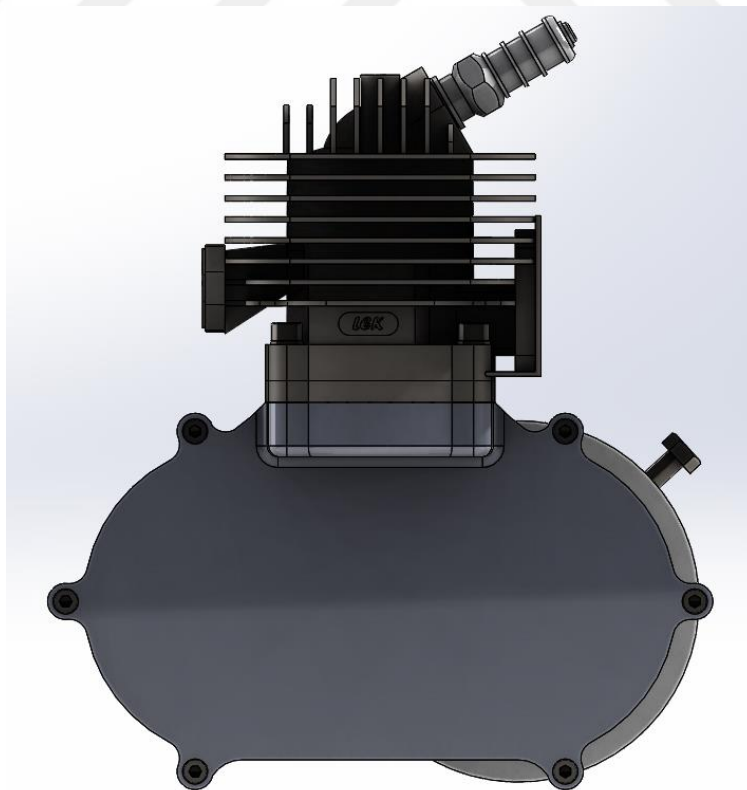


Figure 4.24: Front view of rhombic drive mechanism engine

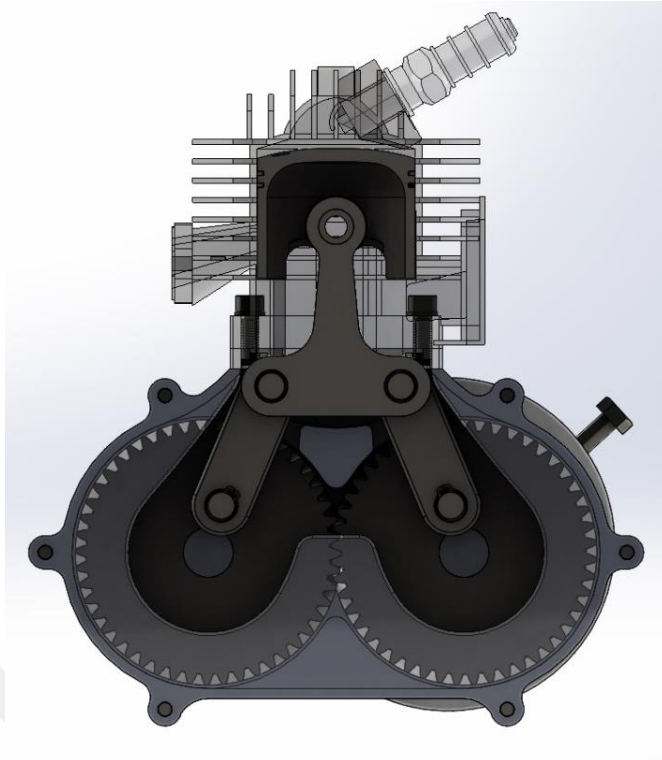


Figure 4.25: Transparent front view of rhombic drive mechanism engine

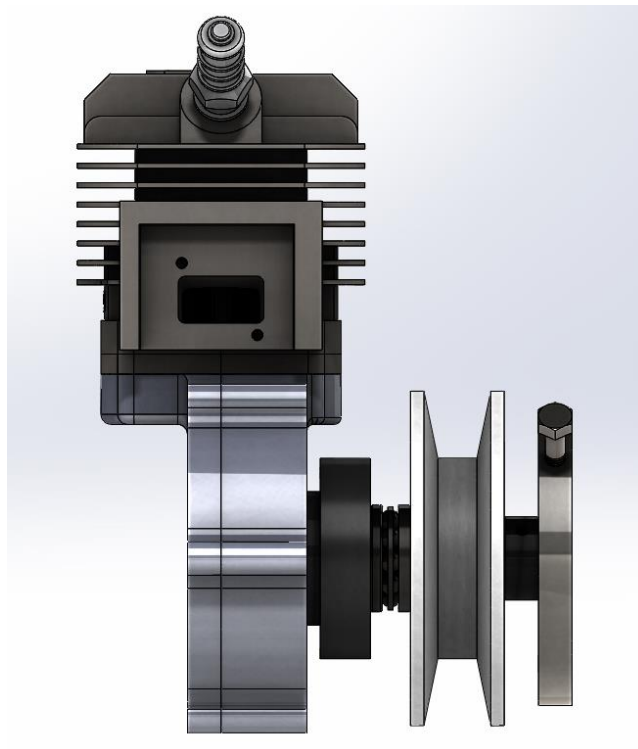


Figure 4.26: Right view of rhombic drive mechanism engine

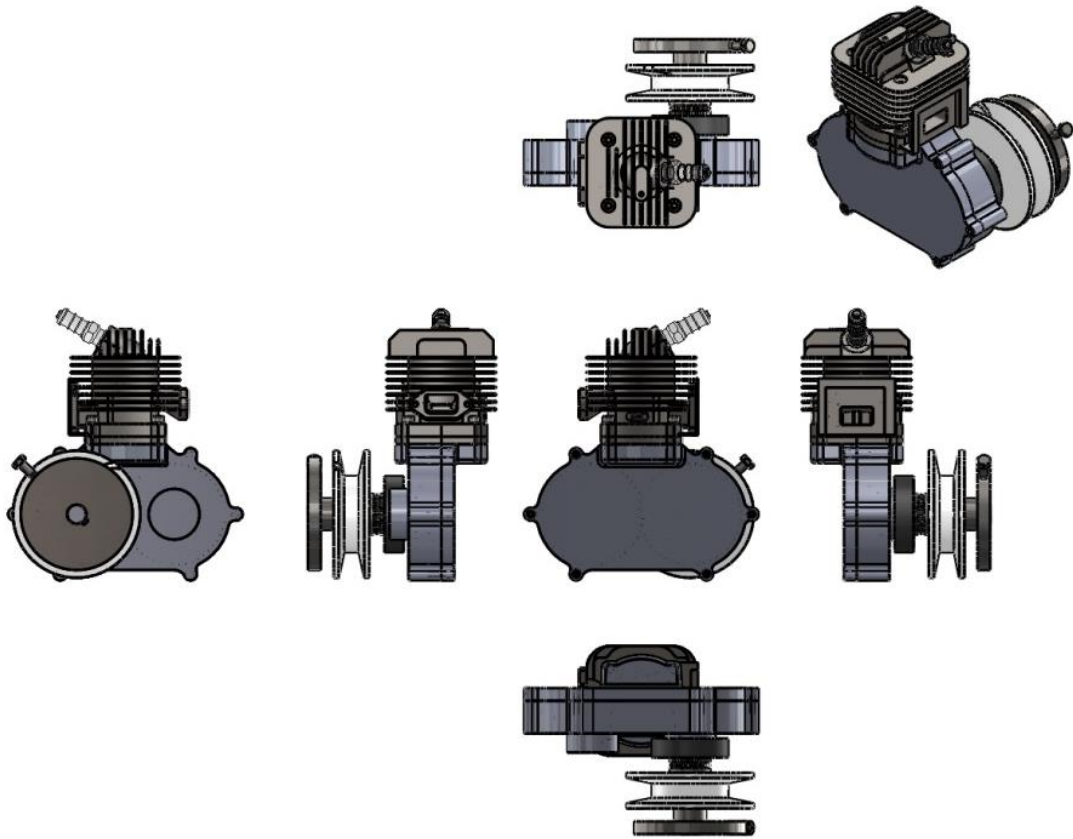


Figure 4.27: Six standard views of the rhombic drive engine at 3rd angle projection

4.2 Manufacturing of the Engine

Manufacturing process was carried out in following three categories:

- Manufactured components,
- Supplied spare components of mass production air cooled single cylinder two-stroke SI engine and lastly,
- Market components according to design requirements.

These are shown in Figure 4.28.

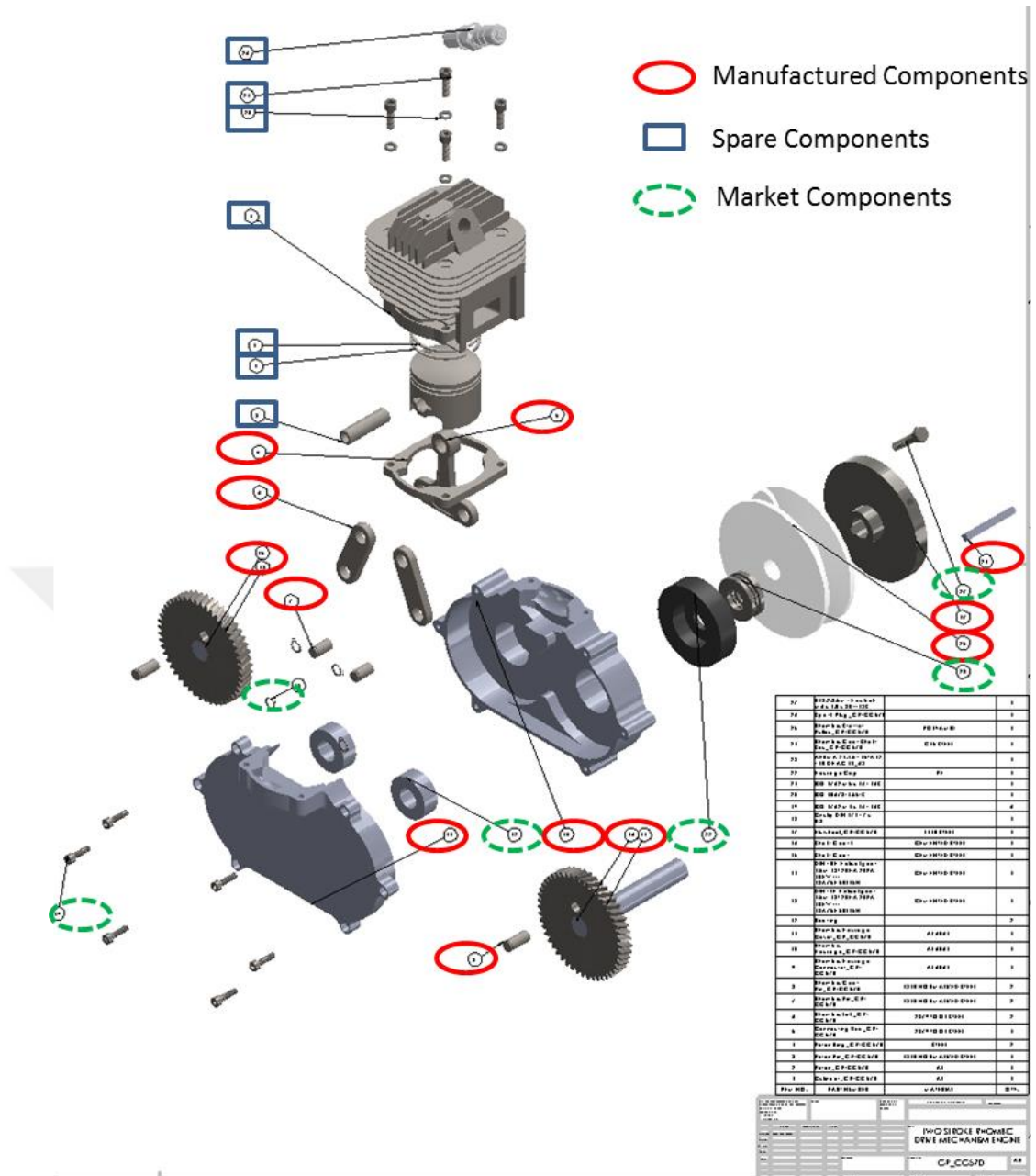


Figure 4.28: Exploded view of the rhombic drive mechanism engine

4.2.1 Manufactured Components

Manufactured parts were one connecting rod, two rhombic pins, two gear pins, two rhombic links, LH and RH side helical gears with integrated shafts, one housing, one cover, one housing connector, one flywheel, and one pull start pulley according

to rhombic drive requirements and analysis results. Some of the parts are shown in Figure 4.29-36 below. Given figures are not in true size ratios.



Figure 4.29: Connecting rod



Figure 4.30: Rhombic links



Figure 4.31: LH and RH helical gears



Figure 4.32: Housing internal surface.

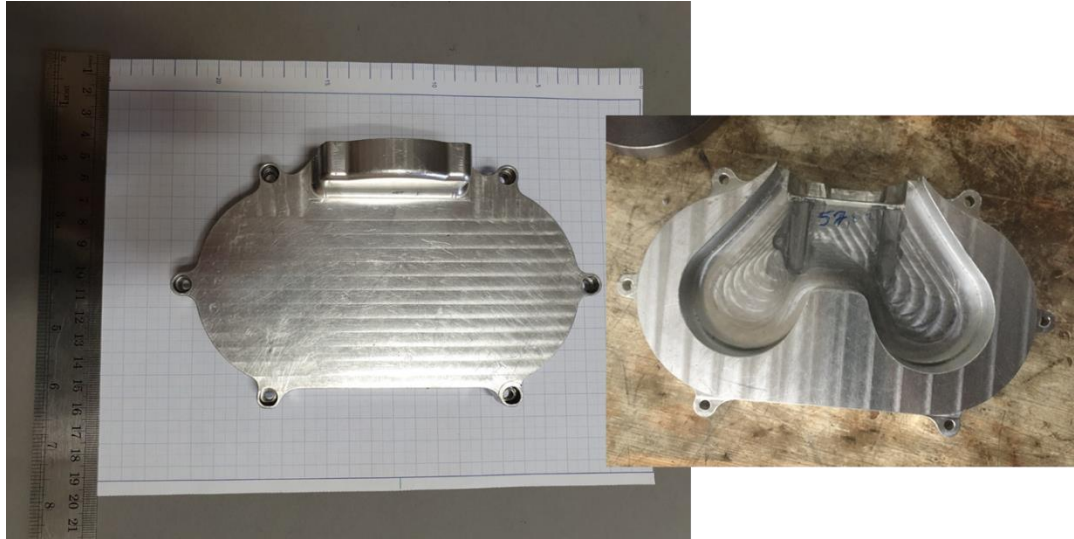


Figure 4.33: Cover external and internal surfaces



Figure 4.34: Housing connector.



Figure 4.35: Flywheel.

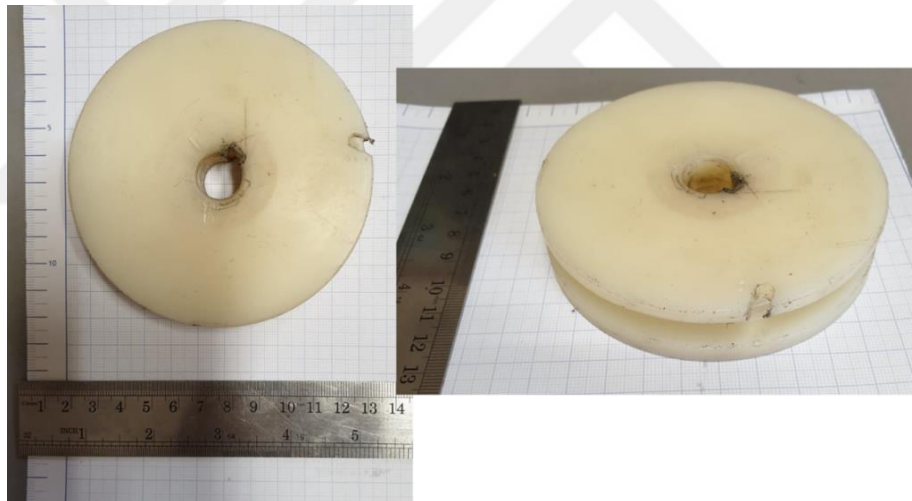


Figure 4.36: Pull start pulley.

4.2.2 Spare Components

Parts are spare component of a mass production engine such as cylinder, piston, piston pin, piston rings, spark plug, intake manifold, carburettor, and exhaust sealing. These could be found at the market Some of the spare parts are given in Figure 4.37-40.



Figure 4.37: Cylinder



Figure 4.38: Piston, piston pin, and piston rings



Figure 4.39: Intake manifold

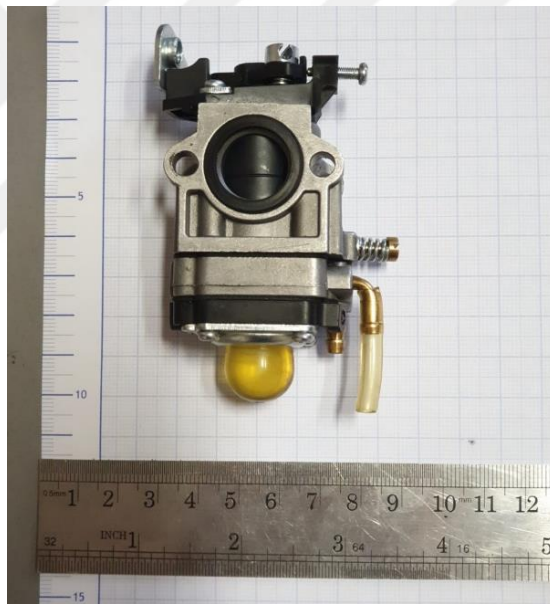


Figure 4.40: Carburettor

4.2.3 Market Components

Parts were supplied w.r.t. design such as ball bearings for gear shafts, retaining rings, bushings for rhombic pins and gear pins, housing cap, thrust ball bearing, rope,

fastening elements, and external ignition system devices. Ball bearings used for gear shafts in the housing are shown in Figure 4.41.



Figure 4.41: Ball bearings for gear shafts

All the components were assembled and construction was obtained as shown in Figures 4.42-48.

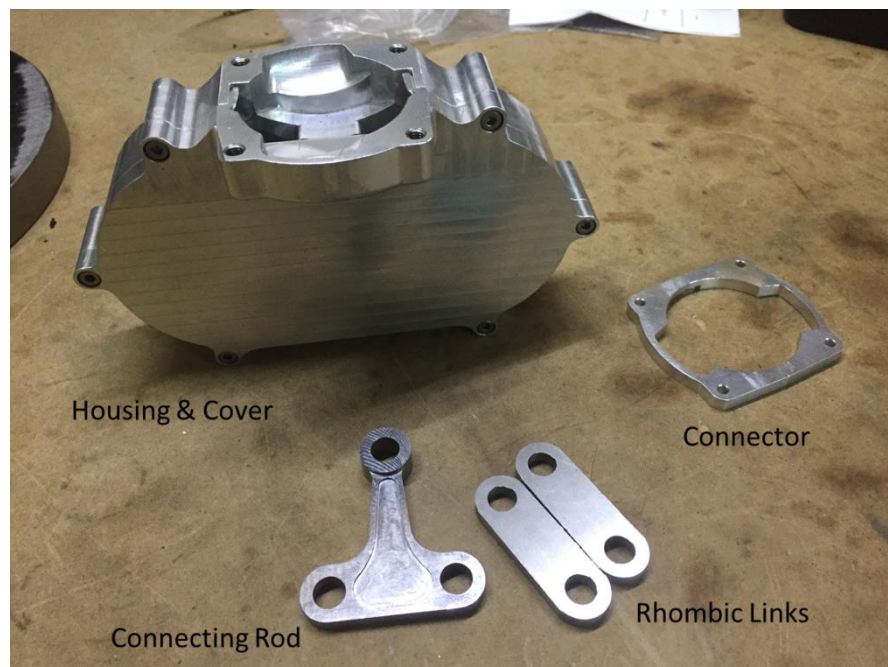


Figure 4.42: Assembled housing and cover with other parts.

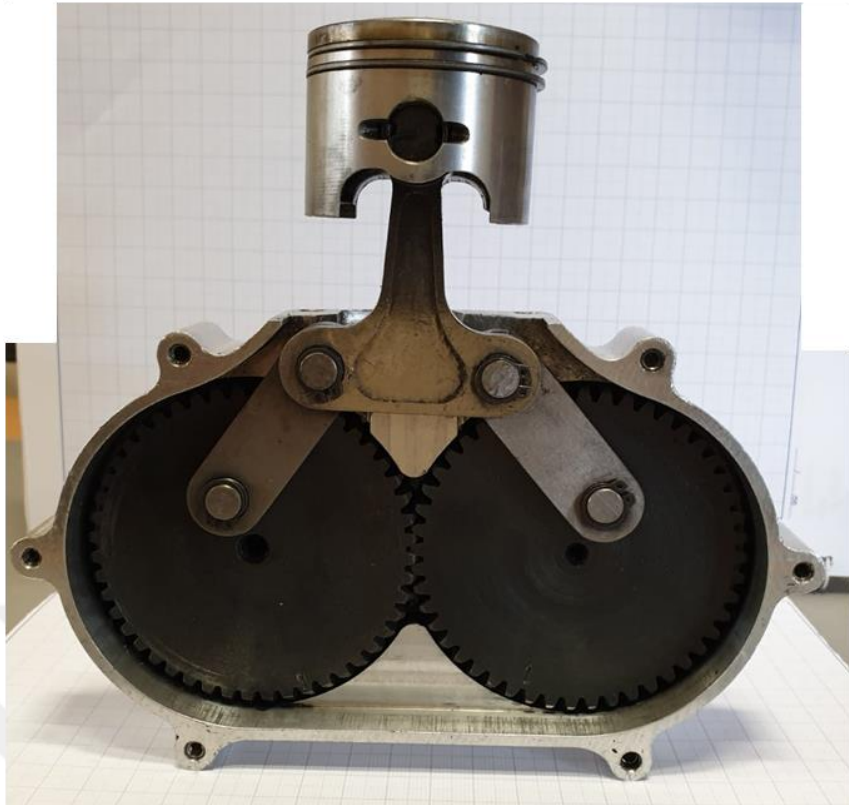


Figure 4.43: Front view of the rhombic mechanism

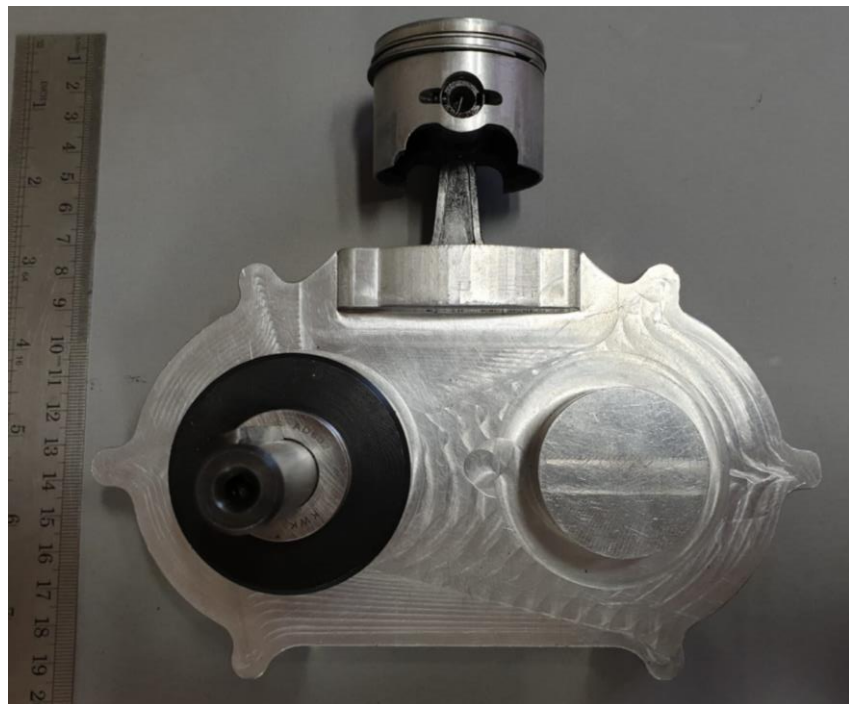


Figure 4.44: Rear view of the housing

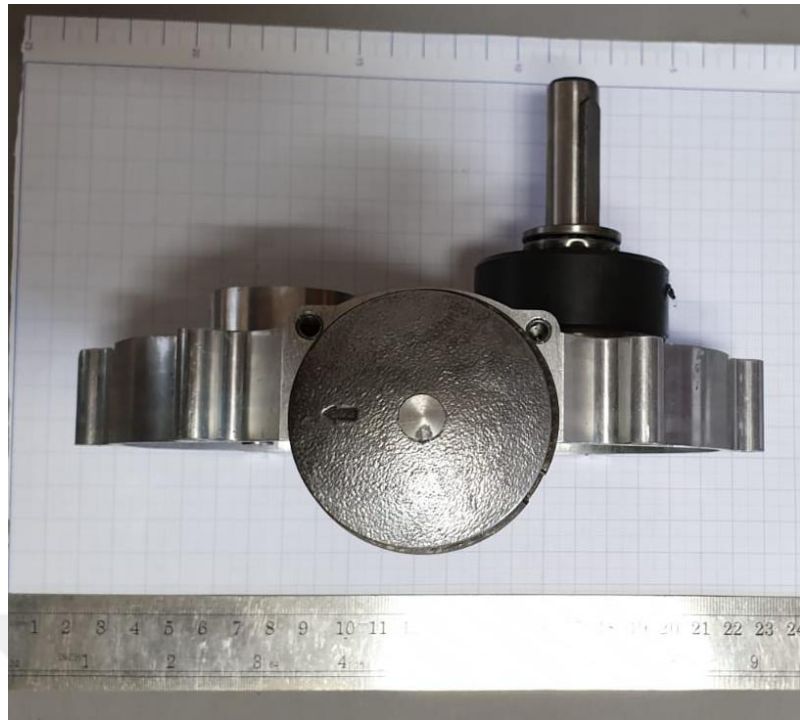


Figure 4.45: Top view of the rhombic mechanism.

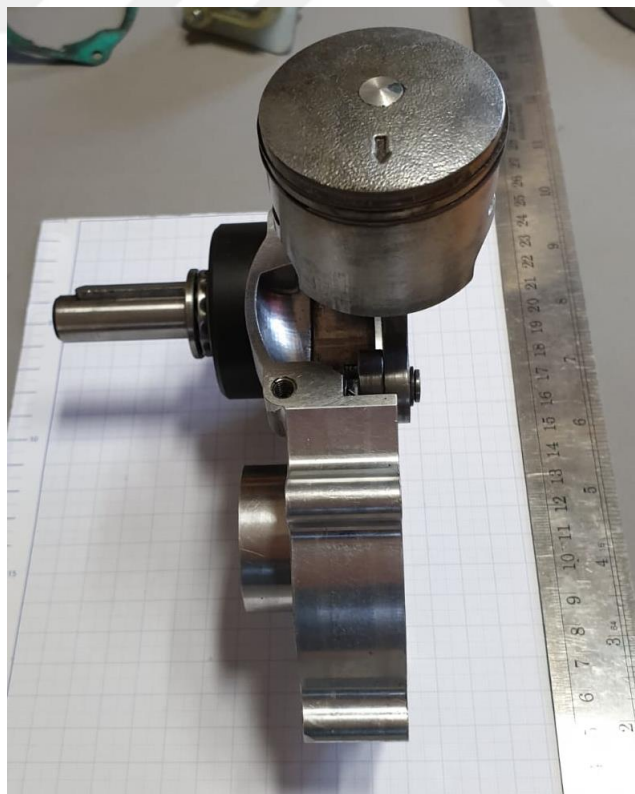


Figure 4.46: Left side of the rhombic mechanism



Figure 4.47: Isometric view of the engine.



Figure 4.48: Rear view of the engine

CHAPTER 5

EXPERIMENTAL STUDIES

Single cylinder, two-stroke spark ignition prototype engine with rhombic drive mechanism was tested to analyse its performance and emissions. In this chapter, experimental setup is introduced. General view of the setup is shown in Figure 5.1.



Figure 5.1: Experimental setup.

Firstly, to test the prototype engine, pull start pulley with 1 m length rope which was commonly used at two-stroke engines for simple first drive was adapted to the output shaft behind the flywheel. Rotation of the pulley on the output shaft with a harmony was provided by a keyset and key along the longitudinal axis of the

shaft. Due to frictional loading conditions in the experiment, a thrust ball bearing was seated onto the output shaft to absorb longitudinal forces. The pulley and the bearing are shown in Figure 5.2. Rolled on rope to the circumference of the pulley was prepared to pull manually.



Figure 5.2: Pull start pulley and thrust ball bearing on the output shaft.

Then an external ignition system was mounted to the setup. Basically this system consisted of a coil, an electronic ignition control module, a magnetic pickup sensor, 12 V battery and connection cables. Circuit components of the ignition system are seen in Figure 5.3.

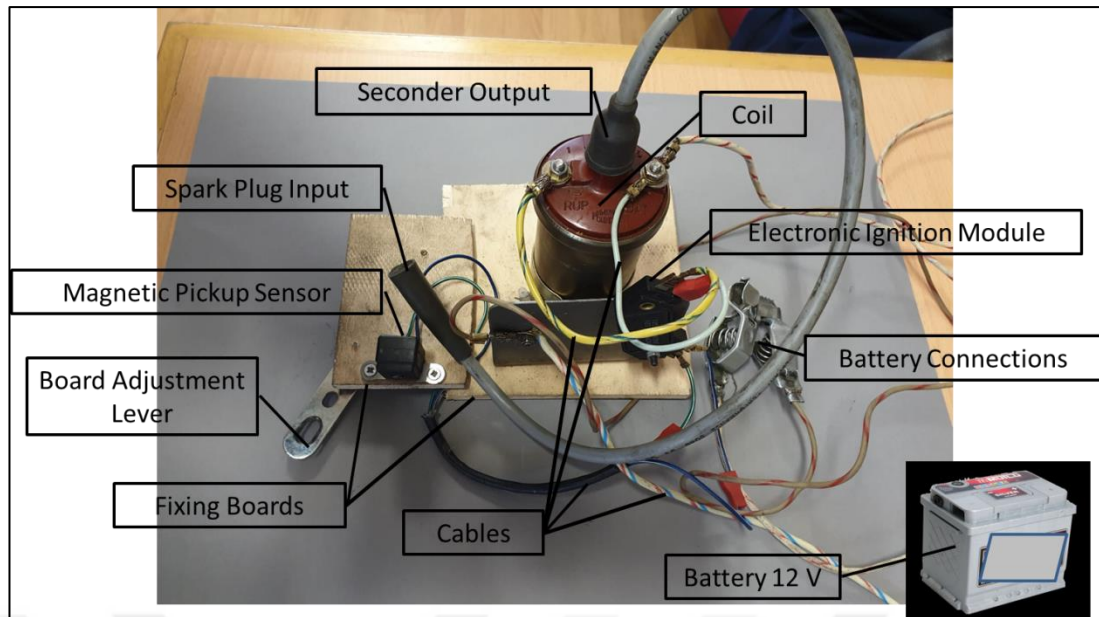


Figure 5.3: Circuit components of the ignition system.

The flywheel was drilled and threaded to insert a screw which was used for measurement of engine speed and external ignition system impulse as shown in Figure 5.4. We adjusted the ignition advance on the fixed 18° crank angle bTDC.



Figure 5.4: Initiator for magnetic pickup sensor and engine speed measurement sensor.

Magnetic pickup sensor was activated with magnetic field changing by means of the inserted screw to the flywheel. UNIPOINT 12 V UNI0810 G01 electronic ignition module was used to control ignition.

Settlement of the ignition system on the experimental setup is shown in Figure 5.5.

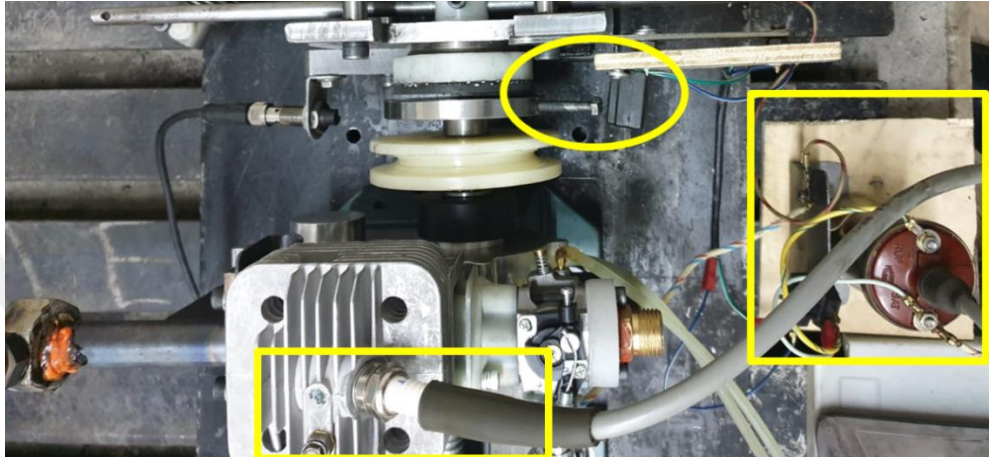


Figure 5.5: Settlement of the external ignition system on the setup.

Experiments were planned to carry on $\frac{1}{4}$ throttle loading at the beginning due to observing engine behaviour and working conditions. We used selected engine throttle and fixed to the $\frac{1}{4}$ loading shown in Figure 5.6.

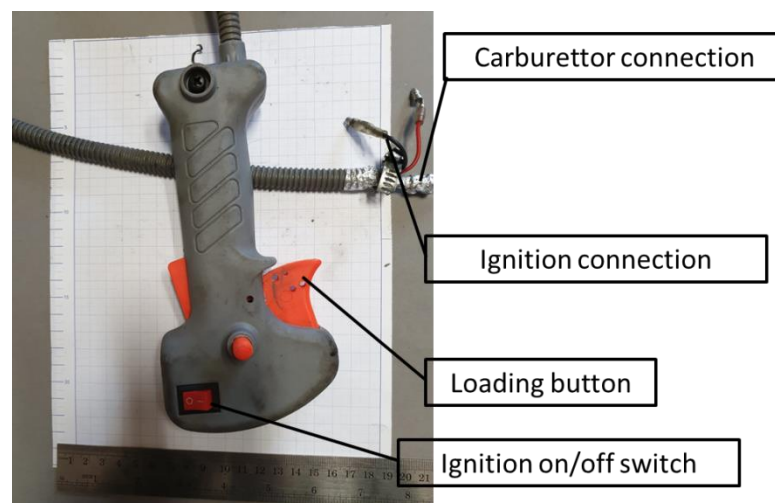


Figure 5.6: Throttle adjustment system

5.1 Dynamometer

Engine torque is normally measured with a dynamometer which has electromagnetically, hydraulically, or mechanical friction to brake rotated engine. The engine is clamped on a test bed and the shaft is connected to the dynamometer rotor. Rotor stationary is balancing the stator. When rotor is rotated torque exerts to the stator and measured with weight, springs or pneumatic means as shown in Figure 5.7 [44].

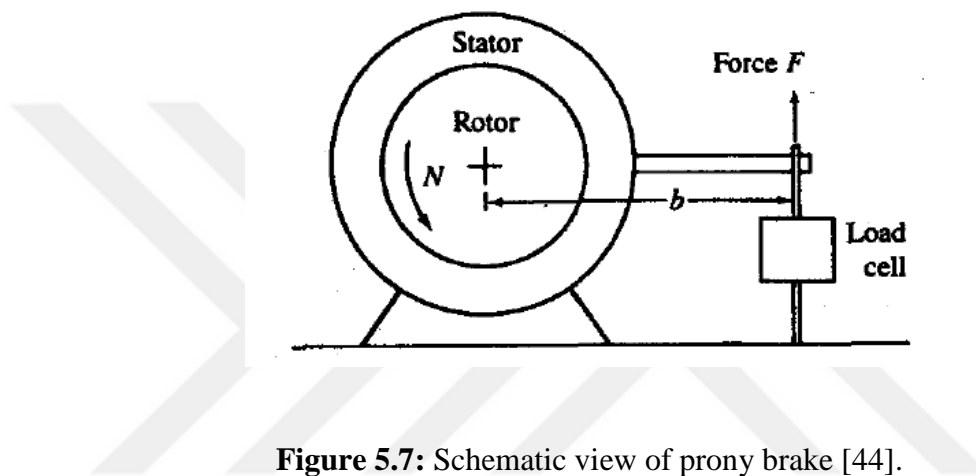


Figure 5.7: Schematic view of prony brake [44].

Prony brake dynamometer absorbs energy in a mechanical friction brake to measure engine torque. Prony brakes have simple loading and measurement methods.

Prony type dynamometer mainly consisted of a loading brake system, a load cell for measurement of the mass, and a force arm. Also over the dynamometer there was an engine speed measurement sensor which took the impulse from the inserted screw to the flywheel shown at external ignition system before. Loading was accomplished with the loading wheel. Friction brake was seated onto two ball bearings along the longitudinal axis and translational motion was performed on four bars. There was a machine vice to mount the engines. Machine vice and dynamometer bench were mounted to the bench tracks for fixing. When friction brake is contacted to the engine, force arm starts to apply force to the load cell. Force arm from the midpoint was fixed and balanced onto the friction brake shaft with a screw. The dynamometer is shown in Figure 5.8.

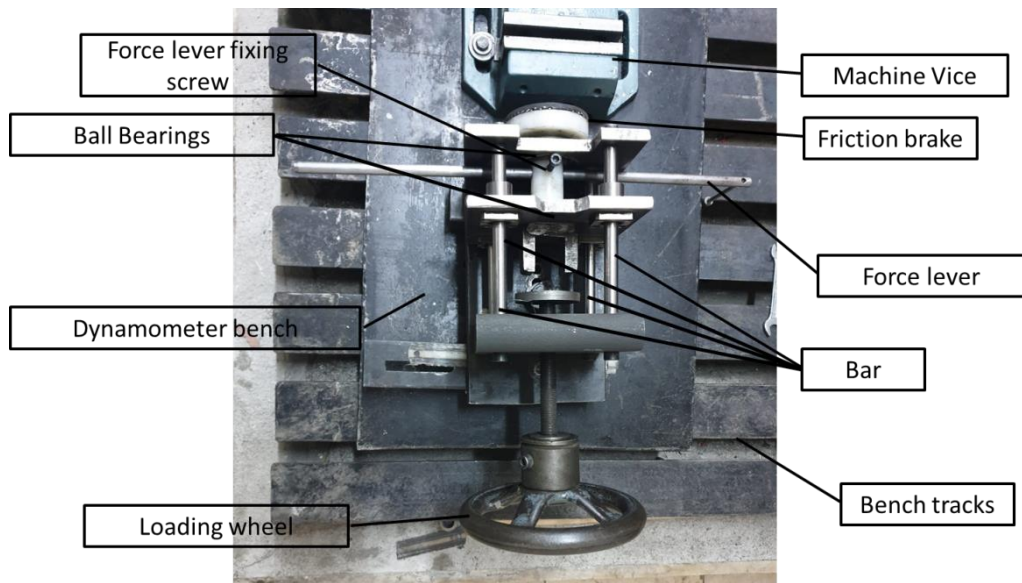


Figure 5.8: Prony type dynamometer

The load cell is ESIT BB model which has 20 kg measurement capacity and 1 g measurement precision. A 0.2 m length force arm was used to calculate torque. The device and the arm are shown in Figure 5.9 and in Figure 5.10.

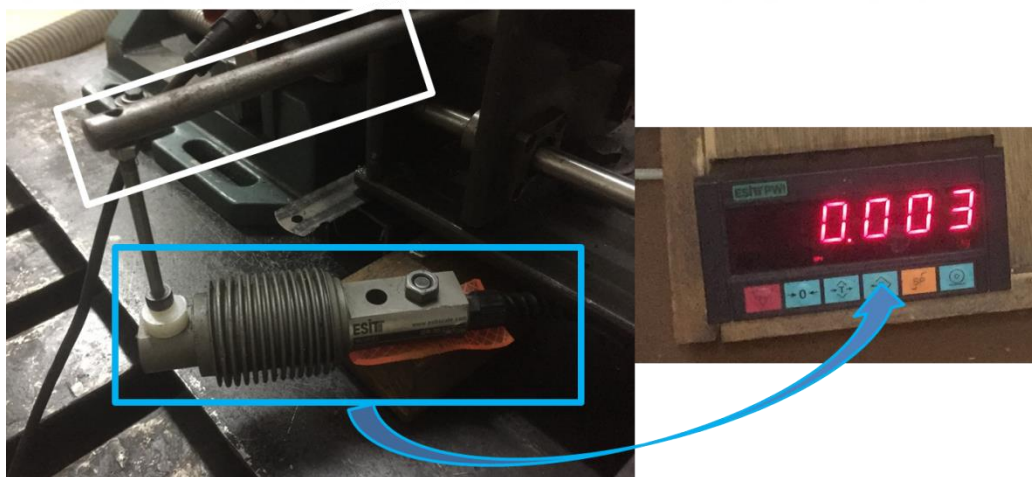


Figure 5.9: Load cell and force arm

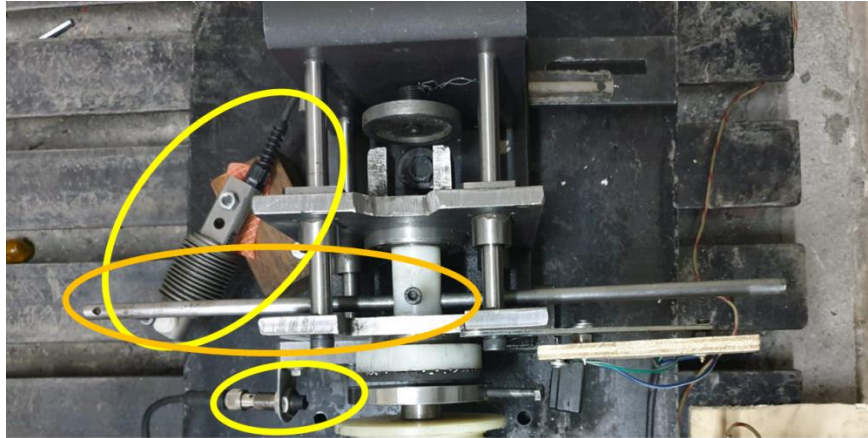


Figure 5.10: Layout of the load cell, force arm and engine speed sensor

Engine was mounted to the machine vice with a plate to prevent damage on the housing and cover of the engine. The plate is shown in Figure 5.11

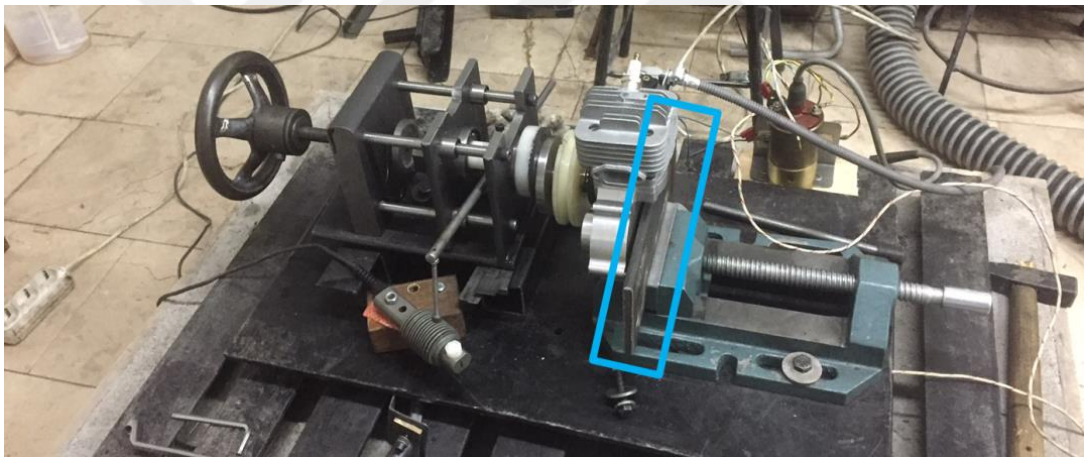


Figure 5.11: Engine mounting to the machine vice

Engine speed sensor sends the signal to a tachometer, ENDA, and this impulse of the engine is converted rotational speed in rpm. The tachometer is shown in Figure 5.12



Figure 5.12: Engine tachometer

5.2 Measurement of Fuel Consumption

Engine fuel consumption was measured with a 0.1 g precision CAS ED-H model electronic scale (Figure 5.13). Stopwatch was used for the consumption rate in seconds.



Figure 5.13: CAS ED-H model electronic scale

5.3 Exhaust Emission Device

Muffler of the engine was removed and to measure emissions, an exhaust duct was produced. Emission device probe was inserted to the duct and sealing was provided. A UEGO Lambda sensor was adopted to the duct. Engine exhaust emissions were observed with Bosch exhaust gas analyser. CO, CO₂, HC, NO, lambda and O₂ could be measured. Exhaust duct and device are shown in Figure 5.14 and Figure 5.15, respectively.

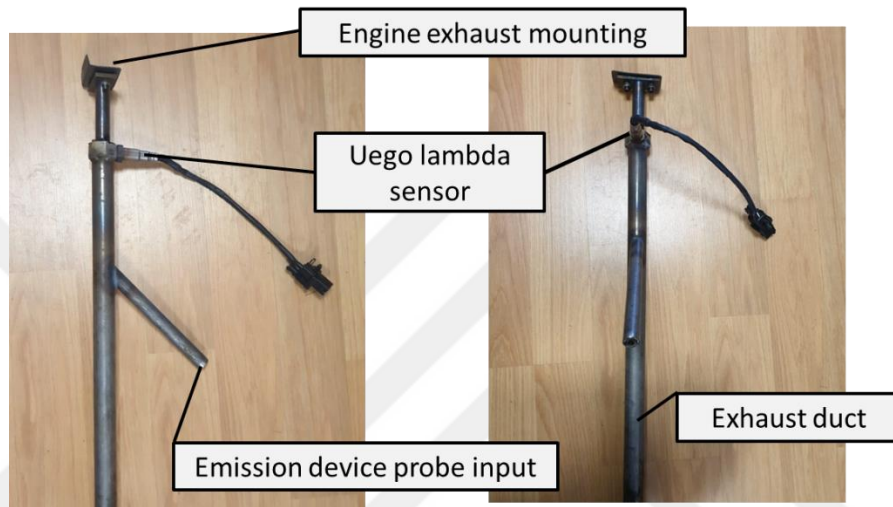


Figure 5.14: Exhaust duct and sensor inputs.

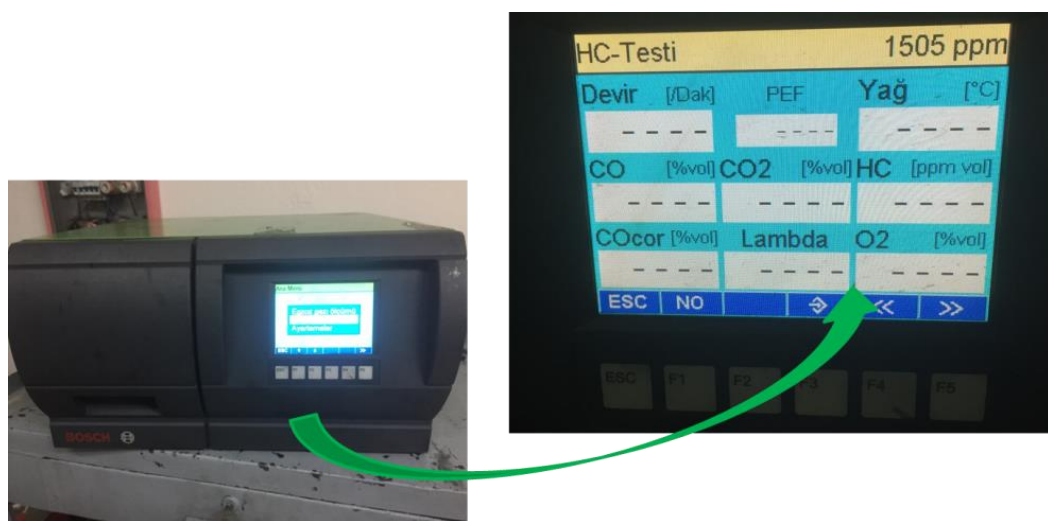


Figure 5.15: Bosch exhaust gas analyser.

In Table 5.1, technical properties of the used exhaust analyser device are given below.

Table 5.1: Technical properties of Bosch BEA350 exhaust analyser device [55].

Parameter	Measurement Range	Accuracy
CO [% volume]	0 – 10	0.001
HC [ppm]	0 – 9999	1
NO [ppm]	0 – 5000	≤ 1
CO ₂ [% volume]	0 – 18	0.01
O ₂ [% volume]	0 – 22	0.01
Lambda	0.5 – 9.9999	0.001

5.4 Temperature Measurement

Due to being a prototype engine, interior fan was not designed and so to provide enough cooling external fan was used that is shown in Figure 5.16



Figure 5.16: External cooling fan

Exhaust duct temperature was followed with an inserted temperature probe into the duct. Also cylinder temperature was measured with a probe contacting near side of the combustion chamber among the cooling fins. Temperature measurement device is shown in Figure 5.17.



Figure 5.17: Temperature measurement device

Experimental setup measurement accuracies and uncertainties are given in Table 5.2.

Table 5.2: Accuracy of the measurement and the uncertainty in the calculated result [56].

Accuracies and uncertainties	
Load (g)	Accuracy= ± 0.1
Speed (rpm)	Accuracy= ± 1
Temperature ($^{\circ}\text{C}$)	Accuracy= ± 2
Torque (Nm)	Uncertainty= $\pm 0.1\%$
Power (W)	Uncertainty= $\pm 1\%$

CHAPTER 6

RESULTS AND DISCUSSION

This chapter is planned to evaluate results of thermodynamic analysis and experiments for designed and manufactured engine. Thermodynamic analysis were performed on a developed Matlab software program and

- Pressure - Volume,
- Pressure - Crank Angle,
- Piston Force - Crank Angle,
- Volume - Crank Angle,
- Stroke - Crank Angle,
- Temperature - Crank Angle,
- Net Work - Crank Angle,
- Heat - Crank Angle
- Cumulative Heat - Crank Angle
- Convection Heat Transfer Coefficient - Crank Angle

relations were obtained for the designed single cylinder, two-stroke SI engine with rhombic drive mechanism and the selected mass production engine from the market. At the program engine speed was taken 3500 rpm. Results were compared.

On the other hand, second parts of the chapter, experimental results are given which were carried out on a fixed ignition advance, 18° crank angle bTDC, and engine speed at the range 1700 to 3000 rpm. Torque, power and fuel consumption w.r.t. engine speeds are evaluated. Exhaust emissions such as CO, HC, NO and CO₂, are given.

6.1 Evaluation of the Thermodynamic Analysis

Thermodynamic cycles are completed in one revolution of crank shaft in two-stroke engines and position changing of the piston inside the cylinder is defined according to crank angle (CA). At rhombic drive engine crankshaft was removed instead, gear and link mechanism was inserted. Gear position changing w.r.t.

revolution is also called crank angle to compare designed engine with the conventional selected engine for preventing ambiguity.

Both engines total cylinder volume were nearly same (57.96 cc for slider-crank mechanism engine and 57.98 cc for rhombic drive engine). Cycles were assumed that starting from the BDC for both engines. Due to the designed purpose of two-stroke engines, compression and expansion strokes occur during the piston reciprocating motion between BDC and TDC. That's is why power output is two times more than the four-stroke engines theoretically. But in reality that is not possible mostly with charging cases. Piston motion towards to TDC compresses the charged air fuel mixture and also previous cycle residual gases stem from blowdown to combustion chamber.

Process durations were taken same but due to velocity differences on the mechanism, piston speed was lower at rhombic mechanism. That means charging of the rhombic mechanism takes more time w.r.t. slider-crank mechanism. But compression was dedicated for a shorter time at the same case due to accessing to the TDC with a higher speed. Slider-crank mechanism arrived TDC at 180° CA while rhombic was 212° CA. Maximum velocities of the engines were obtained as usual at point where acceleration was zero. Maximum instantaneous piston velocity was at the 75° CA and 284° CA with 6.69 m/s for slider-crank mechanism on the other hand 72° CA and 286° CA 5.67 m/s for rhombic drive mechanism. Max acceleration was 3038 m/s^2 for slider-crank mechanism but 2690 m/s^2 for rhombic drive mechanism. These are shown in Figure 6.1 (a) (b) and (c), respectively.

Volume crank angle changing diagram was obtained in developed Matlab program as shown in Figure 6.2. Due to the mechanism difference, piston arrived 32° CA later to the TDC at rhombic drive mechanism.

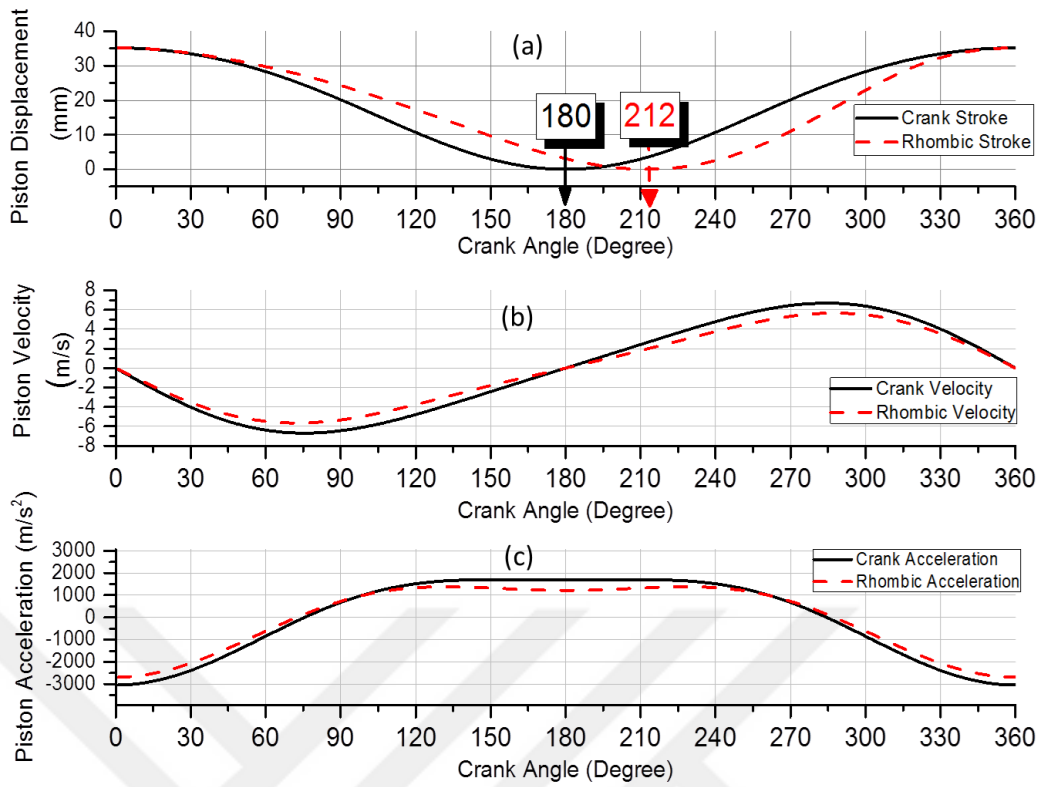


Figure 6.1: Piston displacement, velocity, acceleration-crank angle diagrams

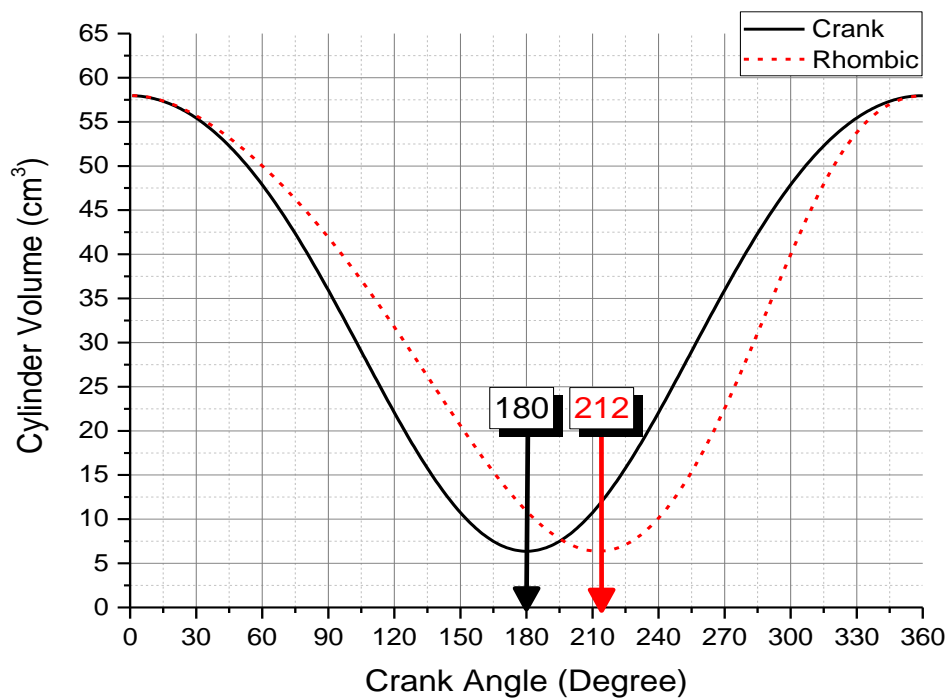


Figure 6.2: Volume-crank angle diagrams

Figure 6.3 and Figure 6.4 show indicated cylinder pressure w.r.t. crank angle and pressure change w.r.t. cylinder volume respectively. Both engine maximum pressure was obtained at 10° CA aTDC. Maximum pressure was taken at 222° CA with 4188 kPa for rhombic drive while 190° CA with 4003 kPa for crank mechanism engine. Pressure increases efficiently after exhaust port is closed. The duration between the transfer port and the exhaust port closes is defined with trapping compression ratios as a function of volume change. For rhombic mechanism trapping compression ratio was 5.44 while 5.57 for slider-crank mechanism. Geometric compression ratios were same for both engines which was 9.1.

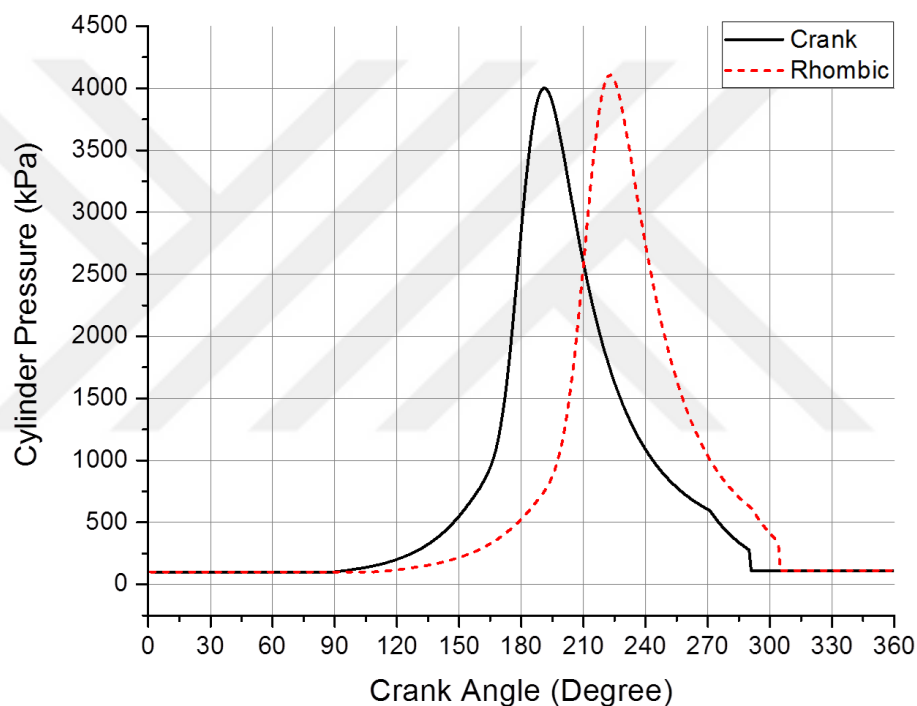


Figure 6.3: Cylinder pressure-crank angle diagram

In Figure 6.4, pressure changing w.r.t. volume was overlapped to compare the mechanism from the point of same volume ratio. It seems there are no so much difference between the two mechanisms. At rhombic drive, transfer port opening caused earlier scavenge for the exhaust gases. Duration of the expansion after the combustion end was 60° CA until exhaust port opening and 80° CA until transfer port opening at slider-crank mechanism. But at rhombic drive, duration for these were shorter which was 56° CA until exhaust port opening and 71° CA until transfer

port opening. Difference at transfer port opening duration was more than the exhaust port opening duration that is why fresh charging quantity at rhombic drive will be less but that will be compensated with shorter scavenge duration of the fresh charge through the exhaust.

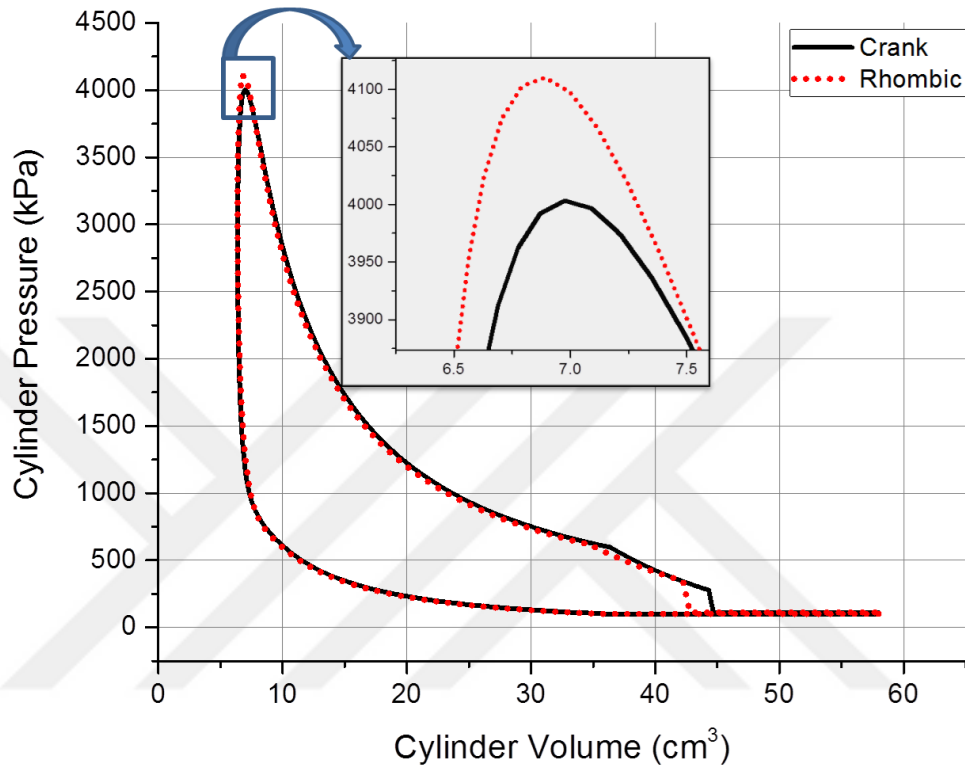


Figure 6.4: Cylinder pressure-volume diagram.

As a relation with pressure also maximum temperature was obtained at 227° CA with 2785 K for rhombic drive when we obtained 198° CA with 2746 K for slider-crank mechanism engine. Due to having less piston velocity during the expansion period, cylinder temperature will be decreased more at rhombic drive than the slider-crank mechanism engine. Temperature change w.r.t. crank angle for both engines is given in Figure 6.5.

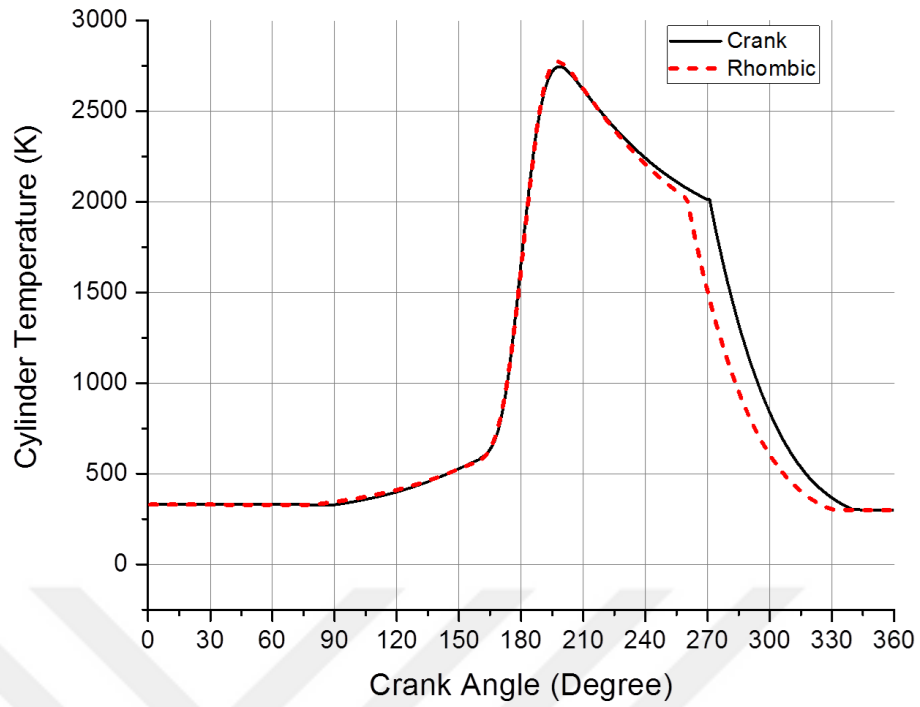


Figure 6.5: Cylinder temperature-crank angle diagram.

In Figure 6.6 net work of both engines is compared. 43.2 J was obtained from the slider-crank mechanism, whereas 42.3 J was gained from the rhombic mechanism engine in a cycle.

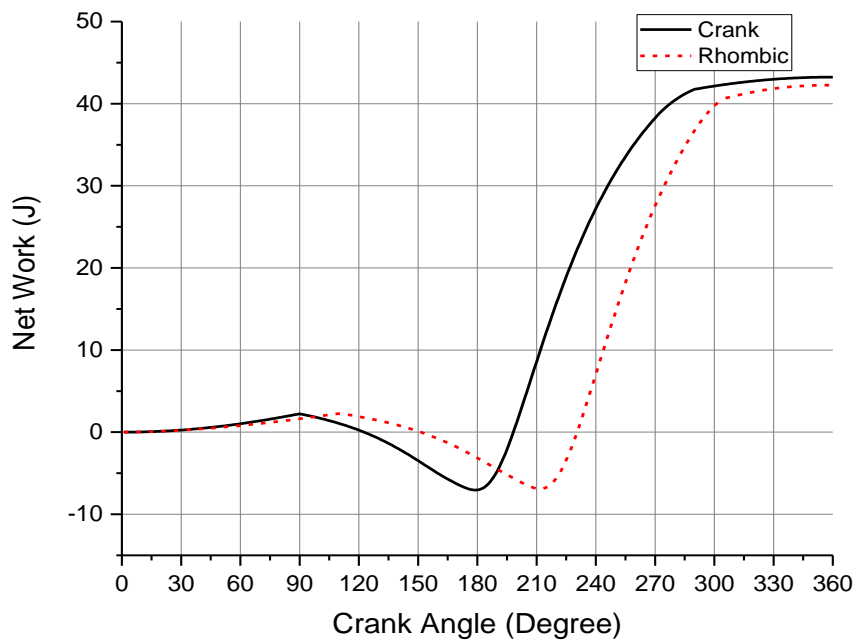


Figure 6.6: Cylinder net work-crank angle diagram.

During the combustion period, which was kept identical for each engine on the Wiebe function, heat release was considerably same. In Figure 6.7, heat release w.r.t. CA is given for both engines. Burning of the mixture was assumed 50° CA for each. Therefore, angular distribution of heat release for slider-crank and rhombic drive engine was $6.56 \text{ J}/^\circ$. Cumulative heat release at one cycle was 132.95 J . Regarding to flame speed mostly heat release occurred around the point where maximum pressure was obtained. Cumulative heat release w.r.t. angular change is given in Figure 6.8 below.

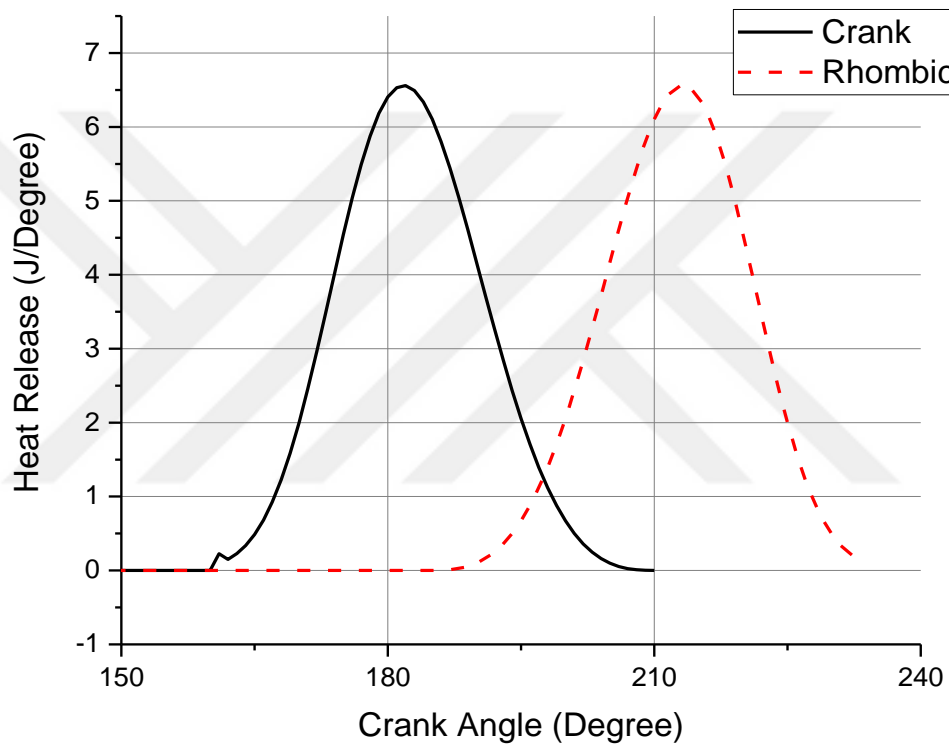


Figure 6.7: Cylinder heat release-crank angle diagram.

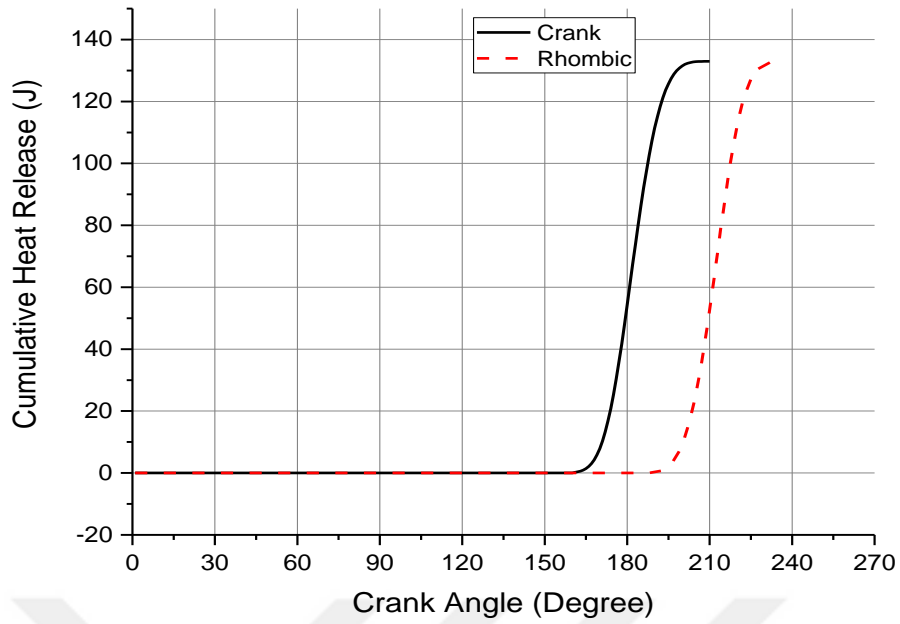


Figure 6.8: Cylinder cumulative heat release-crank angle diagram.

Due to having a bit higher maximum cylinder pressure, rhombic drive engine heat transfer coefficient was also a bit higher. This is shown in Figure 6.9. It is clear that during the expansion stroke, heat transfer coefficient reduction is a bit higher at rhombic drive which is probably stem from slower piston speed during the period.

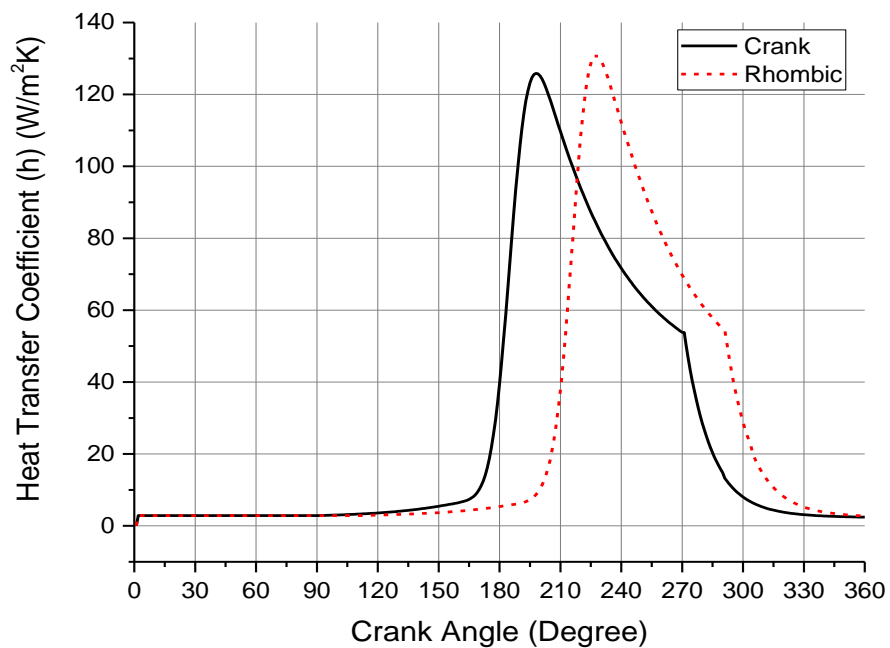


Figure 6.9: Cylinder heat transfer coefficient-crank angle diagram.

With the faster reduction in heat transfer coefficient during the expansion period of rhombic drive, as a result, heat transfer quantity was less than the slider-crank mechanism. In Figure 6.10, heat transfer quantity w.r.t. crank angle is shown. 0.01207 J/° was obtained as a maximum value at 230° CA. Also for slider-crank mechanism result was not so different. It was 0.01196 J/°

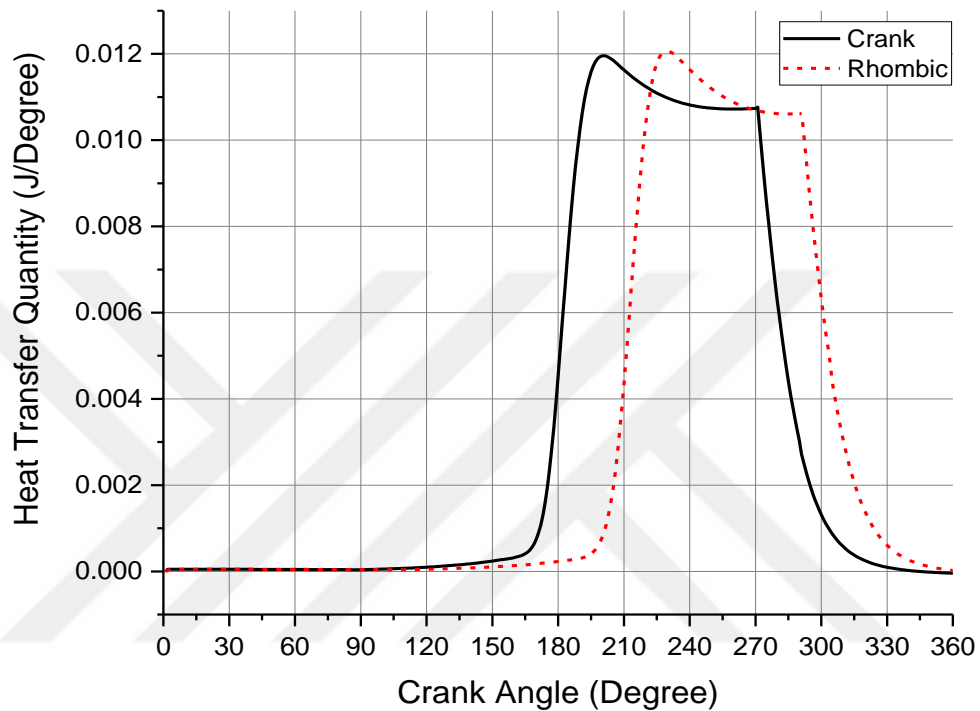


Figure 6.10: Cylinder heat transfer quantity-crank angle diagram.

In Figure 6.11 angular change on gas force is given for both engines. Due to having more maximum cylinder pressure, rhombic drive gas force was also higher than the slider mechanism engine which was 7.5 kN at 222° CA and 7.17 kN at 190° CA, respectively.

Mechanical efficiency of rhombic drive was 85.89%, while this was 86.21% for slider-crank mechanism.

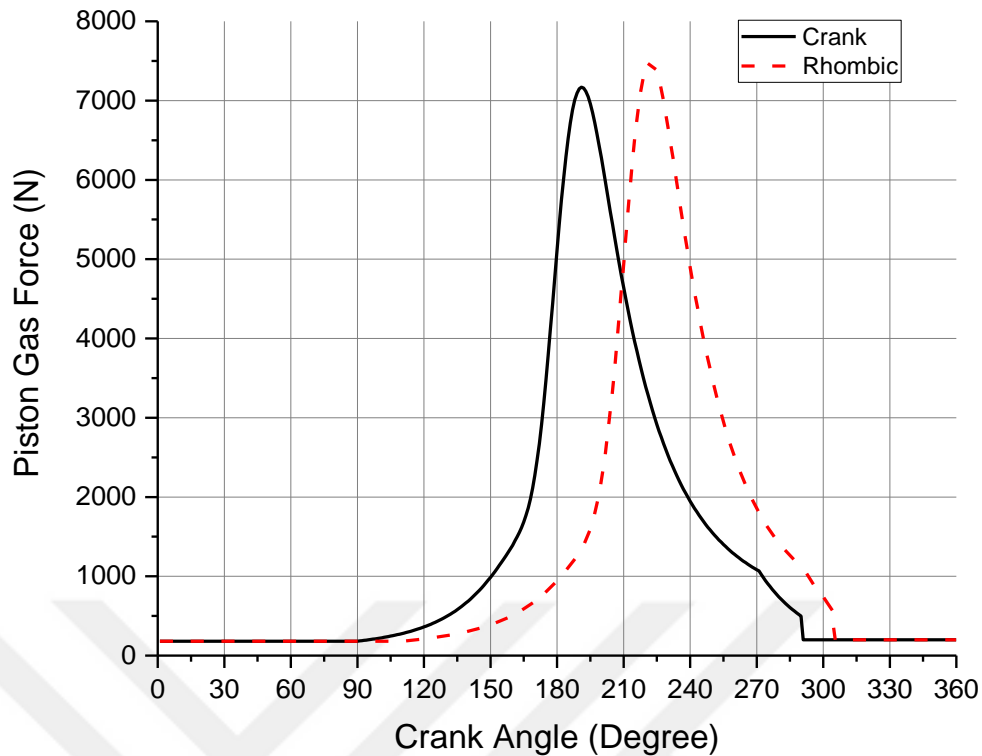


Figure 6.11: Piston gas force-crank angle diagram.

6.2 Evaluation of the Experimental Results

Experimental results of rhombic drive engine were taken on the range from 1700 rpm to 3000 rpm at $\frac{1}{4}$ throttle opening. Engine torque was increased with increasing engine speed but after a point, torque started to decrease due to reduction on charging efficiency with increment on flow resistances at high speeds. Maximum torque of output shaft was obtained 0.98 Nm at around 2400 rpm. It was observed that, engine idle speed was around 1100 rpm. At the range of operation, engine kept its stability. Engine power tends to increase till a point as a function of engine torque and engine speed but at high engine speeds, increment on engine speed could be not enough to sustain its increase and started to decrease with more reduction on torque. At $\frac{1}{4}$ throttle condition, maximum power was obtained about 0.3 kW. Effective (brake) torque and effective power w.r.t. engine speed is given in Figure 6.12 below.

Brake specific fuel consumption was measured as 205 g/kWh at around 2450 rpm. Increase on BSFC after 2450 rpm was attributed to poor charging, reduced

mechanical efficiency and increase on residual exhaust gases inside the cylinder. According to engine speed BSFC is given in Figure 6.13.

In Figure 6.14, thermal efficiency w.r.t. engine speed is given. Maximum thermal efficiency was obtained at around 2400 rpm with the polynomial fitting value 23.55%.

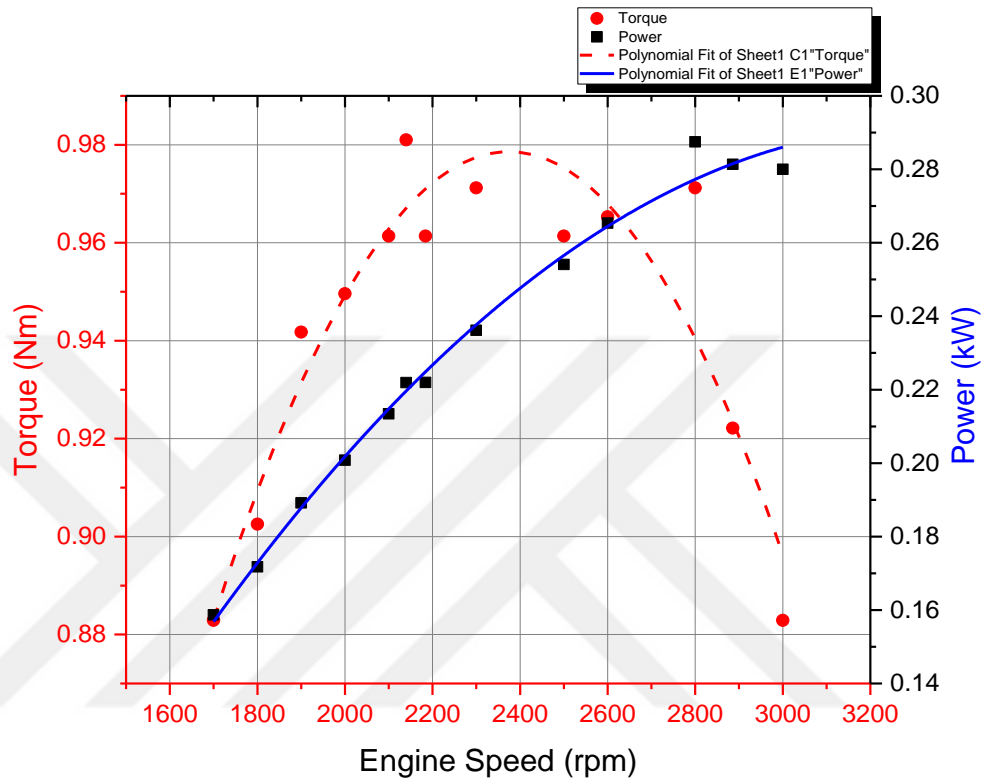


Figure 6.12: Effective torque-effective power w.r.t. engine speed diagram.

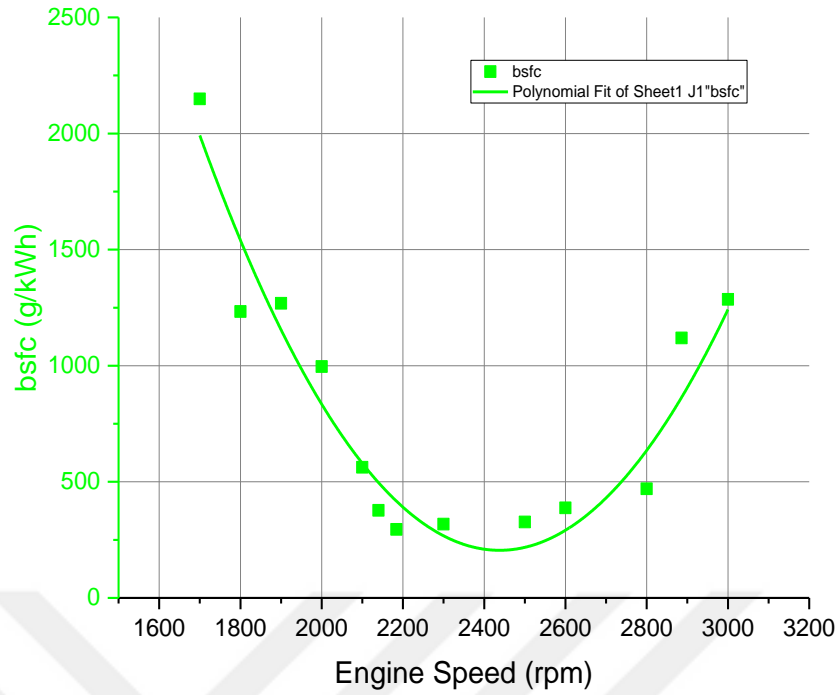


Figure 6.13: Brake specific fuel consumption w.r.t. engine speed diagram.

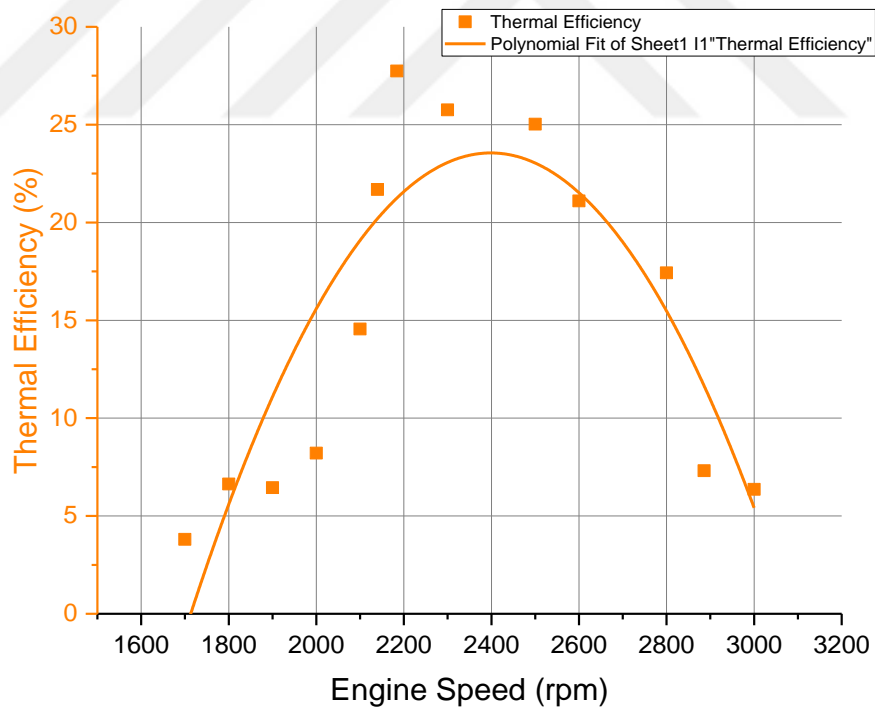


Figure 6.14: Thermal efficiency w.r.t. engine speed diagram

In Figure 6.15, CO, HC, NO, and also CO₂ change at the range of engine speed, 1700-2000 rpm, is given. CO pollutant is mostly affected by poor combustion process and main contribution to the exhaust pollutant is induced by scavenging process of the two-stroke engines. Unburned fuel is ejected during opened exhaust port. With increasing engine speed port opening duration will be less and as a result HC emission will be reduced. But rich mixture conditions will cause an increase again in HC curve. NO tends to decrease with reduction of peak combustion temperatures. Also due to mixing rate of lubricant with fuel, emissions will be affected and that will cause increasing of HC rates in total with lower flame speeds. On the other hand, emissions also seem to be better with more air intake conditions to burn with fuel molecules while approaching to the most effective torque speed. CO₂ component of the exhaust gas is decreased with misfire due to the increasing engine speed.

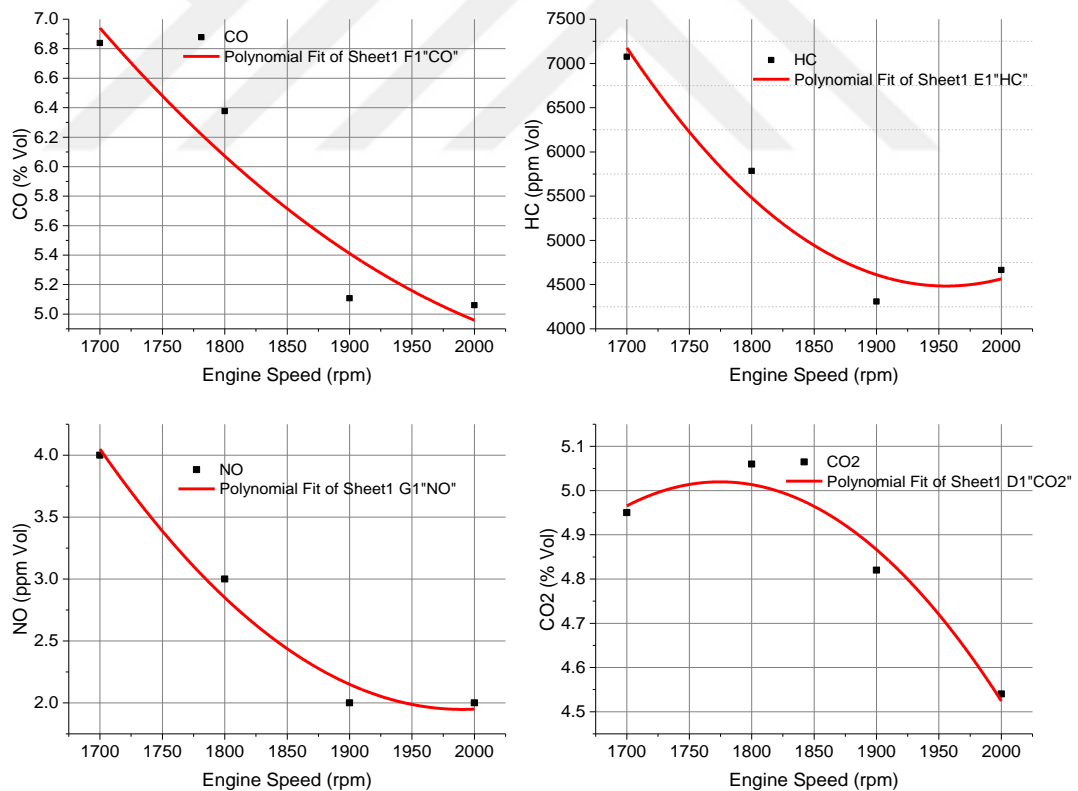


Figure 6.15: CO, HC, NO, CO₂ pollutant change w.r.t. engine speed.

CHAPTER 7

CONCLUDING REMARKS

In this study, a novel mechanism, rhombic drive, was designed for a two-stroke single cylinder air cooled spark ignition engine which could be an alternative of slider-crank mechanism. Design stage includes kinematic and thermodynamic analysis of the rhombic drive engine, 3D modelling and strength analysis with a finite element model in CAE software. Then a prototype of the engine was manufactured. Engine performance characteristics and some of the pollutants such as CO, HC, and CO₂ were examined.

Kinematic and thermodynamic analysis of the rhombic driven engine were expressed and some of the design parameters were kept fixed such as geometrical compression ratio, total cylinder volume, stroke, combustion duration, used fuel, volumetric efficiency, lambda and engine speed to compare with a slider-crank mechanism engine which is a mass production one in the market. Stroke, piston velocity and acceleration, pressure, volume, temperature, net work, heat release, heat transfer coefficient, gas forces on the piston were calculated as a function of crank in a developed Matlab program. It is observed that kinematic differences cause port timing change but two engines have no crucial dominance thermodynamically over each other. Maximum cylinder pressure is 185 kPa higher at rhombic drive than the slider-crank mechanism, so gas force on the rhombic drive piston is 0.33 kN more and the maximum temperature is only 39 K higher. On the other hand, net work is 0.9 J less. Theoretical thermal efficiencies of rhombic drive and slider-crank mechanism are 31.14% and 31.87%, respectively. In consideration of kinematic and thermodynamic analysis rhombic drive engine 3D model was obtained and strength analysis was run with inertia relief conditions in CAE software for the manufacturing.

Rhombic driven prototype engine was tested from the point effective torque, brake power and brake specific fuel consumption at the determined throttle and ignition advance conditions. Total mass of the rhombic drive is considerably reduced

when compared with the selected mass production engine which has 0.4 kg difference for the nearly same brake power.

Recommendations for future work; cylinder port area and places of the ports could be optimized for the new kinematic conditions to manage compression and expansion efficiently. Performance tests and emission measurement could be done for different operating parameters such as, ignition advances, compression ratio, etc. Also forced charging could make a compact engine as well from the point of power to weight ratio. GDI fuel system could be tried on to make independent crankcase volume and better combustion period. That configuration will also provide a separate lubrication system, as a result, durability of the engine will be increased and less pollutant emerge from the exhaust. Engine could be operated with alternative fuels to observe performance and emission change. Heat transfer correlations could be matched with other offers in the literature and with experimental results. Rhombic drive engine has advantage on power to weight ratio so could be used at light aerial vehicles and also could be preferred to use as a range extender on the vehicles.

REFERENCES

1. Ausserer, J., Polanka, M., Baranski, J., Grinstead, K. et al. (2017). Measurement of Loss Pathways in Small, Two-Stroke Internal- Combustion Engines. *SAE Int. J. Engines* 10(2):2017, doi: 10.4271/2017-01-9276.
2. Pulkrabek, Willard W. (2014). *Engineering Fundamentals of the Internal Combustion Engine*. England: Pearson Education Limited.
3. Newton, K., Steeds, W., Garrett, T.K. (1983). *The Motor Vehicle*. England: 10th Edition, Butterworths.
4. <https://www.britannica.com/technology/two-stroke-cycle> (09.02.2019).
5. <https://www.karlbenez.com/2013/04/karl-benz.html> (09.02.2019).
6. Blair, Gordon P. (1996). *Design and Simulation of Two-Stroke Engines*. Warrandale, PA: Society of Automotive Engineers, Inc.
7. https://en.wikipedia.org/wiki/Schnuerle_porting (09.02.2019).
8. <https://www.revolvvy.com/page/C.-F.-Caunter> (09.02.2019).
9. Nora, M.D., Metzka, T.D., Lanzanova, H.Z. (2016). Effects of valve timing, valve lift and exhaust backpressure on performance and gas exchanging of a two-stroke GDI engine with overhead valves. *Energy Conversion and Management* Volume 123, 1, Pages 71-83.
10. Senatorea, A., Buonoa, D., Frosina, E., Pratib, M.V., Valentino, G., Poles, F. (2015). Performances And Emissions Of A 2-Stroke Diesel Engine Fueled With Biofuel Blends. *Energy Procedia* 81 (2015) 918 – 929 .
11. Cantore, G., Mattarelli, E., Rinaldini, C.A. (2014). A new design concept for 2-Stroke aircraft Diesel engines. *Science Direct Energy Procedia* 45 739 –748.

12. Herold, R.E., Wahl, M.H., Regner G. and Lemke J.U.(2011). Thermodynamic Benefits of Opposed-Piston Two- Stroke Engines. *SAE International Published* <https://doi.org/10.4271/2011-01-2216>.
13. Carlucci, A.P., Ficarella, A., Laforgia, D., Renna, A. (2015). Supercharging system behaviour for high altitude operation of an aircraft 2-stroke Diesel engine. *Energy Conversion and Management* 101 470–480.
14. Carlucci, A.P., Ficarella, A., Trullo, G. (2016). Performance optimization of a Two-Stroke supercharged diesel engine for aircraft propulsion. *Energy Conversion and Management* 122 279–289.
15. [https://www.neander-motors.com/en/state-of-the-art/neander-solution/\(2017\)](https://www.neander-motors.com/en/state-of-the-art/neander-solution/(2017)); Neander Motor Vehicles AG, (09.02.2019)
16. Rucker, R. D. (2000). An Analysis of the Parallel Combustion Two-Stroke Engine, *SAE* 2000-01-1022.
17. Boretti, A. and Jiang, S. (2015). Two-Stroke Direct Injection Jet Ignition Engines for Unmanned Aerial Vehicles. *SAE Technical Paper* 2015-01-2424, doi: 10.4271/2015-01-2424.
18. Nuccio, P. and Marzano M. R. (2003). Performance Improvement of Two-Stroke SI Engines for Motor-Gliders and Ultra-Light Aircraft by Means of a GDI System. *SAE* 2003-32-0002.
19. Shankar,R. K., Priyanka, E.B., Saravanan, B. (2015). Performance Analysis of Gasoline Direct Injection in Two-Stroke Spark-ignition Engines. *International Journal of Advanced Research in Electrical, Electronics and Instrumentation Engineering*, Vol. 4, Issue 6.
20. Savioli, T., Zardin, B. Borghi, M. (2017). Development of a 2-stroke GDI Engine. *Science Direct Energy Procedia* 126(201709) 1091-1098.
21. Antonelli, E., Nuccio, P., Dongiovanni, C., Marzano, M.R. (2004). A New GDI 2-Stroke Engine to Meet Future Emission Limits: The Design and Prototype Architecture. *SAE* 2004-32-0041.

22. Dube, A. and Ramesh, A. (2016). Influence of Injection Parameters on the Performance and Emissions of a Direct Injection Two-Stroke SI Engine. *SAE Technical Paper* 2016-01-1052.
23. <https://patentimages.storage.googleapis.com/81/a9/2d/88bb381b6ce694/US2609802.pdf> (17.02.2019).
24. Kaya, G. (2017). “İki Zamanlı Ters Doğru Akışlı Buji İle Ateşlemeli Bir Motorun Tasarımı, İmalı ve Performans Testleri” Doktora Tezi, Karabük Üniversitesi Fen Bilimleri Enstitüsü
25. archive.maas.museum/australia_innovates/index32a3.html?behaviour=view_article&Section_id=1020&article_id=10041 (17.02.2019).
26. https://www.researchgate.net/publication/301243069_A_New_Rotary_Valve_for_2-Stroke_Engines_Enabling_Over-Expansion (09.02.2019).
27. Aksoy, F., Solmaz, H., Karabulut, H., Çınar, C., Ozgoren, Y.O., Polat, S. (2016). A thermodynamic approach to compare the performance of rhombic drive and crank drive mechanisms for a beta type Stirling engine. *Applied Thermal Engineering* 93(2016) 359-367.
28. Solmaz, H., Karabulut, H. (2014). Performance comparison of a novel configuration of beta-type Stirling engines with rhombic drive engine, *Energy Conversion and Management* 78(2014) 627-633.
29. Chin,-H., Cheng, Y.J.Y. (2012). Combining dynamic and thermodynamic models for dynamic simulation of a beta-type Stirling engine with rhombic drive mechanism. *Renewable Energy* 37(2012) 161-173.
30. Hassani, E.H., Boutammachte, N., Knorr, J., Hannaoui, E.M. (2013). Study of a low temperature Stirling engine driven by a rhombic drive mechanism. *International Journal of Energy and Environmental Engineering* 2013,4:40.
31. Shendage, D.J., Kedare, S.B., Bapat, S.L. (2011). An analysis of beta type Stirling engine with rhombic drive mechanism. *Renewable Energy* 36(2011) 289-297.

32. Karabulut, H., Aksoy, F., Öztürk, E. (2009). Thermodynamic analysis of a β type Stirling engine with a displacer driving mechanism by means of a lever. *Renewable Energy* 34(2009) 202-208.
33. Cheng, Y.J.Y. (2010). Numerical model for predicting thermodynamic cycle and thermal efficiency of a beta-type Stirling engine with rhombic drive mechanism. *Renewable Energy* 35(2010) 2590-2601.
34. Polat, S. (2010). “Dört zamanlı, tek silindri, değişken sıkıştırma oranlı bir dizel motorunun bilgisayar yardımı ile teorik simülasyonu ve performans analizi” Yüksek Lisans Tezi, Gazi Üniversitesi Fen Bilimleri Enstitüsü.
35. Böğrek, A., (2011) “İdeal Otto Çevriminin Teorik Analizi” Yüksek Lisans Tezi, Selçuk Üniversitesi Fen Bilimleri Enstitüsü.
36. <http://www.rsc.org/periodic-table> (09.02.2019).
37. Yılmaz, E. (2018).”Rhombik Mekanizmalı Buji İle Ateşlemeli Bir Motorun Tasarımı Ve Analizleri”, Doktora Tezi, Gazi Üniversitesi Fen Bilimleri Enstitüsü.
38. İpçi, D., Karabulut, H. (2016). Dynamic and Thermodynamic Examination of a Two Stroke Internal Combustion Engine. *Journal of Polytechnic*;19 (2): 141-154.
39. Öztürk, E. (2003).”İki Zamanlı Direkt Püskürtmeli Bir Dizel Motorunun Bilgisayar Yardımı İle Performans Analizi” Yüksek Lisans Tezi, Gazi Üniversitesi Fen Bilimleri Enstitüsü.
40. Ferguson, C. R., and Kirkpatrick, A. T. (2014). *Internal combustion engine applied thermosciences*. New Jersey, John Wiley & Sons.
41. Cengel, Y.A. and Boles, M.A. (2006), *Thermodynamics: An Engineering Approach. Fifth Edition*. New York: McGraw Hill.
42. Sonntag R., Borgnakke C., Van, W. G. (1998). *Fundamentals of Thermodynamics 5th Edition*. New York :Wiley.

43. Planck, M. (1910) *Treaties on Thermodynamics, 3rd Edition*. Dover Publications Inc.
44. Heywood, J. B. (1988). *Internal combustion engine fundamentals*. New York,: McGraw-Hill Book Company.
45. Polat, S. (2013). Bir Dizel Motorun Bilgisayar Yardımı ile Termodinamik ve Performans Analizi. *Gazi Üniversitesi Fen Bilimleri Dergisi, Part C, Tasarım ve Teknoloji*, 1(3):139-151.
46. Yeliana, C., Cooney, J., Worm, D., Michalek, J. N. (2008). Wiebe Function Parameter Determination For Mass Fraction Burn Calculation In An Ethanol-Gasoline Fuelled SI Engine. *Journal of KONES Powertrain and Transport*, Vol. 15, No. 3
47. Bakara, R.A., Wee, C.C., Minga, G.L. (2003) Heat Transfer Analysis in Air-Cooled Two-Stroke Engine Prototype, *Researchgate Publication, Publisher: Engineering and Technology Conference*, January 2003.
48. Brusiania, F., Falfaria, S., Fortea, C., Cazzolia, G., Verziagib, P., Ferrarib, M., Cataneseb, D. (2015). Definition of a CFD Methodology to Evaluate the Cylinder Temperature Distribution in Two-Stroke Air Cooled Engines. *Energy Procedia*, Volume 81, Pages 765-774.
49. Mitianiec, W., Buczek, K. (2007). Analysis Of Thermal Loads In Air Cooled SI Engine. *Journal of KONES Powertrain and Transport*, Vol.14, No. 3.
50. Spitsov, O. (2013). “Heat transfer inside internal combustion engine: modelling and comparison with experimental data” M.Sc Thesis, Lappeenranta University of Technology, Faculty of Technology, Degree Programme in Energy Technology.
51. Çetinkaya, S., (2005), *Taşıt Mekaniği*, Ankara, Nobel Yayın Dağıtım.
52. http://www.thyssenkruppmaterials.co.th/Cold_Work_Steel_2379.html (09.02.2019).
53. <http://www.otaisteel.com/products/cold-work-tool-steel/1-2379-steel/> (09.02.2019).

54. <https://www.indiamart.com/proddetail/tool-steel-din-1-2379-7229586348.html> (09.02.2019).
55. https://www.etsp.ru/documents/catalog_engine.pdf (09.02.2019).
56. Çınar, C., Aksoy, F., Erol, D. (2011). The effect of displacer material on the performance of a low temperature differential Stirling engine. *International Journal of Energy* DOI:10.1002/er.1861.



CURRICULUM VITAE

PERSONAL INFORMATION

Name Surname : Erol Gültekin
Nationality : Turkish
Place and Date of Birth : Ardanuç / 1984
Marital Status : Married
Adress : University of Turkish Aeronautical Association, Faculty of
Engineering, Dept. of Mechanical Engineering
E-mail : egultekin@thk.edu.tr
Phone : 90 312 589 61 08

EDUCATION

Ph.D : UTAA, Mechanical and Aeronautical Engineering - Ongoing
M.Sc. : Uludağ and Torino Polytechnic Universities/
Dept. of Mechanical Engineering – 2011
B.Sc. : Gazi University / Dept. of Automotive Teaching – 2008
High School : Hürriyet Anatolian Technical High School/ Dept. of Aircraft Body
And Engine - 2003

EXPERIENCE

2012-Ongoing, University of Turkish Aeronautical Association, Lecturer
2011-2012, Rollmech Automotive Inc., R&D Benchmark / Value Analysis
Engineer
2010-2011, Turkish Armed Forces., Land Forces Command / Lecturer
2008-2010, Bosch Rexroth AG., Bosch Production System / Master Science
Employee

FOREIGN LANGUAGE

English, German.